

Chapter 5

Characterization of Space-time Processes

5.1 Introduction

In this chapter we will develop techniques for characterizing space-time random processes and their interaction with arrays and apertures. It produces the statistical basis for the remainder of the text, where we emphasize a statistical approach rather than a deterministic approach to array analysis and synthesis.

In the discussion of classical array processing the input to the array was assumed to be a sinusoidal plane-wave signal. It was characterized by its frequency and wavenumber or by its frequency and direction of arrival. In most of our discussions, we focused on a single frequency, and the beamformer weights were fixed complex numbers.

In the statistical approach, the input to the array consists of desired signals, interfering signals, and noise. Some or all of these inputs are modeled as sample functions of space-time random processes.

These processes may be spread over regions of $\omega\text{-}\mathbf{k}$ space. The array processor operates on the array output to estimate a waveform, detect a signal, or estimate parameters of a signal. These operations are the vector extensions of the scalar detection, estimation, and modulation problems that were solved in DEMT I [VT68], [VT01a] and DEMT III [VT71], [VT01b]. The first step was to operate on the continuous time functions to obtain a set of random variables that were used to solve the detection or estimation problem. We used a Karhunen-Loëve (KL) expansion that was applicable to non-stationary processes and finite time intervals and generated statistically

independent Gaussian random variables when the input was a Gaussian random process. This approach can be extended to the vector case.

In most applications and in the majority of the research literature, an alternative approach using sampling is employed. These samples are normally referred to in the literature as **snapshots**. In Section 5.2, snapshot models in the frequency domain and time domain are developed. The objective of the snapshot generation process is to operate on the sensor output and generate a sequence of vectors. Appropriate processing is performed on this vector sequence.

Section 5.3 develops models for spatially spread random processes. A second-moment characterization of the random fields is developed. If processing consists of linear filters and quadratic error criteria, then the second-moment characterization is adequate. However, if we want to develop optimum detectors and estimators, then a complete statistical characterization is necessary. Gaussian space-time processes are defined that are completely characterized by the second moments.

In Section 5.4, the output statistics of arrays and apertures are developed for the case in which the input is a space-time random process. For an array the primary statistic of interest is the **spatial spectral matrix**, \mathbf{S}_x , of the snapshot vectors. We will show how the classical beam patterns developed in chapters 2–4 interact with the frequency-wavenumber characterization of space-time processes.

In Section 5.5, an eigendecomposition of the $N \times N$ spatial spectral matrix \mathbf{S}_x is performed. The resulting eigenvalues and eigenvectors play a key role in many of the subsequent discussions. The concept of signal and noise subspaces is introduced. The subspace concept also plays a key role in subsequent discussions.

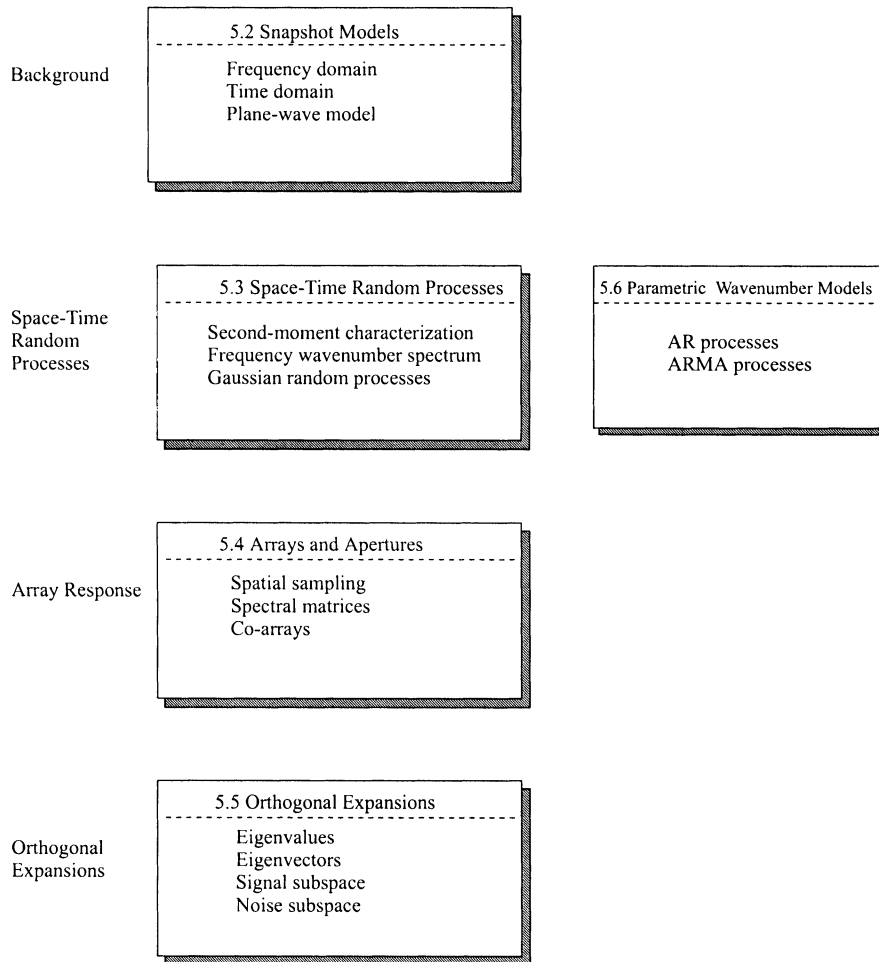
Section 5.6 develops parametric models for the frequency-wavenumber spectrum. Various rational transfer function models such as auto-regressive (AR) and auto-regressive moving average (ARMA) models are developed.

Section 5.7 provides a brief summary of the chapter. The structure of Chapter 5 is shown in Table 5.1.

5.2 Snapshot Models

In this section, the snapshot models that play a key role in the subsequent discussion are developed. In Section 5.2.1, frequency-domain snapshot models are developed. In Section 5.2.2, time-domain snapshot models are developed. In Section 5.2.3, the results are summarized.

Table 5.1 Structure of Chapter 5.



5.2.1 Frequency-domain Snapshot Models

In many applications, we implement the beamforming in the frequency domain. The model is shown in Figure 5.1. The first box converts the sensor input vector from the time domain to the frequency domain. The second box processes the frequency-domain vector to obtain a scalar frequency-domain function. The third box converts the frequency-domain function into a scalar time-domain waveform. The functions in each box are now described.

The objective of the first processor is to generate a set of complex vectors that can be processed to form a beam. We refer to these complex vectors as

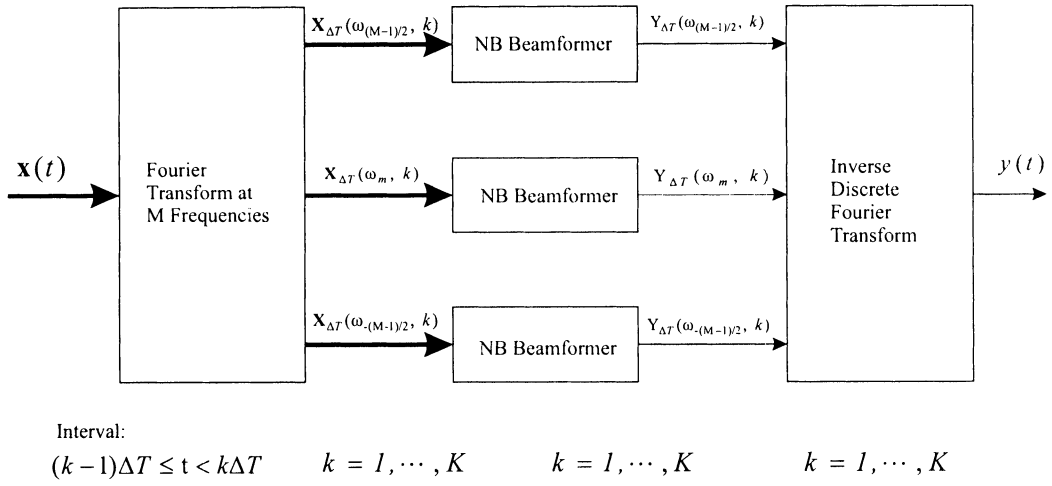


Figure 5.1 Frequency-domain beamformer.

frequency-domain snapshots.

In order to generate these vectors, first divide the total observation interval T into K disjoint intervals of length ΔT . These intervals are indexed with k ,

$$\begin{aligned}
 k &= 1 & 0 \leq t < \Delta T \\
 k &= 2 & \Delta T \leq t < 2\Delta T \\
 &\vdots & \\
 k &= k & (k-1)\Delta T \leq t < k\Delta T \\
 &\vdots & \\
 k &= K & (K-1)\Delta T \leq t < K\Delta T.
 \end{aligned} \tag{5.1}$$

As part of the development, we will develop criteria for choosing ΔT .

The first requirement is that ΔT must be significantly greater than the propagation time across the array. Define

$$\Delta T_{\max} \triangleq \max_{d=1, \dots, D} \left\{ \max_{i,j} [\Delta T_{ij}^{(d)}] \right\}, \tag{5.2}$$

where $\Delta T_{ij}^{(d)}$ is the travel time between the i and j elements for the d th signal. In a linear array, the maximum propagation time corresponds to a signal arriving from endfire and equals the length of the array divided by

the velocity of propagation. Then we require

$$\Delta T \gg \Delta T_{max}. \quad (5.3)$$

The second requirement on ΔT will be determined by the bandwidth of the input signals and the shape of their temporal spectra. We discuss this requirement shortly.

To motivate the approach, we recall our approach to detection and estimation problems in DEMT I [VT68], [VT01a]. We decomposed the waveform of interest using a series expansion whose coefficients were statistically independent Gaussian random variables. This approach led to a Karhunen-Loëve expansion and an eigenfunction problem. We did the vector version of the problem in Section 3.7 of DEMT I (pp. 220–224). For stationary processes and a long time interval, the KL expansion becomes a Fourier series expansion. This result motivates the frequency-domain snapshot model. We define this model and analyze the covariance between its components as a function of ΔT .

We assume that the input is a zero-mean bandpass process centered at ω_c . The signal at the origin is $x(t)$. The bandpass spectrum of $x(t)$ and its lowpass equivalent are shown in Figure 5.2.

We first consider the interval $(0, \Delta T)$ and define¹

$$\begin{aligned} \mathbf{X}_{\Delta T}(\omega_m) &= \frac{1}{\sqrt{\Delta T}} \int_0^{\Delta T} \mathbf{x}(t) e^{-j(\omega_c + m\omega_\Delta)t} dt, \\ m &= -\frac{M-1}{2}, \dots, 0, \dots, \frac{M-1}{2}, \end{aligned} \quad (5.4)$$

where the m th Fourier series frequency is

$$\omega_m = \omega_c + m\omega_\Delta, \quad (5.5)$$

and the resolution of the transform is

$$\omega_\Delta = \frac{2\pi}{\Delta T}. \quad (5.6)$$

The expression in (5.4) assumes M is odd. For M even, the limits are $m = -M/2, \dots, 0, \dots, \frac{M}{2}-1$. The value of M will depend on the bandwidth of the bandpass process. For M odd,

$$M = \lfloor B_s \cdot \Delta T \rfloor + 1, \quad (5.7)$$

¹This discussion is based on Hodgkiss and Nolte [HN76]. Several of their key formulas are due to Blackman [Bla57].

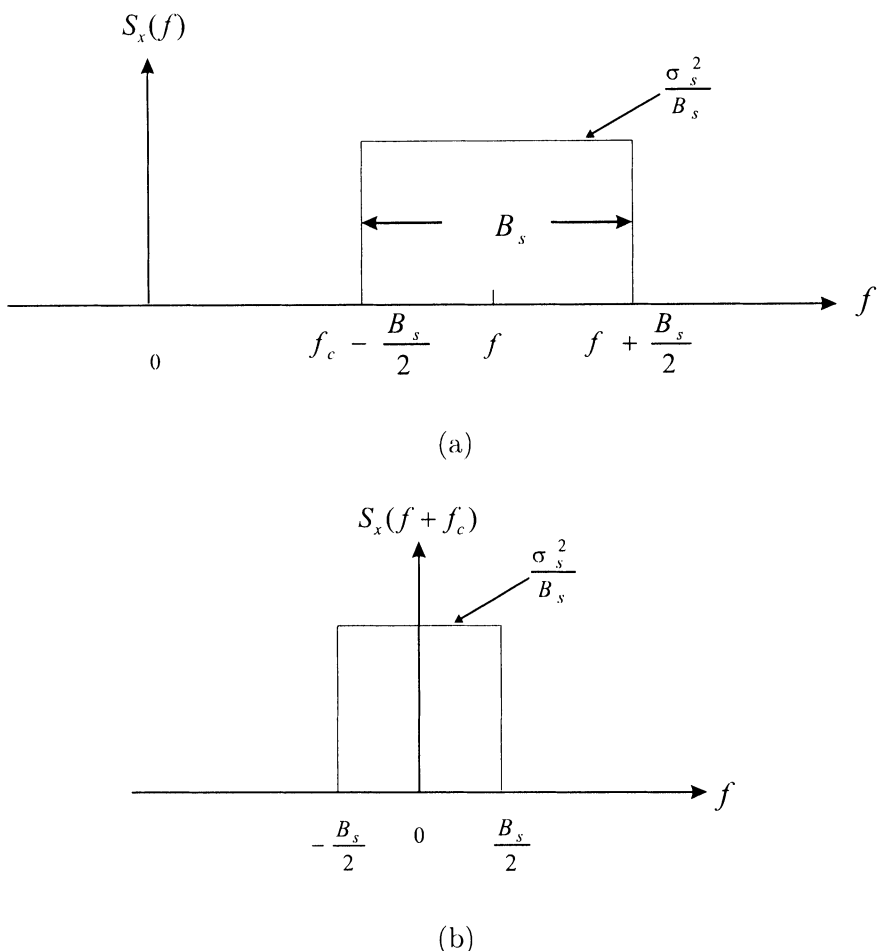


Figure 5.2 Bandpass signal spectrum and corresponding lowpass spectrum.

where $\lfloor B_s \cdot \Delta T \rfloor$ denote the largest integer less than $B_s \cdot \Delta T$. Each of the $\mathbf{X}_{\Delta T}(\omega_m)$ is an N -dimensional complex vector corresponding to the Fourier series coefficient at ω_m . We refer to each of the ω_m as the center frequency of a **frequency bin** whose width is ω_Δ .

We want to derive an expression for the covariance matrix $\mathbf{X}_{\Delta T}(\omega_{m_1})$ and $\mathbf{X}_{\Delta T}(\omega_{m_2})$. The covariance matrix is

$$\begin{aligned} \mathbf{S}_{\mathbf{x}_{\Delta T}}(m_1, m_2) &\triangleq E \left[\mathbf{X}_{\Delta T}(\omega_{m_1}) \mathbf{X}_{\Delta T}^H(\omega_{m_2}) \right] \\ &= \frac{1}{\Delta T} \int_0^{\Delta T} \int_0^{\Delta T} \mathbf{R}_x(t-u) e^{-j\omega_c(t-u)} e^{-jm_1\omega_\Delta t + jm_2\omega_\Delta u} dt du. \end{aligned} \quad (5.8)$$

This can be written as

$$\begin{aligned} \mathbf{S}_{\mathbf{x}_{\Delta T}}(m_1, m_2) &= \frac{1}{\Delta T} \int_{-\infty}^{\infty} \int_0^{\Delta T} \int_0^{\Delta T} \frac{1}{2\pi} \mathbf{S}_{\mathbf{x}}(\omega) e^{j(\omega - \omega_c)(t-u)} \\ &\quad \cdot e^{-jm_1\omega_\Delta t} e^{jm_2\omega_\Delta u} dt du d\omega, \end{aligned} \quad (5.9)$$

where $\mathbf{S}_{\mathbf{x}}(\omega)$ is the spectral matrix of the process. Defining

$$\omega_L = \omega - \omega_c, \quad (5.10)$$

(5.9) reduces to

$$\begin{aligned} \mathbf{S}_{\mathbf{x}_{\Delta T}}(m_1, m_2) &= e^{-j\pi(m_1 - m_2)} \int_{-\infty}^{\infty} \mathbf{S}_{\mathbf{x}}(\omega_L + \omega_c) \\ &\quad \cdot \left\{ \frac{1}{\omega_\Delta} \text{sinc}\left(\pi\left(\frac{\omega_L}{\omega_\Delta} - m_1\right)\right) \text{sinc}\left(\pi\left(\frac{\omega_L}{\omega_\Delta} - m_2\right)\right) \right\} d\omega_L. \end{aligned} \quad (5.11)$$

For $m_1 = m_2 = m$, (5.11) reduces to

$$\mathbf{S}_{\mathbf{x}_{\Delta T}}(m, m) = \int_{-\infty}^{\infty} \mathbf{S}_{\mathbf{x}}(\omega_L + \omega_c) \left\{ \frac{\text{sinc}^2\left(\pi\left(\frac{\omega_L}{\omega_\Delta} - m\right)\right)}{\omega_\Delta} \right\} d\omega_L. \quad (5.12)$$

We first consider the diagonal terms that correspond to the covariance at a single sensor. For the n th sensor,

$$[\mathbf{S}_{\mathbf{x}_{\Delta T}}(m, m)]_{nn} = \int_{-\infty}^{\infty} [\mathbf{S}_{\mathbf{x}}(\omega_L + \omega_c)]_{nn} \left\{ \frac{\text{sinc}^2\left(\pi\left(\frac{\omega_L}{\omega_\Delta} - m\right)\right)}{\omega_\Delta} \right\} d\omega_L. \quad (5.13)$$

In Figure 5.3, we show the components of the integrand for various values of ω_Δ . Figure 5.3(a) shows the $\text{sinc}^2(\cdot)$ function for several values of m . In Figure 5.3(b), we plot $[\mathbf{S}_x(\omega_L + \omega_c)]_{nn}$ versus (ω_L/ω_Δ) for the case in which

$$B_s \cdot \Delta T = 16. \quad (5.14)$$

We typically use the frequency-domain snapshot approach when the time-bandwidth product $B_s \cdot \Delta T$ is large. In practice, $B_s \cdot \Delta T$ products from 16 to 512 are common. The value of ω_Δ determines the frequency resolution of the model and $2\pi B_s/\omega_\Delta$ determines the number of terms in the Fourier series expression.

In the limit, as $\Delta T \rightarrow \infty$, the term in braces in (5.13) approaches an impulse and

$$\lim_{\Delta T \rightarrow \infty} \{[\mathbf{S}_{x_{\Delta T}}(m, m)]_{nn}\} = [\mathbf{S}_x(\omega_c + m\omega_\Delta)]_{nn}. \quad (5.15)$$

This result is the Wiener-Khinchin theorem (e.g., [Hel91]). A similar result holds for the off-diagonal terms, so the matrix version of (5.15) is

$$\lim_{\Delta T \rightarrow \infty} \{\mathbf{S}_{x_{\Delta T}}(m, m)\} = \mathbf{S}_x(\omega_c + m\omega_\Delta). \quad (5.16)$$

We now consider a simple example to illustrate the behavior as a function of $B_s \cdot \Delta T$.

Example 5.2.1

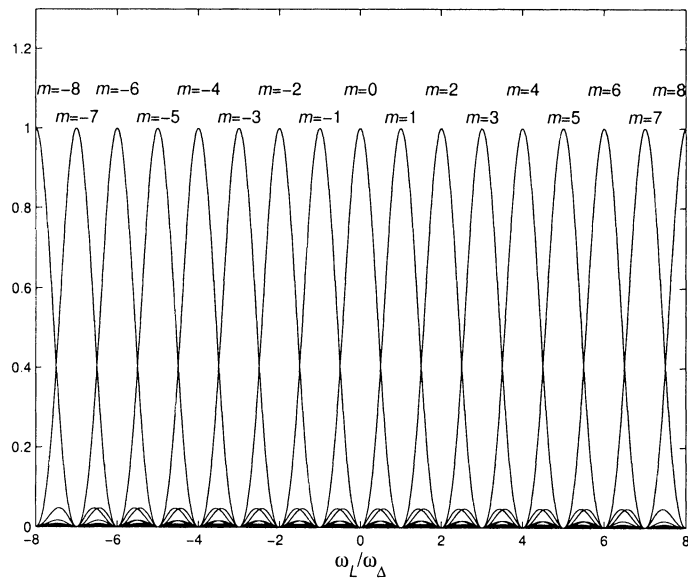
The spectrum of the signal is shown in Figure 5.2. We evaluate the integral in (5.12) for

$$B_s \cdot \Delta T = 2^l, \quad l = 0, \dots, 8. \quad (5.17)$$

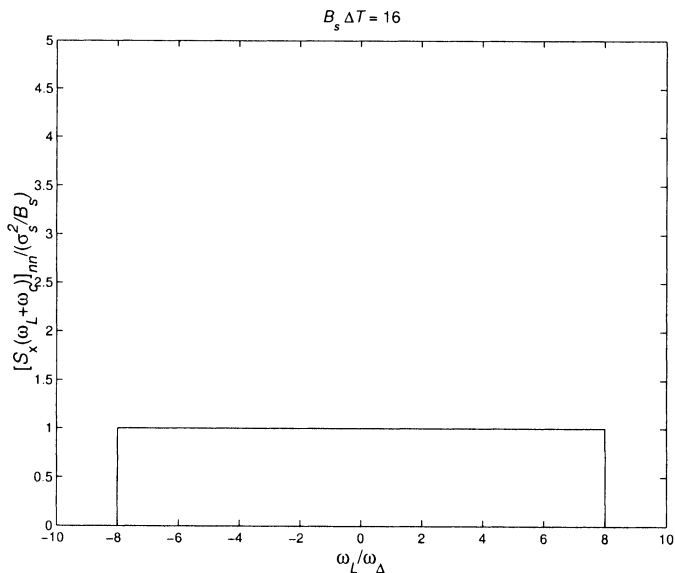
In Table 5.2, we show the normalized value, $[\mathbf{S}_{x_{\Delta T}}(m, m)]_{nn} / (\sigma_s^2 / B_s)$ for the given values of l and selected values of $|m|$.

Table 5.2

$ m $	0	1	2	4	8	16	32	64	128
0	0.7737	0.0787	0.0140	0.0032	0.0008	0.0002	0.0000	0.0000	0.0000
1	0.9028	0.4750	0.0318	0.0067	0.0016	0.0004	0.0001	0.0000	0.0000
2	0.9499	0.9346	0.4874	0.0166	0.0034	0.0008	0.0002	0.0000	0.0000
3	0.9747	0.9731	0.9665	0.4937	0.0084	0.0017	0.0004	0.0001	0.0000
4	0.9873	0.9871	0.9865	0.9832	0.4968	0.0042	0.0008	0.0002	0.0000
5	0.9937	0.9936	0.9936	0.9932	0.9916	0.4984	0.0021	0.0004	0.0001
6	0.9968	0.9968	0.9968	0.9968	0.9966	0.9958	0.4992	0.0011	0.0002
7	0.9984	0.9984	0.9984	0.9984	0.9984	0.9983	0.9979	0.4996	0.0005
8	0.9992	0.9992	0.9992	0.9992	0.9992	0.9992	0.9992	0.9989	0.4998



(a)



(b)

Figure 5.3 Functions in integrand: (a) sinc²(\cdot) functions for various m ; (b) spectrum of bandpass process ($B_s \cdot \Delta T = 16$).

We see that, for $B_s \cdot \Delta T \geq 16$, the approximation in (5.15) is accurate.

In practice, many of the spectra of interest are not flat. However, if the spectrum is constant over an interval $\pm 2\omega_\Delta - \pm 3\omega_\Delta$ around $m\omega_\Delta$, then we can use the approximation,

$$[\mathbf{S}_{x_{\Delta T}}(m, m)]_{nn} \simeq [\mathbf{S}_x(\omega_c + m\omega_\Delta)]_{nn} = [\mathbf{S}_x(\omega_m)]_{nn}. \quad (5.18)$$

Example 5.2.1 and the approximation in (5.18) deal with the diagonal terms in $\mathbf{S}_{x_{\Delta T}}(m, m)$. To investigate the off-diagonal terms we assume a plane-wave model. Carrying out a similar analysis, we find that if the spectrum is constant over $\pm 2\omega_\Delta - \pm 3\omega_\Delta$, then we can use the approximation

$$\mathbf{S}_{x_{\Delta T}}(m, m) \simeq \mathbf{S}_x(\omega_c + m\omega_\Delta) = \mathbf{S}_x(\omega_m). \quad (5.19)$$

The frequency-domain snapshot model is most appropriate for large $B_s \cdot \Delta T$ products. However, it is useful to consider the case in which

$$B_s \cdot \Delta T \ll 1. \quad (5.20)$$

Now the $\text{sinc}^2(\cdot)$ is approximately unity over the interval where the spectrum is non-zero and we can approximate the integral for $m = 0$ by

$$\begin{aligned} [\mathbf{S}_{x_{\Delta T}}(0, 0)]_{nn} &\simeq \int_{-\pi B_s}^{\pi B_s} \frac{\sigma_s^2}{B_s} \cdot \frac{1}{\omega_\Delta} d\omega \\ &= \sigma_s^2 \Delta T = [\mathbf{S}_x(\omega_c)]_{nn} \cdot \Delta T. \end{aligned} \quad (5.21)$$

We also use the approximation,

$$[\mathbf{S}_{x_{\Delta T}}(m, m)]_{nn} \simeq 0, \quad m \neq 0. \quad (5.22)$$

If we use the approximations in (5.21) and (5.22), then the beamformer only processes one frequency bin. This case is the narrowband frequency-domain snapshot model.

The frequency-domain snapshot model is occasionally used for the case when

$$B_s \cdot \Delta T = 1. \quad (5.23)$$

In Example 5.2.1, the actual values of $[\mathbf{S}_{x_{\Delta T}}(m, m)]_{nn}$ for various $B_s \cdot \Delta T$ are calculated. For $B_s \cdot \Delta T = 1$,

$$[\mathbf{S}_{x_{\Delta T}}(m, m)]_{nn} = \begin{cases} 0.773 & m = 0 \\ 0.079 & |m| = 1 \\ 0.014 & |m| = 2. \end{cases} \quad (5.24)$$

Thus, the approximation in (5.21) is not precise. However, if the desired signal, the interfering signals, and the sensor noise all have flat spectrum over the bandwidth, then the scaling factor (0.773) will be the same. All of the beamformer weights will depend on ratios of the various spectra so the use of (5.21) will not affect the beamformer design or its performance.

The approximation in (5.22) means that the narrowband beamformer is not utilizing the information in the $m \neq 0$ frequency bins. From (5.4), we note that $\mathbf{X}_{\Delta T}(\omega_m)$ for $m = 0$ is just the average value of the envelope over the interval ΔT (multiplied by $\sqrt{\Delta T}$ for normalization purposes). In our subsequent work we assume that we utilize

$$M = \begin{cases} 1 & , \quad B_s \cdot \Delta T \leq 1 \\ B_s \cdot \Delta T + 1 & , \quad B_s \cdot \Delta T = 2, 3, \dots \end{cases} \quad (5.25)$$

and that $B_s \cdot \Delta T$ is large enough that the approximation in (5.19) is valid.²

If we are going to process multiple frequency bins, we need to analyze the statistical behavior for $m_1 \neq m_2$. The expression for $\mathbf{S}_{\mathbf{x}_{\Delta T}}(m_1, m_2)$ is given in (5.11). The relevant $\text{sinc}^2(\cdot)$ functions are shown in Figure 5.3(a). For $m_1 \neq m_2$, the two $\text{sinc}(\cdot)$ functions are orthogonal so that, if the elements in $[\mathbf{S}_{\mathbf{x}}(\omega)]$ are constant over an interval $\pm 2\omega_{\Delta}$ or $\pm 3\omega_{\Delta}$ on either side of $(\omega_c + m\omega_{\Delta})$, the magnitude will approach zero. Hodgkiss and Nolte [HN76] have calculated the values for a flat spectrum over the frequency range ($-B_s/2 \leq f \leq B_s/2$) and find that if

$$B_s \cdot \Delta T \geq 16, \quad (5.26)$$

the values are essentially zero (see Problem 5.2.3).

We implement a similar expansion in the k th interval to obtain the vector $\mathbf{X}_{\Delta T}(\omega_m, k)$. Due to the stationarity of the process, the spatial covariance matrix is not a function of k . In addition,

$$\begin{aligned} E \left[\mathbf{X}_{\Delta T}(\omega_{m_1}, k) \mathbf{X}_{\Delta T}^H(\omega_{m_2}, l) \right] &\cong 0, \quad k \neq l \\ m_1, m_2 &= -\frac{M-1}{2}, \dots, \frac{M-1}{2}, \end{aligned} \quad (5.27)$$

for large $B_s \cdot \Delta T$ (see Problem 5.2.4).

Thus, the frequency-domain snapshot model generates a sequence of N -dimensional complex vectors at M discrete frequencies, ω_m .

²The $B_s \cdot \Delta T = 1$ case is really not a good fit in the frequency-domain snapshot model. The discussion after (5.24) partially justifies its use. In practice, we would normally use the time-domain model in Section 5.2.2 if all of the signals and interferers are narrowband around ω_c .

In our subsequent discussions, we assume that the approximation in (5.19) is valid and that the snapshots for different m and/or different k are uncorrelated. In the next section, we show that if $\mathbf{x}(t)$ is a real Gaussian random process, then the snapshots for $m_i, i = -(M-1)/2, \dots, (M-1)/2$, and $k, k = 1, \dots, K$ are joint circular complex Gaussian random vectors. Thus, the snapshots for different m and/or different k are statistically independent.

5.2.1.1 Gaussian model

In many of our subsequent developments, $\mathbf{x}(t)$ is modeled as a real vector Gaussian random process. We want to show that the $\mathbf{X}_{\Delta T}(\omega_m, k)$ are joint circular complex Gaussian random vectors.³ First consider the case in which $\mathbf{x}(t)$ is a zero-mean process.

Then, the real part and the imaginary part of $\mathbf{X}_{\Delta T}(\omega_m, k)$ are real zero-mean Gaussian random vectors:

$$\begin{aligned}\mathbf{X}_{\Delta T,C}(\omega_m, k) &\triangleq \text{Re}(\mathbf{X}_{\Delta T}(\omega_m, k)) = \frac{1}{\sqrt{\Delta T}} \int_0^{\Delta T} \mathbf{x}(t) \cos \omega_m t dt, \\ m &= -\frac{M-1}{2}, \dots, 0, \dots, \frac{M-1}{2},\end{aligned}\quad (5.28)$$

and

$$\begin{aligned}\mathbf{X}_{\Delta T,S} \triangleq \text{Im}(\mathbf{X}_{\Delta T}(\omega_m, k)) &= -\frac{1}{\sqrt{\Delta T}} \int_0^{\Delta T} \mathbf{x}(t) \sin \omega_m t dt, \\ m &= -\frac{M-1}{2}, \dots, 0, \dots, \frac{M-1}{2}.\end{aligned}\quad (5.29)$$

However, in order for $\mathbf{X}_{\Delta T}(\omega_m, k)$ to be a circular complex Gaussian random vector, we require

$$E \left[\mathbf{X}_{\Delta T,C}(\omega_m, k) \mathbf{X}_{\Delta T,C}^T(\omega_m, k) \right] = E \left[\mathbf{X}_{\Delta T,S}(\omega_m, k) \mathbf{X}_{\Delta T,S}^T(\omega_m, k) \right], \quad (5.30)$$

and

$$E \left[\mathbf{X}_{\Delta T,C}(\omega_m, k) \mathbf{X}_{\Delta T,S}^T(\omega_m, k) \right] = \mathbf{0}. \quad (5.31)$$

The conditions in (5.30) and (5.31) can also be written as,

$$E \left[\mathbf{X}_{\Delta T}(\omega_m, k) \mathbf{X}_{\Delta T}^T(\omega_m, k) \right] = \mathbf{0}. \quad (5.32)$$

³Complex Gaussian random processes are discussed in Appendix A of DEMT III [VT71], [VT01b]. Other discussions are available in Fuhrman [Fuh98], Miller [Mil74], and Neeser and Massey [NM93].

The equalities in (5.30) and (5.31) can be verified by using the same steps as in (5.4)–(5.12) to compute the various terms. Expressing $\cos \omega_m t$ and $\sin \omega_m t$ in exponential form gives integrals similar to those in (5.9).

Therefore, for a circular complex Gaussian random vector, the probability density can be expressed in terms of a single correlation matrix,

$$\mathbf{S}_{\mathbf{x}_{\Delta T}}(\omega_m) = E \left[\mathbf{X}_{\Delta T}(\omega_m, k) \mathbf{X}_{\Delta T}^H(\omega_m, k) \right]. \quad (5.33)$$

The probability density for the zero-mean case is

$$\begin{aligned} \mathbf{p}_{\mathbf{x}_{\Delta T}}(\mathbf{X}_{\Delta T}(\omega_m, k)) \triangleq & \frac{1}{\pi^N |\mathbf{S}_{\mathbf{x}_{\Delta T}}(\omega_m)|} \\ & \exp \left\{ - \left[\mathbf{X}_{\Delta T}(\omega_m, k) \mathbf{S}_{\mathbf{x}_{\Delta T}}^{-1} \mathbf{X}_{\Delta T}^H(\omega_m, k) \right] \right\}. \end{aligned} \quad (5.34)$$

For the non-zero mean case, define the mean vector as

$$\mathbf{m}_{\Delta T}(\omega_m, k) = E [\mathbf{X}_{\Delta T}(\omega_m, k)], \quad (5.35)$$

and the covariance matrix as

$$\mathbf{K}_{\mathbf{x}_{\Delta T}}(\omega_m) \triangleq E \left[[\mathbf{X}_{\Delta T}(\omega_m, k) - \mathbf{m}_{\Delta T}(\omega_m, k)] [\mathbf{X}_{\Delta T}^H(\omega_m, k) - \mathbf{m}_{\Delta T}^H(\omega_m, k)] \right]. \quad (5.36)$$

Note that the mean vector is usually a function of k (time), while the covariance matrix is constant due to the stationary assumption. The probability density is

$$\begin{aligned} \mathbf{p}_{\mathbf{x}_{\Delta T}}(\mathbf{x}_{\Delta T}(\omega_m, k)) \triangleq & \frac{1}{\pi^N |\mathbf{K}_{\mathbf{x}_{\Delta T}}(\omega_m)|} \exp \left\{ - [\mathbf{X}_{\Delta T}(\omega_m, k) \right. \\ & \left. - \mathbf{m}_{\Delta T}(\omega_m, k)] \cdot \mathbf{K}_{\mathbf{x}_{\Delta T}}^{-1}(\omega_m) [\mathbf{X}_{\Delta T}^H(\omega_m, k) - \mathbf{m}_{\Delta T}^H(\omega_m, k)] \right\}. \end{aligned} \quad (5.37)$$

The probability density in (5.37) will play a central role in many of the subsequent discussions. The condition in (5.30) and (5.31) considered a single snapshot vector, $\mathbf{X}_{\Delta T}(\omega_m, k)$. In addition, the snapshots at different frequencies, $\mathbf{X}_{\Delta T}(\omega_{m_1}, k)$ and $\mathbf{X}_{\Delta T}(\omega_{m_2}, k)$ are jointly circular complex Gaussian random vectors for $-(M-1)/2 \leq m_1 \leq (M-1)/2, -(M-1)/2 \leq m_2 \leq (M-1)/2, m_1 \neq m_2$, and $k = 1, \dots, K$. The snapshots in different time intervals, $\mathbf{X}_{\Delta T}(\omega_{m_1}, k_1)$ and $\mathbf{X}_{\Delta T}(\omega_{m_2}, k_2)$ are jointly circular complex Gaussian random vectors for $-(M-1)/2 \leq m_1 \leq (M-1)/2, -(M-1)/2 \leq m_2 \leq (M-1)/2, k_1 = 1, \dots, K, k_2 = 1, \dots, K, k_1 \neq k_2$. These results can be verified in the same manner as the single snapshot result.

Therefore, whenever (5.26) and (5.27) are satisfied, the frequency-domain snapshots can be modeled as statistically independent circular complex Gaussian random vectors. When (5.26) is valid,

$$\mathbf{m}_{\Delta T}(\omega_m, k) \simeq \mathbf{m}_x(\omega_m, k), \quad (5.38)$$

$$\mathbf{K}_{x_{\Delta T}}(\omega_m) \simeq \mathbf{K}_x(\omega_m), \quad (5.39)$$

and

$$\mathbf{S}_{x_{\Delta T}}(\omega_m) \simeq \mathbf{S}_x(\omega_m), \quad (5.40)$$

In this case, (5.34) becomes,

$$\begin{aligned} p_{x_{\Delta T}}(\mathbf{X}_{\Delta T}(\omega_m, k)) = & \frac{1}{\pi^N |\mathbf{S}_x(\omega_m)|} \exp \\ & \left\{ - [\mathbf{X}_{\Delta T}(\omega_m, k) \mathbf{S}_x^{-1}(\omega_m) \mathbf{X}_{\Delta T}^H(\omega_m, k)] \right\} \end{aligned} \quad (5.41)$$

for the zero-mean case. Similarly, (5.37) becomes,

$$\begin{aligned} p_{x_{\Delta T}}(\mathbf{X}_{\Delta T}(\omega_m, k)) = & \frac{1}{\pi^N |\mathbf{K}_x(\omega_m)|} \exp \\ & \left\{ - [\mathbf{X}_{\Delta T}(\omega_m, k) - \mathbf{m}_x(\omega_m, k)] \mathbf{K}_x^{-1}(\omega_m) [\mathbf{X}_{\Delta T}^H(\omega_m, k) - \mathbf{m}_x^H(\omega_m, k)] \right\}. \end{aligned} \quad (5.42)$$

The statistical independence result means that the joint densities of the snapshots for different m and k factor into a product of the individual densities.

5.2.1.2 Plane-wave snapshot model

In this section we develop the frequency-domain snapshot model for the case in which the desired signals and interfering signals can be modeled as plane waves. A family of models is developed that plays a central role in many of the subsequent developments. The models can be divided into two cases. In the first case, the desired signals are either deterministic signals or unknown nonrandom signals. In the second case, the desired signals are sample functions of a Gaussian random process. For each case, several examples are discussed.

In case 1, the output of the array is an $N \times 1$ complex vector,

$$\mathbf{x}(t) = \mathbf{x}_s(t) + \mathbf{n}(t), \quad (5.43)$$

where $\mathbf{x}_s(t)$ is either a deterministic signal or an unknown nonrandom signal⁴ and $\mathbf{n}(t)$ is a sample function of a zero-mean Gaussian random process. The frequency-domain snapshot model is

$$\begin{aligned}\mathbf{X}_{\Delta T}(\omega_m, k) &= \mathbf{X}_{s,\Delta T}(\omega_m, k) + \mathbf{N}_{\Delta T}(\omega_m, k), \\ m &= 0, \dots, M-1, \quad k = 1, \dots, K.\end{aligned}\quad (5.44)$$

In subsequent equations the range of m and k is the same as in (5.44) and is omitted.

Example 5.2.2

In this example, there is a single plane-wave desired signal,

$$\mathbf{X}_{s,\Delta T}(\omega_m, k) = \mathbf{v}(\omega_m, \mathbf{k}_s) F_{s,\Delta T}(\omega_m, k). \quad (5.45)$$

The source-signal snapshot, $F_{s,\Delta T}(\omega_m, k)$, is modeled in one of two ways. In the first way, $F_{s,\Delta T}(\omega_m, k)$ is assumed to be the snapshot of a known (or deterministic) signal. This model is appropriate in many communications or radar problems. In the second way, $F_{s,\Delta T}(\omega_m, k)$ is assumed to be the snapshot of an unknown, but nonrandom waveform. This model is appropriate in many passive sonar or direction-finding applications.

The probability density is a non-zero mean circular complex density,

$$\begin{aligned}p_{\mathbf{x}_{\Delta T}}(\mathbf{X}_{\Delta T}(\omega_m, k)) &= \frac{1}{\pi^N |\mathbf{S}_{\mathbf{n}_{\Delta T}}|} \exp \\ &\left\{ -[\mathbf{X}_{\Delta T} - \mathbf{v}(\mathbf{k}_s) F_{s,\Delta T}] \mathbf{S}_{\mathbf{n}_{\Delta T}}^{-1} [\mathbf{X}_{\Delta T} - \mathbf{v}(\mathbf{k}_s) F_{s,\Delta T}]^H \right\},\end{aligned}\quad (5.46)$$

where the ω_m and k arguments are suppressed on the right side of the equation. The covariance matrix is the spatial spectral matrix of the noise. Initially, $\mathbf{S}_{\mathbf{n}}$ is assumed to be known. The mean of the density is either known (deterministic signal) or unknown (unknown nonrandom signal). Using the approximations in Section 5.2.1.1, (5.46) reduces to

$$p_{\mathbf{x}_{\Delta T}}(\mathbf{X}_{\Delta T}(\omega_m, k)) = \frac{1}{\pi^N |\mathbf{S}_{\mathbf{n}}|} \exp \left\{ -[\mathbf{X}_{\Delta T} - \mathbf{v}(\mathbf{k}_s) F_{s,\Delta T}] \mathbf{S}_{\mathbf{n}}^{-1} [\mathbf{X}_{\Delta T} - \mathbf{v}(\mathbf{k}_s) F_{s,\Delta T}]^H \right\}. \quad (5.47)$$

For the spatial case of spatial white noise,

$$\mathbf{S}_{\mathbf{n}} = \sigma_{\omega}^2 \mathbf{I}, \quad (5.48)$$

and (5.47) reduces to

$$\begin{aligned}p_{\mathbf{x}_{\Delta T}}(\mathbf{X}_{\Delta T}(\omega_m, k)) &= (\pi^N \sigma_{\omega}^2 N)^{-1} \exp \\ &\left\{ -\frac{1}{\sigma_{\omega}^2} [\mathbf{X}_{\Delta T} - \mathbf{v}(\mathbf{k}_s) F_{s,\Delta T}] [\mathbf{X}_{\Delta T} - \mathbf{v}(\mathbf{k}_s) F_{s,\Delta T}]^H \right\}.\end{aligned}\quad (5.49)$$

Example 5.2.3

In this example, there is a single plane-wave desired signal, and $(D-1)$ plane-wave interfering signals, and additive noise. All of the source signals are either deterministic

⁴These two terms are defined in Example 5.2.2.

signals or unknown nonrandom signals. Then,

$$\mathbf{X}_{\Delta T}(\omega_m, k) = \mathbf{v}(\omega_m, \mathbf{k}_s) F_{s,\Delta T}(\omega_m, k) + \sum_{i=1}^{D-1} \mathbf{v}(\omega_m, \mathbf{k}_i) F_{i,\Delta T}(\omega_m, k) + \mathbf{N}_{\Delta T}(\omega_m, k). \quad (5.50)$$

A composite $N \times D$ array manifold matrix is defined as

$$\mathbf{V}(\omega_m, \mathbf{k}) = [\mathbf{v}(\omega_m, \mathbf{k}_s) \ \mathbf{v}(\omega_m, \mathbf{k}_1) \ \cdots \ \mathbf{v}(\omega_m, \mathbf{k}_{D-1})], \quad (5.51)$$

and a composite source signal vector is defined as

$$\mathbf{F}_{\Delta T}(\omega_m, k) = [F_{s,\Delta T} \ F_{1,\Delta T} \ \cdots \ F_{D-1,\Delta T}]^T. \quad (5.52)$$

Then the snapshot vector can be written as

$$\mathbf{X}_{\Delta T}(\omega_m, \mathbf{k}) = \mathbf{V}(\omega_m, \mathbf{k}) \mathbf{F}_{\Delta T}(\omega_m, k) + \mathbf{N}_{\Delta T}(\omega_m, k). \quad (5.53)$$

Using the approximations in Section 5.2.1.1, the probability density is

$$p_{\mathbf{x}_{\Delta T}}(\mathbf{X}_{\Delta T}(\omega_m, k)) = \frac{1}{\pi^N |\mathbf{S}_n|} \exp \left\{ -[\mathbf{X}_{\Delta T} - \mathbf{V}(\mathbf{k}) \mathbf{F}_{\Delta T}] \mathbf{S}_n^{-1} [\mathbf{X}_{\Delta T} - \mathbf{V}(\mathbf{k}) \mathbf{F}_{\Delta T}]^H \right\}, \quad (5.54)$$

where the ω_m and k arguments are suppressed on the right side of (5.54).

Example 5.2.4

In this example, there is a single plane-wave desired signal, $(D - 1)$ plane-wave interfering signals, and additive noise. The desired signal is modeled as a deterministic or unknown nonrandom signal. The $(D - 1)$ plane-wave interfering signals are modeled as sample functions of Gaussian random processes. The snapshot vector is the same as in (5.50),

$$\mathbf{X}_{\Delta T}(\omega_m, k) = \mathbf{v}(\omega_m, \mathbf{k}_s) F_{s,\Delta T}(\omega_m, k) + \sum_{i=1}^{D-1} \mathbf{v}(\omega_m, \mathbf{k}_i) F_{i,\Delta T}(\omega_m, k) + \mathbf{N}_{\Delta T}(\omega_m, k) \quad (5.55)$$

A composite $N \times (D - 1)$ interference array manifold matrix is defined as

$$\mathbf{V}_I(\omega_m, \mathbf{k}_1) = [\mathbf{v}(\omega_m, \mathbf{k}_1) \ \cdots \ \mathbf{v}(\omega_m, \mathbf{k}_{D-1})], \quad (5.56)$$

and a composite source interference vector is defined as

$$\mathbf{F}_{I,\Delta T}(\omega_m, k) = [F_{1,\Delta T} \ \cdots \ F_{D-1,\Delta T}(\omega_m, k)]^T. \quad (5.57)$$

The interference source spectral matrix is defined as

$$\mathbf{S}_{I,\Delta T}(\omega_m) \triangleq E [\mathbf{F}_{I,\Delta T}(\omega_m, k) \mathbf{F}_{I,\Delta T}^H(\omega_m, k)], \quad (5.58)$$

which is approximated by

$$\mathbf{S}_{I,\Delta T}(\omega_m) \simeq \mathbf{S}_I(\omega_m). \quad (5.59)$$

The noise-plus-interference spectral matrix is defined as

$$\mathbf{S}_{IN}(\omega_m) = \mathbf{V}_I(\omega_m, \mathbf{k}_I) \mathbf{S}_I(\omega_m) \mathbf{V}_I^H(\omega_m, \mathbf{k}_I) + \mathbf{S}_n(\omega_m). \quad (5.60)$$

The probability density is

$$p_{\mathbf{x}_{\Delta T}}(\mathbf{X}_{\Delta T}(\omega_m, k)) =$$

$$\frac{1}{\pi^N |\mathbf{S}_{IN}(\omega_m)|} \exp \left\{ -[\mathbf{X}_{\Delta T} - \mathbf{v}(\mathbf{k}_s) F_{\Delta T}] \mathbf{S}_{IN}^{-1}(\omega_m) [\mathbf{X}_{\Delta T} - \mathbf{v}(\mathbf{k}_s) F_{\Delta T}]^H \right\}. \quad (5.61)$$

These three models are used for applications in which the source signals are modeled as nonrandom or deterministic waveforms.

In case 2, the output of the array is an $N \times 1$ complex vector,

$$\mathbf{x}(t) = \mathbf{x}_s(t) + \mathbf{n}(t), \quad (5.62)$$

and both $\mathbf{x}_s(t)$ and $\mathbf{n}(t)$ are zero-mean Gaussian random processes. The frequency-domain snapshot model is

$$\mathbf{X}_{\Delta T}(\omega_m, k) = \mathbf{X}_{s,\Delta T}(\omega_m, k) + \mathbf{N}_{\Delta T}(\omega_m, k). \quad (5.63)$$

Example 5.2.5

In this example, there is a single plane-wave desired signal, $(D - 1)$ plane-wave interfering signals, and additive noise. All of the source signals are zero-mean Gaussian random processes. The expressions in (5.50)–(5.53) all apply to this case. Now, the $D \times D$ signal-plus-interference source spectral matrix is defined as

$$\mathbf{S}_{SI,\Delta T}(\omega_m) = E [\mathbf{F}_{\Delta T}(\omega_m, k) \mathbf{F}_{\Delta T}^H(\omega_m, k)], \quad (5.64)$$

where $\mathbf{F}_{\Delta T}(\omega_m, k)$ is defined in (5.52). The spectral matrix in (5.64) is approximated by

$$\mathbf{S}_{SI}(\omega_m) \simeq \mathbf{S}_f(\omega_m). \quad (5.65)$$

The total snapshot spectral matrix is

$$\begin{aligned} \mathbf{S}_{\mathbf{x}_{\Delta T}} &= E [\mathbf{X}_{\Delta T}(\omega_m) \mathbf{X}_{\Delta T}^H(\omega_m)] \\ &= \mathbf{V}(\omega_m, \mathbf{k}) \mathbf{S}_{SI,\Delta T}(\omega_m) \mathbf{V}^H(\omega_m, \mathbf{k}) + \mathbf{S}_{N,\Delta T}(\omega_m), \end{aligned} \quad (5.66)$$

which is approximated by

$$\mathbf{S}_{\mathbf{x}}(\omega_m) = \mathbf{V}(\omega_m, \mathbf{k}) \mathbf{S}_f(\omega_m) \mathbf{V}^H(\omega_m, \mathbf{k}) + \mathbf{S}_n(\omega_m). \quad (5.67)$$

The probability density is

$$p_{\mathbf{x}_{\Delta T}}(\mathbf{X}_{\Delta T}(\omega_m, k)) = \frac{1}{\pi^N |\mathbf{S}_{\mathbf{x}}|} \exp \left\{ -\mathbf{X}_{\Delta T} \mathbf{S}_{\mathbf{x}}^{-1} \mathbf{X}_{\Delta T}^H \right\}, \quad (5.68)$$

where the ω_m and k are suppressed on the right side of (5.68).

The four models in these examples will have a central role in most of our subsequent discussions.

5.2.1.3 Beamforming

We now discuss the other two boxes in Figure 5.1. In the second box, each frequency bin is processed with a narrowband beamformer centered at ω_m . The output in each bin is a complex scalar Gaussian random variable,

$$Y_{\Delta T}(m\omega_{\Delta}), \quad m = -\frac{M-1}{2}, \dots, 0, \dots, \frac{M-1}{2}. \quad (5.69)$$

Chapter 6 develops optimum narrowband beamformers assuming that the appropriate spatial spectral matrices (e.g., $\mathbf{S}_x(\omega_m)$ or $\mathbf{S}_n(\omega_m)$) are known. Chapter 7 develops the adaptive versions.

The final step is to construct the beamformer output that is a scalar complex Gaussian random process,

$$y(t) = \frac{1}{\sqrt{\Delta T}} \sum_{m=-\frac{M-1}{2}}^{\frac{M-1}{2}} Y_{\Delta T}(m\omega_{\Delta}) e^{j m \omega_{\Delta} t}. \quad (5.70)$$

5.2.2 Narrowband Time-domain Snapshot Models

In this section, a time-domain model that is appropriate for narrowband waveforms is developed. In Section 6.13, time-domain models for the broadband case are developed.

First consider the case of a single plane-wave input. The input at the reference sensor located at the origin is a real bandpass signal,

$$f(t) = \sqrt{2} \operatorname{Re} \left\{ \tilde{f}(t) e^{j \omega_c t} \right\}. \quad (5.71)$$

The input at the n th sensor is

$$\begin{aligned} f_n(t) &= f(t - \tau_n) \\ &= \sqrt{2} \operatorname{Re} \left\{ \tilde{f}(t - \tau_n) e^{j \omega_c (t - \tau_n)} \right\}, \end{aligned} \quad (5.72)$$

where τ_n is the time delay from the origin to the n th sensor. The narrowband assumption implies

$$\tilde{f}(t - \tau_n) \simeq \tilde{f}(t), \quad n = 0, \dots, N - 1. \quad (5.73)$$

Using (5.73) in (5.72) gives

$$f_n(t) = \sqrt{2} \operatorname{Re} \left\{ \tilde{f}(t) e^{-j \omega_c \tau_n} e^{j \omega_c t} \right\}. \quad (5.74)$$

We normally perform a quadrature demodulation of the sensor outputs prior to time-domain processing. The quadrature demodulation process is shown in Figure 5.4. Figure 5.4(a) shows the actual demodulation process. Figure 5.4(b) shows its complex representation in the time domain. Figure 5.4(c) shows its complex representation in the frequency domain. The lowpass filter has a bandwidth of B_s Hz.

The complex output of the quadrature demodulator at the n th sensor is

$$\tilde{f}_n(t) = \tilde{f}(t)e^{-j\omega_c t_n}. \quad (5.75)$$

We recognize the exponential term as the n th element of the array manifold vector $\mathbf{v}(\mathbf{k})$. Thus, the complex vector output of the array (after quadrature demodulation) is

$$\tilde{\mathbf{f}}(t) = \tilde{f}(t)\mathbf{v}(\mathbf{k}), \quad (5.76)$$

where $\tilde{f}(t)$ is a scalar zero-mean complex Gaussian random process. The covariance matrix at time t is

$$\mathbf{R}_{\tilde{\mathbf{f}}}(0) = E[\tilde{\mathbf{f}}(t)\tilde{\mathbf{f}}^H(t)] = \mathbf{v}(\mathbf{k})R_f(0)\mathbf{v}^H(\mathbf{k}). \quad (5.77)$$

However, $R_f(0)$ is just the power in the signal process, so (5.77) can be written as

$$\mathbf{R}_{\tilde{f}}(0) = \sigma_s^2 \mathbf{v}(\mathbf{k})\mathbf{v}^H(\mathbf{k}), \quad (5.78)$$

where σ_s^2 is the signal power.

Generalizing this result to the case of D signals and adding a white noise component gives

$$\mathbf{R}_{\tilde{\mathbf{x}}}(0) = \mathbf{V}(\mathbf{k})\mathbf{R}_{\tilde{\mathbf{f}}}(0)\mathbf{V}^H(\mathbf{k}) + \sigma_w^2 B_s \mathbf{I}. \quad (5.79)$$

The B_s factor in the second term results from passing the white noise through the filter in the quadrature demodulator. If we assume that $\tilde{f}(t)$ is bandlimited to $-B_s/2 \leq f \leq B_s/2$ Hz, then we sample $\mathbf{x}(t)$ every $1/B_s$ seconds to obtain a time domain snapshot model. We denote the snapshots of the complex envelope as

$$\tilde{\mathbf{x}}(k), \quad k = 1, 2, \dots, K. \quad (5.80)$$

Then

$$\mathbf{R}_{\tilde{\mathbf{x}}}(k) \triangleq E[\tilde{\mathbf{x}}(k)\tilde{\mathbf{x}}^H(k)] = \mathbf{V}(\mathbf{U})\mathbf{R}_{\tilde{\mathbf{f}}}(0)\mathbf{V}^H(\mathbf{U}) + \sigma_w^2 B_s \mathbf{I}, \quad k = 1, 2, \dots, K. \quad (5.81)$$

Quadrature demodulation

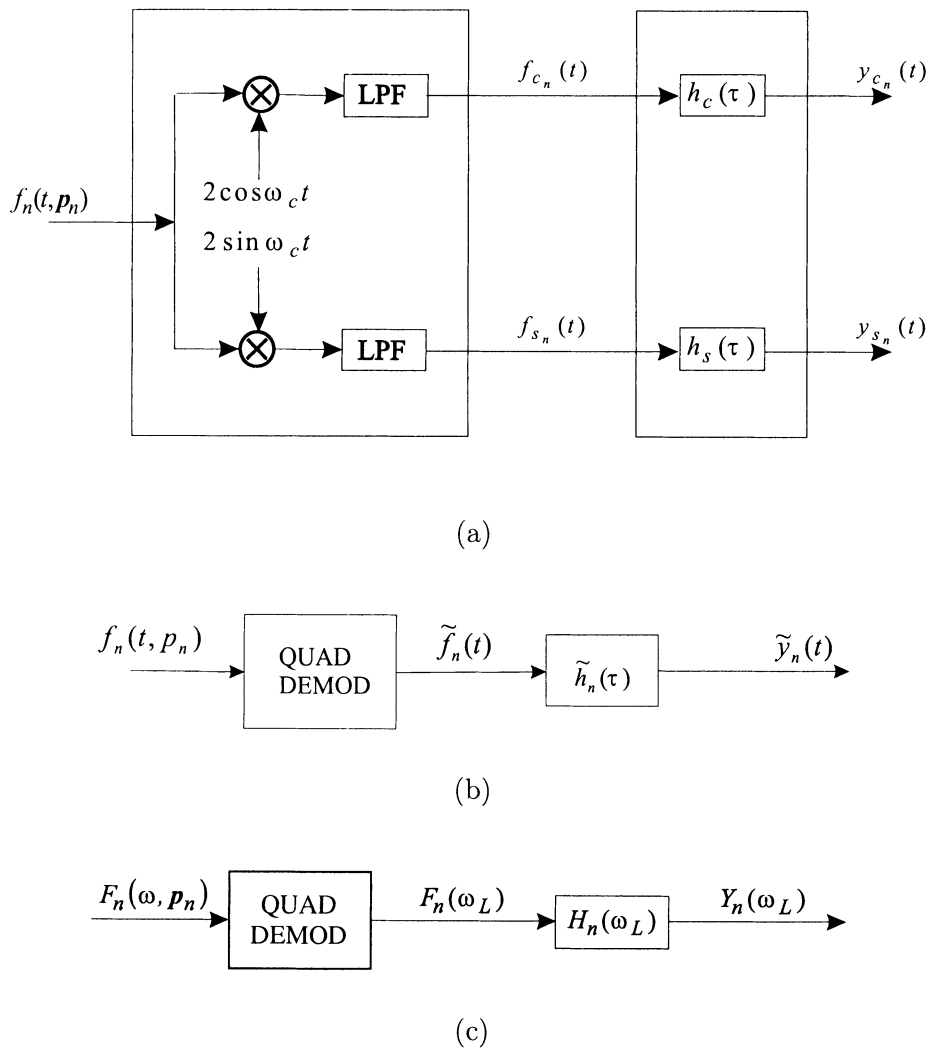


Figure 5.4 Quadrature demodulation.

If we further assume that the components of $\tilde{\mathbf{f}}(t)$ have a flat spectrum, as shown in Figure 5.2(b), then

$$E \left[\tilde{\mathbf{x}}(k_1) \tilde{\mathbf{x}}^H(k_2) \right] = 0, \quad k_1 \neq k_2. \quad (5.82)$$

Thus, the narrowband time-domain model generates a sequence of statistically independent, zero-mean complex Gaussian random vectors whose covariance matrix is given by (5.81).

Comparing (5.81) and (5.67), we see that

$$\mathbf{R}_{\tilde{\mathbf{x}}}(k) = \mathbf{S}_{\mathbf{x}_{\Delta T}}(0) \cdot B_s. \quad (5.83)$$

The spatial characteristics are identical in the narrowband frequency-domain snapshot model and the narrowband time-domain snapshot model. Therefore the narrowband beamformers that operate on the snapshots will be identical.

5.2.3 Summary

In this section, we have developed snapshot models in the frequency domain and the time domain. These models define the sampling of the sensor output that we perform prior to further processing. We have discussed the models in the context of beamforming because that is the application we develop in Chapters 6 and 7. The same models are appropriate when we develop parameter estimation in Chapters 8 and 9 and detection theory in Chapter 10.

The first key result is that the sampling process generates a sequence of complex Gaussian random vectors. We assume that the vectors in different frequency bins and different observation intervals are statistically independent.

The second key result is that, for the narrowband case, the frequency-domain snapshot model and the time-domain snapshot model have identical spatial statistics, so the subsequent processing will be identical.

The frequency-domain snapshot model is used in most of our subsequent discussion because it applies to both the broadband and narrowband cases.

In the next section, a general model for space-time random processes is considered. This model allows us to model spatially spread random processes as well as the finite plane-wave model in Section 5.2.1.2 when the source signals are statistically independent. It does not allow us to model correlated plane waves. For readers whose primary interest is in applications that can be modeled with D plane waves, the next section can be skipped at first reading.

5.3 Space-time Random Processes

In many applications, the signal or noise source has a continuous distribution in space. For these cases, a space-time model of the source process must be developed.

Assume that the complex signal $f(t, \mathbf{p})$ is a scalar waveform that is defined over time and space.⁵ We model $f(t, \mathbf{p})$ as a complex random process over the time interval (T_i, T_f) and the spatial region $\mathbf{p} \in \Re^N$. Normally, \Re will be a 3-D space.

We are interested in both a second-moment characterization of the process and a complete characterization of the process.⁶ The second-moment characterization of the process is adequate to deal with linear operations on the process. A complete characterization is necessary to formulate optimum detection and estimation problems. We restrict our complete characterization to Gaussian space-time processes. We develop the second-moment characterization in Section 5.3.1 and define the Gaussian process model in Section 5.3.2.

5.3.1 Second-moment Characterization

The mean of the space-time field, $f(t, \mathbf{p})$, is defined as

$$m_f(t, \mathbf{p}) = E[f(t, \mathbf{p})], \quad T_i \leq t \leq T_f, \quad \mathbf{p} \in \Re^N, \quad (5.84)$$

and the space-time covariance as

$$\begin{aligned} K_f(t_1, t_2 : \mathbf{p}_1, \mathbf{p}_2) &= E\left\{[f(t_1, \mathbf{p}_1) - m_f(t_1, \mathbf{p}_1)][f^*(t_2, \mathbf{p}_2) - m_f^*(t_2, \mathbf{p}_2)]\right\} \\ &\quad T_i \leq t_1, t_2 \leq T_f, \quad \mathbf{p}_1, \mathbf{p}_2 \in \Re^N. \end{aligned} \quad (5.85)$$

In the subsequent discussion we assume that $m_f(t, \mathbf{p}) = 0$.

In the general case the random process can be non-stationary and non-homogeneous. In Part I of DEMT [VT68], [VT01a], we analyzed scalar non-stationary processes and saw that mathematics were more complicated than the stationary case, but the concepts were unchanged. The same results carry over to space-time processes.

In many cases of interest, the process is temporally wide-sense stationary. Then,

$$K_f(t_1, t_2 : \mathbf{p}_1, \mathbf{p}_2) = K_f(\tau : \mathbf{p}_1, \mathbf{p}_2), \quad (5.86)$$

⁵See Appendix A of DEMT, Part III of [VT71], [VT01b] for a discussion of complex processes.

⁶See Sections 5.3.1 and 5.3.3 of DEMT, Part I [VT68], [VT01a] for the corresponding scalar process discussion.

where

$$\tau = t_1 - t_2. \quad (5.87)$$

Note that, in a practical application, the stationarity only has to hold over a time interval that is long compared to the processing time.

In many cases of interest, the process is homogeneous or spatially stationary over a region that is large compared to the spatial dimensions of the aperture or array. Then,

$$K_f(t_1, t_2 : \mathbf{p}_1, \mathbf{p}_2) = K_f(t_1, t_2 : \Delta\mathbf{p}), \quad (5.88)$$

where

$$\Delta\mathbf{p} = \mathbf{p}_1 - \mathbf{p}_2. \quad (5.89)$$

For cases that satisfy both conditions, the process is time-stationary and space-homogeneous,

$$K_f(t_1, t_2 : \mathbf{p}_1, \mathbf{p}_2) = K_f(\tau : \Delta\mathbf{p}). \quad (5.90)$$

We focus most of our attention on random processes that satisfy (5.90).

We define the *temporal frequency spectrum-spatial correlation function*,

$$S_f(\omega : \Delta\mathbf{p}) = \int_{-\infty}^{\infty} K_f(\tau : \Delta\mathbf{p}) e^{-j\omega\tau} d\tau, \quad (5.91)$$

which is the Fourier transform with respect to τ of the space-time covariance function. When $\Delta\mathbf{p} = 0$, $S_f(\omega : 0)$ is the frequency spectrum at a point in space.

Similarly, we can define a *temporal correlation-spatial wavenumber spectrum* as

$$F_f(\tau : \mathbf{k}) = \int \cdot \int_{\Re^N} d\Delta\mathbf{p} K_f(\tau : \Delta\mathbf{p}) e^{j\mathbf{k}^T \Delta\mathbf{p}}. \quad (5.92)$$

Note that the region of integration depends on the dimension of spatial domain (linear, planar, or volumetric). Although we define this function for completeness, we will not use it very often in the subsequent discussion.

A function of major interest is the *frequency-wavenumber spectrum*,

$$P_f(\omega : \mathbf{k}) = \int \cdot \int_{\Re^N} d\Delta\mathbf{p} S_f(\omega : \Delta\mathbf{p}) e^{j\mathbf{k}^T \Delta\mathbf{p}}. \quad (5.93)$$

If we assume a three-dimensional space, then

$$P_f(\omega : \mathbf{k}) = \int_{-\infty}^{\infty} \int_{-\infty}^{\infty} \int_{-\infty}^{\infty} d\Delta\mathbf{p} S_f(\omega : \Delta\mathbf{p}) e^{j\mathbf{k}^T \Delta\mathbf{p}}, \quad (5.94)$$

and the inverse transform is

$$S_f(\omega : \Delta \mathbf{p}) = \int_{-\infty}^{\infty} \int_{-\infty}^{\infty} \int_{-\infty}^{\infty} \frac{d\mathbf{k}}{(2\pi)^3} P_f(\omega : \mathbf{k}) e^{-j\mathbf{k}^T \Delta \mathbf{p}}. \quad (5.95)$$

$P_f(\omega : \mathbf{k})$ can also be expressed in terms of $K_f(\tau : \Delta \mathbf{p})$ as

$$P_f(\omega : \mathbf{k}) = \int_{-\infty}^{\infty} d\tau \int \cdot \int_{\mathbb{R}^N} d\Delta \mathbf{p} K_f(\tau : \Delta \mathbf{p}) e^{-j(\omega\tau - \mathbf{k}^T \Delta \mathbf{p})}. \quad (5.96)$$

If we assume a 3-D space, then

$$P_f(\omega : \mathbf{k}) = \int_{-\infty}^{\infty} d\tau \int_{-\infty}^{\infty} \int_{-\infty}^{\infty} \int_{-\infty}^{\infty} d\Delta \mathbf{p} K_f(\tau : \Delta \mathbf{p}) e^{-j(\omega\tau - \mathbf{k}^T \Delta \mathbf{p})}. \quad (5.97)$$

$P_f(\omega : \mathbf{k})$ has properties analogous to the frequency spectrum for scalar processes.

In particular, $f(t, \mathbf{p})$ can be represented as a Stieltjes integral,

$$f(t, \mathbf{p}) = \int_{-\infty}^{\infty} \cdots \int_{-\infty}^{\infty} e^{j(\omega t - \mathbf{k}^T \mathbf{p})} dF(\omega; \mathbf{k}), \quad (5.98)$$

where \mathbf{k} has a definition consistent with the space domain (e.g., [Doo53], [Yag57], [Yag60]).

The following properties hold:

$$E \left[|dF(\omega_2 : \mathbf{k}_2) - dF(\omega_1 : \mathbf{k}_1)|^2 \right] = \int_{\omega_1}^{\omega_2} \frac{d\omega}{2\pi} \int_{\mathbf{k}_1}^{\mathbf{k}_2} \frac{d\mathbf{k}}{(2\pi)^N} P_f(\omega : \mathbf{k}), \quad (5.99)$$

and

$$E [(dF(\omega_2 : \mathbf{k}_2) - dF(\omega_1 : \mathbf{k}_1)) (dF(\omega_4 : \mathbf{k}_4) - dF(\omega_3 : \mathbf{k}_3))^*] = 0, \quad (5.100)$$

when

$$(\omega_1, \omega_2) \times (\mathbf{k}_1, \mathbf{k}_2) \cap (\omega_3, \omega_4) \times (\mathbf{k}_3, \mathbf{k}_4) = 0. \quad (5.101)$$

In other words, disjoint frequency-wavenumber bands are uncorrelated.

This is the spatial generalization of a spectral decomposition of a scalar random process. Therefore, we can consider random processes that satisfy (5.99) to be composed of a superposition of uncorrelated plane waves with temporal frequency ω and wavenumber k .

If, in addition, we impose the condition that the process $f(t, \mathbf{p})$ satisfies the homogeneous wave equation, then we have the constraint

$$\frac{\omega}{c} = |\mathbf{k}|. \quad (5.102)$$

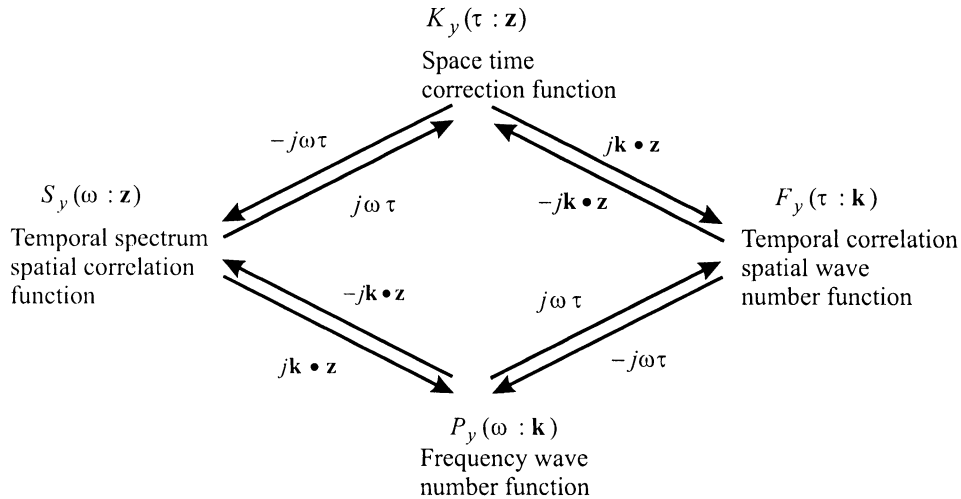


Figure 5.5 Second-moment representations for stationary homogeneous space-time random processes. [From [Bag76]]

This defines a structure that signals propagating in a medium must satisfy. Further, this implies that at any particular ω the frequency-wavenumber function is nonzero only on a sphere of radius $\frac{2\pi}{\lambda} = |\mathbf{k}| = \frac{\omega}{c}$ and is concentrated in that sphere. This constraint is not necessary for $f(t : \mathbf{p})$ to correspond to a propagating process. For example, one may have propagation in three dimensions and yet consider a representation over a 2-D surface, since the 2-D wavenumber value corresponds unambiguously to a 3-D surface except for its sign.

The advantage of this representation for homogeneous fields is that it allows us to make many statements regarding the processing for our signals, which are completely dual to analogous frequency-domain operations when processing temporal waveforms. Naturally, there is a close relationship among the various transforms discussed, which are summarized in Figure 5.5.

When we consider frequency-wavenumber spectra in different dimensions, it is important to understand their relationship. From (5.95), we have the 3-D transform,

$$S_{3f}(\omega : \Delta p_x, \Delta p_y, \Delta p_z) = \int_{-\infty}^{\infty} \int_{-\infty}^{\infty} \int_{-\infty}^{\infty} \frac{d\mathbf{k}_3}{(2\pi)^3} P_{3f}(\omega : \mathbf{k}_3) e^{-j[k_x \cdot \Delta p_x + k_y \cdot \Delta p_y + k_z \cdot \Delta p_z]}, \quad (5.103)$$

where we have added the subscript “3” to denote the dimension. Similarly,

from (5.95), we have the 2-D transform,

$$S_{2f}(\omega : \Delta p_x, \Delta p_y) = \int_{-\infty}^{\infty} \int_{-\infty}^{\infty} \frac{d\mathbf{k}_2}{(2\pi)^2} P_{2f}(\omega : \mathbf{k}_2) e^{-j[k_x \cdot \Delta p_x + k_y \cdot \Delta p_y]}, \quad (5.104)$$

for a representation in the xy -plane. We observe that

$$S_{2f}(\omega : \Delta p_x, \Delta p_y) = S_{3f}(\omega : \Delta p_x, \Delta p_y, 0). \quad (5.105)$$

Using (5.105) in (5.103),

$$\begin{aligned} S_{2f}(\omega : \Delta p_x, \Delta p_y) &= \int_{-\infty}^{\infty} \int_{-\infty}^{\infty} \int_{-\infty}^{\infty} \frac{d\mathbf{k}_3}{(2\pi)^3} P_{3f}(\omega : \mathbf{k}_3) e^{-j[k_x \cdot \Delta p_x + k_y \cdot \Delta p_y]} \\ &= \int_{-\infty}^{\infty} \int_{-\infty}^{\infty} \frac{dk_x dk_y}{(2\pi)^2} \left[\int_{-\infty}^{\infty} \frac{dk_z}{2\pi} P_{3f}(\omega : \mathbf{k}_3) \right] e^{-j[k_x \cdot \Delta p_x + k_y \cdot \Delta p_y]}. \end{aligned} \quad (5.106)$$

Equating the right sides of (5.106) and (5.104) gives

$$P_{2f}(\omega : \mathbf{k}_2) = \int_{-\infty}^{\infty} \frac{dk_z}{2\pi} P_{3f}(\omega : \mathbf{k}_3). \quad (5.107)$$

Similarly,

$$P_{1f}(\omega : k_x) = \int_{-\infty}^{\infty} \frac{dk_y}{2\pi} P_{2f}(\omega : \mathbf{k}_2). \quad (5.108)$$

In chapters 2 and 3, we normally used the z -axis for 1-D representations. Then,

$$P_{1f}(\omega : k_z) = \int_{-\infty}^{\infty} \int_{-\infty}^{\infty} \frac{dk_x dk_y}{(2\pi)^2} P_{3f}(\omega : \mathbf{k}). \quad (5.109)$$

We consider a simple example.

Example 5.3.1: Directional Signal

The simplest signal of interest is a plane wave propagating in a direction with speed c as illustrated in Figure 5.6. The space-time process has the form

$$f(t, \mathbf{p}) = f \left[t - \frac{\mathbf{a}^T \mathbf{p}}{c} \right], \quad (5.110)$$

where $f(t)$ is a zero-mean stationary random process with spectrum $S_f(\omega)$.

Then, the space-time correlation function is

$$\begin{aligned} K_f(\tau : \Delta \mathbf{p}) &= E \left(f \left(t - \frac{\mathbf{a}^T \mathbf{p}}{c} \right) f^* \left(t - \tau - \frac{\mathbf{a}^T (\mathbf{p} - \Delta \mathbf{p})}{c} \right) \right) \\ &= K_f \left(\tau - \frac{\mathbf{a}^T \Delta \mathbf{p}}{c} \right). \end{aligned} \quad (5.111)$$

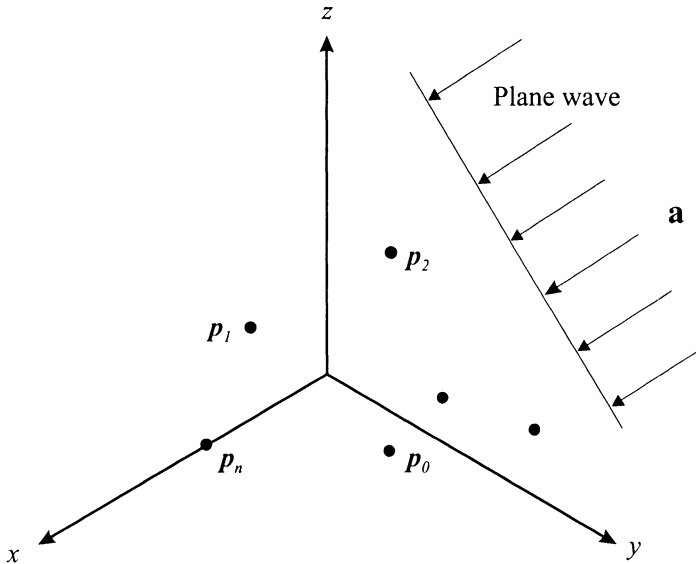


Figure 5.6 Model of plane wave propagation.

The temporal frequency spectrum spatial correlation function is

$$S_{3f}(\omega : \Delta \mathbf{p}) = S_f(\omega) e^{-j\left(\frac{\omega}{c}\right)(\mathbf{a}^T \Delta \mathbf{p})} = S_f(\omega) e^{j\frac{2\pi}{\lambda} \mathbf{u}^T \Delta \mathbf{p}}. \quad (5.112)$$

Consequently, we have the cross-spectrum of a plane wave at two different locations that is related to the spectrum of the process at a single point by a simple linear phase shift that reflects the propagation delay between the two points.

Transforming with respect to the spatial variable, we obtain the frequency-wavenumber function

$$P_{3f}(\omega : \mathbf{k}) = \int \int_{\Re^N} d\Delta \mathbf{p} S_f(\omega : \Delta \mathbf{p}) e^{j\mathbf{k}^T \Delta \mathbf{p}} = S_{f_o}(\omega) \delta\left(\mathbf{k} - \frac{\omega}{c} \mathbf{a}\right), \quad (5.113)$$

where

$$\delta\left(\mathbf{k} - \frac{\omega}{c} \mathbf{a}\right) = \delta\left(k_x - \frac{\omega}{c} a_x\right) \delta\left(k_y - \frac{\omega}{c} a_y\right) \delta\left(k_z - \frac{\omega}{c} a_z\right), \quad (5.114)$$

is a 3-D impulse function, which in Cartesian coordinates can be written as a product of impulse functions of a single variable.

For a planar representation in the xy -plane,

$$\begin{aligned} P_{2f}(\omega : k_x, k_y) &= \delta(k_x - k_{sx}) \delta(k_y - k_{sy}) \\ &= \delta\left(k_x - \frac{2\pi}{\lambda} \sin \theta \cos \phi\right) \delta\left(k_y - \frac{2\pi}{\lambda} \sin \theta \sin \phi\right), \end{aligned} \quad (5.115)$$

and for a 1-D representation along the z -axis,

$$P_{1f}(\omega : k_z) = \delta(k_z - k_{sz}) = \delta\left(k_z - \frac{2\pi}{\lambda} \cos \theta\right). \quad (5.116)$$

We find that a plane wave propagating with speed c and direction \mathbf{a} has an impulsive frequency-wavenumber spectrum located at

$$\mathbf{k}_a = \frac{\omega}{c} \mathbf{a}, \quad (5.117)$$

in wavenumber space. We again point out that the space over which this transform is taken must be specified. Theoretically, in a homogeneous isotropic medium the magnitude of the wavenumber \mathbf{k} at a particular frequency should be a constant, indicating that, for three dimensions, the function $P_f(\omega : \mathbf{k})$ is concentrated on a sphere; concentrated on a circle in two dimensions; or concentrated at two points opposite in sign in one dimension.

However, in many cases one considers representing the waves in a 3-D space as projected on a 2-D geometry. This leads to an analysis in which the magnitude of the wavenumber is not a constant at a particular temporal frequency. It should be obvious that any set of statistically independent directional signals propagating as plane waves can be represented with an impulsive frequency-wavenumber function. However, such a representation is not possible if the components are correlated as could possibly be envisioned in some multipath situations. The fundamental difficulty stems from the requirement that components from disjoint regions of wavenumber space must be uncorrelated as specified by (5.98); therefore such a process would not be homogeneous.

We discuss other interesting examples in Sections 5.3.3 and 5.3.4. Before doing that development, we want to define Gaussian space-time processes.

5.3.2 Gaussian Space-time Processes

In Section 2.6 of DEMT I [VT68], [VT01a], we discuss Gaussian random vectors in detail. In Section 3.3.3 of DEMT I [VT68], [VT01a], we discuss scalar Gaussian random processes in detail. We now extend those ideas to vector space-time random processes.

Definition: Let $f(t, \mathbf{p})$ be a space-time random process defined over some time interval $[T_\alpha, T_\beta]$ and spatial region \Re^N with a mean value function $m_f(t, \mathbf{p})$ and covariance function $K_f(t_1, t_2 : \mathbf{p}_1, \mathbf{p}_2)$. If every linear functional

of $f(t, \mathbf{p})$ is a Gaussian random variable, then $f(t, \mathbf{p})$ is a Gaussian space-time random process. In other words, if

$$y = \int_{T_\alpha}^{T_\beta} \int_{\Re^N} g(u : \mathbf{p}) f(u : \mathbf{p}) du d\mathbf{p}, \quad (5.118)$$

and $g(u : \mathbf{p})$ is any linear function that $E[y^2] < \infty$, then in order for $f(u : \mathbf{p})$ to be a Gaussian space-time random process, y must be a Gaussian random variable for every $g(u : \mathbf{p})$ in the above class (denoted by \mathcal{G}).⁷ Several properties follow immediately from this definition.

Property 1: The output of a linear system is a particular linear functional of interest. We denote the impulse response (which is the output at time t and position \mathbf{p}_1 due to a unit impulse input at time u and position \mathbf{p}_2) as $h(t, u : \mathbf{p}_1, \mathbf{p}_2)$. If the input is $f(t, \mathbf{p})$, which is a sample function from a Gaussian space-time random process, the output $y(t, \mathbf{p})$ is also;

$$\int_{T_\alpha}^{T_\beta} \int_{\Re^N} du d\mathbf{p}_2 h(t, u : \mathbf{p}_1, \mathbf{p}_2) f(u : \mathbf{p}_2) = y(t, \mathbf{p}_1). \quad (5.119)$$

The proof is identical to the proof on page 183 of DEMT I [VT68], [VT01a], with appropriate changes in notation.

Property 2: If

$$y_1 = \int_{T_\alpha}^{T_\beta} \int_{\Re^N} g_1(u : \mathbf{p}) f(u : \mathbf{p}) du d\mathbf{p}, \quad (5.120)$$

and

$$y_2 = \int_{T_\alpha}^{T_\beta} \int_{\Re^N} g_2(u : \mathbf{p}) f(u : \mathbf{p}) du d\mathbf{p}, \quad (5.121)$$

where $f(u : \mathbf{p})$ is a Gaussian random process and g_1 and g_2 are in \mathcal{G} , then y_1 and y_2 are jointly Gaussian.

Property 3: If $f(t, \mathbf{p})$ is a Gaussian random process, for any set of times $t_1, t_2, t_3, \dots, t_n$ in the time interval $[T_\alpha, T_\beta]$ and locations $p_1, p_2, p_3, \dots, p_m$ in the set \Re^N , the mn random variables $f_{t_1 \mathbf{p}_1}, f_{t_2 \mathbf{p}_1}, f_{t_3 \mathbf{p}_1}, \dots, f_{t_n \mathbf{p}_1}, f_{t_1 \mathbf{p}_2}, \dots, f_{t_1 \mathbf{p}_m}, \dots, f_{t_n \mathbf{p}_m}$ are jointly Gaussian random variables. To verify this, use a $g(u : \mathbf{p})$ in (5.118), which is a set of impulses,

$$g(u : \mathbf{p}) = \sum_{i=1}^n \sum_{j=1}^m g_{ij} \delta(u - t_i) \delta(\mathbf{p} - \mathbf{p}_j). \quad (5.122)$$

⁷Gaussian space-time random processes are sometimes referred to as Gaussian random fields.

We see that our definition has the desirable property that it uniquely specifies the joint density at any set of times. Frequently, Property 3 is used as the basic definition. The disadvantage of this approach is that it is more difficult to prove that our definition and properties 1 and 2 hold.

The Gaussian process we have defined has two main virtues:

1. The physical mechanisms that produce many processes are such that a Gaussian model is appropriate.
2. The Gaussian process has many properties that make analytic results feasible.

Discussions of physical mechanisms that lead logically to Gaussian processes are available in [DR58] and [DR87].

We encounter multiple processes that are jointly Gaussian. The definition is a straightforward extension of the preceding one.

Definition: Let $f_1(t, \mathbf{p}), f_2(t, \mathbf{p}), \dots, f_N(t, \mathbf{p})$ be a set of random processes defined over the intervals $(T_{\alpha_1}, T_{\beta_1}), (T_{\alpha_2}, T_{\beta_2}), \dots, (T_{\alpha_N}, T_{\beta_N})$, respectively. If every sum of arbitrary functional of $f_i(t, \mathbf{p})$, $i = 1, \dots, N$ is a Gaussian random variable, then the processes $f_1(t, \mathbf{p}), f_2(t, \mathbf{p}), \dots, f_N(t, \mathbf{p})$ are defined to be jointly Gaussian random processes. In other words,

$$y = \sum_{i=1}^N \int_{T_{\alpha_i}}^{T_{\beta_i}} \int_{\Re^N} g_i(u : \mathbf{p}) f_i(u, \mathbf{p}) du d\mathbf{p}, \quad (5.123)$$

is a Gaussian random variable.

Most of our random process models will be Gaussian when we study optimum array processing. This assumption is justified in a wide range of physical problems.

In the next section, more detailed models of signal and noise random processes are developed.

5.3.3 Plane Waves Propagating in Three Dimensions

In this section⁸ we describe a model that allows us to generate the temporal frequency spatial correlation function for a large class of random processes. This enables us to find the frequency-wavenumber spectrum. Isotropic noise is included as a special case.

⁸This section follows [Bag76].

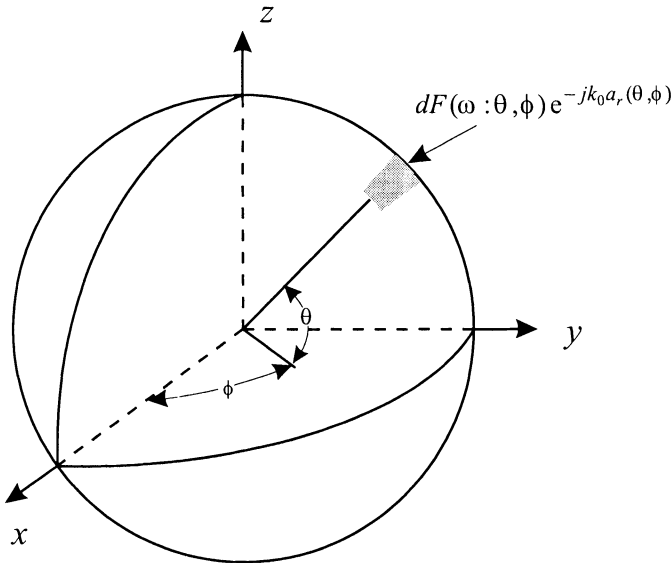


Figure 5.7 Incremental surface area contributing to a plane-wave spatial process.

At temporal frequency ω_o , the noise processes of interest are modeled in three dimensions as positions of infinitesimal plane-wave processes, all radiating towards a common point. These waves may be considered to be generated on the surface of a sphere whose radius is large compared to any geometries or wavelengths of interest. Using the integrated transform representation we have

$$dF(\omega_o, \mathbf{p}) = \int_0^\pi d\theta \int_0^{2\pi} \frac{\sin(\theta)d\phi}{4\pi} dF_0(\omega_o : \theta, \phi) e^{-jk_o \mathbf{a}_r^T(\theta, \phi) \mathbf{p}}, \quad (5.124)$$

where

$$f(t, \mathbf{p}) = \int_{-\infty}^{\infty} dF(\omega_o : \mathbf{p}) e^{j\omega t}, \quad (5.125)$$

$k_o = \frac{2\pi}{\lambda}$, and $\mathbf{a}_r(\theta, \phi)$ is a unit vector in the radial direction. Consequently, $-k_o \mathbf{a}_r(\theta, \phi)$ forms a propagation vector $\mathbf{k}(\theta, \phi)$ at a temporal frequency ω_o radiating towards the center of the sphere, or

$$\mathbf{k}(\theta, \phi) = -k_o \mathbf{a}_r(\theta, \phi) = -\frac{2\pi}{\lambda} \mathbf{a}_r(\theta, \phi) = -\frac{\omega_o}{c} \mathbf{a}_r(\theta, \phi). \quad (5.126)$$

The model is shown in Figure 5.7.

We assume that disjoint regions of the sphere radiate uncorrelated components so that

$$E [dF_0(\omega_o : \theta_1, \phi_1) dF_0^*(\omega_o : \theta_2, \phi_2)] = S_0(\omega_o : \theta_1, \phi_1) \left(\frac{\delta(\theta_1 - \theta_2)\delta(\phi_1 - \phi_2)}{\frac{\sin \theta_1}{4\pi}} \right) \left(\frac{d\omega}{2\pi} \right). \quad (5.127)$$

(The impulse terms should be interpreted formally and should operate simultaneously. The factor of $4\pi/\sin \theta_1$ needs to be introduced because of the use of spherical coordinates.) The temporal spectrum-spatial correlation function is given by

$$E [dF(\omega_o : \mathbf{p}) dF^*(\omega_o : \mathbf{p} - \Delta \mathbf{p})] = S_f(\omega_o : \Delta \mathbf{p}) \frac{d\omega}{2\pi}. \quad (5.128)$$

Using (5.124), we have

$$S_f(\omega_o : \Delta \mathbf{p}) \frac{d\omega}{2\pi} = \int_0^\pi d\theta_1 \int_0^{2\pi} \frac{\sin(\theta_1)}{4\pi} d\phi_1 \int_0^\pi d\theta_2 \int_0^{2\pi} \frac{\sin(\theta_2)}{4\pi} d\phi_2 \cdot E [dF_0(\omega_o : \theta_1, \phi_1) dF_0^*(\omega_o : \theta_2, \phi_2)] \cdot e^{-jk_o \mathbf{a}_r^T(\theta_1, \phi_1) \mathbf{p} + jk_o \mathbf{a}_r^T(\theta_2, \phi_2) (\mathbf{p} - \Delta \mathbf{p})} d\phi_2. \quad (5.129)$$

Equation (5.127) implies that disjoint (θ, ϕ) are uncorrelated, so (5.129) reduces to

$$S_f(\omega_o : \Delta \mathbf{p}) = \int_0^\pi d\theta \int_0^{2\pi} \frac{\sin(\theta)}{4\pi} d\phi S_o(\omega_o : \theta, \phi) e^{-jk_o \mathbf{a}_r^T(\theta, \phi) \Delta \mathbf{p}}, \quad (5.130)$$

which is the first desired result. It enables us to find the temporal frequency spectrum-spatial correlation function for a large class of random processes as a function of $S_o(\omega_o : \theta, \phi)$, which is their temporal frequency function at locations (θ, ϕ) on the sphere.

The form in (5.130) is most useful in cases where $S_o(\omega_o : \theta, \phi)$ is known and we want to find the spatial spectral matrix $\mathbf{S}_f(\omega_o)$ at the array.

The frequency-wavenumber function follows from the Fourier transform relationship. It is useful to define the wavenumber \mathbf{k} in both spherical and Cartesian coordinates:

$$\mathbf{k} = k_x \mathbf{i}_x + k_y \mathbf{i}_y + k_z \mathbf{i}_z = k_r \mathbf{a}_r(\theta_k, \phi_k), \quad (5.131)$$

where $\mathbf{a}_r(\theta_k, \phi_k)$ is a unit radial vector in the same direction as \mathbf{k} . We have

$$\begin{aligned}
P_f(\omega_o : \mathbf{k}) &= \int_{-\infty}^{\infty} \int_{-\infty}^{\infty} \int_{-\infty}^{\infty} d\Delta \mathbf{p} e^{j\mathbf{k}^T \Delta \mathbf{p}} \int_0^{\pi} d\theta \int_0^{2\pi} \frac{\sin(\theta)}{4\pi} d\phi \\
&\quad S_o(\omega_o : \theta, \phi) e^{-jk_o \mathbf{a}_r^T(\theta, \phi) \Delta \mathbf{p}} \\
&= \int_0^{\pi} d\theta \int_0^{2\pi} \frac{\sin(\theta)}{4\pi} \int_{-\infty}^{\infty} \int_{-\infty}^{\infty} d\Delta \mathbf{p} S_o(\omega_o : \theta, \phi) \\
&\quad e^{j(k_r \mathbf{a}_r(\theta_k, \phi_k) - k_o \mathbf{a}_r(\theta, \phi))^T \Delta \mathbf{p}}. \tag{5.132}
\end{aligned}$$

The evaluation of the last integral leads to an impulse, or delta function, in wavenumber space, that is,

$$\begin{aligned}
&\int_{-\infty}^{\infty} \int_{-\infty}^{\infty} \int_{-\infty}^{\infty} d\Delta \mathbf{p} e^{j(k_r \mathbf{a}_r(\theta_k, \phi_k) - k_o \mathbf{a}_r(\theta, \phi))^T \Delta \mathbf{p}} \\
&= (2\pi)^3 \frac{\delta(k_r - k_o) \delta(\theta_k - \theta) \delta(\phi_k - \phi)}{k_o^2 \sin(\theta)}. \tag{5.133}
\end{aligned}$$

When we substitute (5.133) into (5.132), we obtain

$$P_f(\omega_o : \mathbf{k}) = (2\pi)^3 S_o(\omega_o : \theta_k, \phi_k) \frac{\delta(k_r - k_o)}{4\pi k_o^2}. \tag{5.134}$$

We have the intuitive interpretation that the resulting frequency-wavenumber function has the same distribution as the spectra of the plane waves at the various locations on the sphere. The delta function arises because these waves are modeled as pure plane waves analogous to pure tones temporally. By starting with this specification of the noise field we can model a large number of ambient fields that may be encountered.

In many applications it is useful to express the temporal frequency spectrum-spatial correlation function in spherical coordinates. To do this, we write $\mathbf{a}_r(\theta, \phi)$ and $\Delta \mathbf{p}$ in terms of rectangular coordinates,

$$\mathbf{a}_r(\theta, \phi) = -[\sin \theta \cos \phi \ \sin \theta \sin \phi \ \cos \theta]^T, \tag{5.135}$$

and

$$\Delta \mathbf{p} = r_p [\sin \theta_p \cos \phi_p \ \sin \theta_p \sin \phi_p \ \cos \theta_p]^T, \tag{5.136}$$

where

$$r_p = |\Delta \mathbf{p}|. \tag{5.137}$$

Using (5.135) and (5.136) in (5.130) gives

$$\begin{aligned}
S_f(\omega_o : \Delta \mathbf{p}) &= \int_0^{\pi} d\theta \int_0^{2\pi} \frac{\sin \theta}{4\pi} d\phi S_o(\omega_o : \theta, \phi) \cdot \\
&\quad \exp \{jk_o r_p [\sin \theta \sin \theta_p (\cos(\phi - \phi_p)) + \cos \theta \cos \theta_p]\}. \tag{5.138}
\end{aligned}$$

We now consider the special case of isotropic noise. For isotropic noise,

$$S_o(\omega : \theta, \phi) = S_o(\omega). \quad (5.139)$$

Using (5.139) in (5.138) gives

$$\begin{aligned} S_f(\omega_o : \Delta p) &= S_o(\omega_o) \left(\int_0^\pi d\theta \frac{\sin \theta}{4\pi} e^{-jk_o |\Delta p| \cos \theta \cos \theta_p} \right) \\ &\quad \cdot \left(\int_0^{2\pi} e^{-jk_o |\Delta p| \sin \theta \sin \theta_p \cos(\phi - \phi_p)} d\phi \right). \end{aligned} \quad (5.140)$$

We know that the result cannot be a function of (θ_p, ϕ_p) due to the spherical symmetry of the field. Therefore, we can let $\theta_p = 0$. Now (5.140) reduces to

$$S_f(\omega_o : \Delta p) = S_o(\omega_o) \int_0^\pi d\theta \frac{\sin \theta}{2} e^{jk_o \Delta p \cos \theta}. \quad (5.141)$$

Letting $\alpha = \cos \theta$, and integrating , we obtain

$$\begin{aligned} S_f(\omega_o : \Delta p) &= S_o(\omega_o) \frac{\sin k_o \Delta p}{k_o \Delta p} \\ &= S_o(\omega_o) \text{sinc} \left(\frac{2\pi \Delta p}{\lambda} \right). \end{aligned} \quad (5.142)$$

Thus, the temporal frequency spectrum spatial correlation function is a sinc function whose argument is $\frac{2\pi \Delta p}{\lambda}$.

In [Bag76], Baggeroer develops expansions of $S_o(\omega_o : \theta, \phi)$ in terms of spherical harmonics that were introduced by Stratton [Str41] to study electromagnetic fields. We normally use numerical techniques for the non-isotropic cases.

5.3.4 1-D and 2-D Projections

In many of our applications, the array will be 1-D or 2-D. In this case we are interested in the projection onto the appropriate dimension. We consider the one-dimensional case first.

5.3.4.1 Projection onto one dimension

If we project onto one dimension (the z -axis), then $\theta_p = 0$ or π in (5.138). Then,

$$S_f(\omega : \Delta p_z) = \int_0^\pi d\theta \frac{\sin \theta}{4\pi} e^{jk_o \Delta p_z \cos \theta} \int_0^{2\pi} S_o(\omega : \theta, \phi) d\phi. \quad (5.143)$$

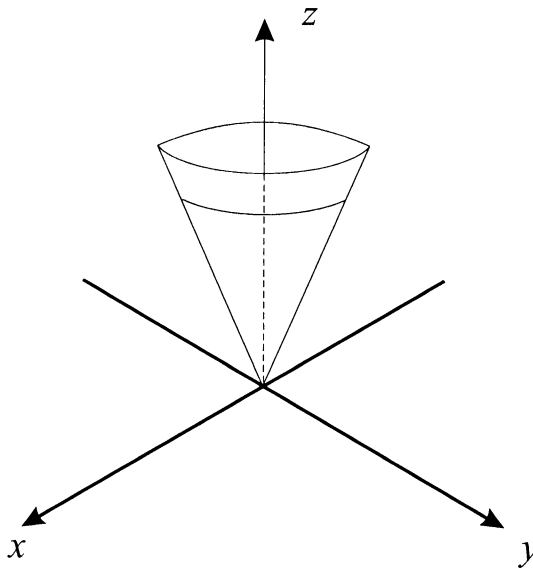


Figure 5.8 Sector signal field.

Since the linear array cannot resolve in the ϕ -direction, define

$$\bar{S}_o(\omega : \theta) = \frac{1}{2\pi} \int_0^{2\pi} S_o(\omega : \theta, \phi) d\phi, \quad (5.144)$$

and (5.143) becomes

$$S_f(\omega : \Delta p_z) = \int_0^\pi d\theta \frac{\sin \theta}{2} e^{jk_o \Delta p_z \cos \theta} \bar{S}_o(\omega : \theta). \quad (5.145)$$

This can be rewritten in terms of the directional cosine u ,

$$u = \cos \theta, \quad (5.146)$$

as

$$S_f(\omega : \Delta p_z) = \frac{1}{2} \int_{-1}^1 du e^{jk_o \Delta p_z u} \bar{S}_{ou}(\omega : u), \quad (5.147)$$

where $\bar{S}_{ou}(\omega : u) = \bar{S}_o(\omega : \cos^{-1}(u))$.

We consider a simple example to illustrate a typical result.

Example 5.3.2

Consider the spatial distribution shown in Figure 5.8.

$$S_o(\omega : \theta, \phi) = \begin{cases} \sigma_f^2, & \theta \leq \theta_0 \\ 0, & \text{elsewhere.} \end{cases} \quad (5.148)$$

The spectrum is constant over a segment of the sphere and is zero elsewhere. It is uniform in the ϕ -variable. Defining,

$$u_0 = \cos \theta_0, \quad (5.149)$$

(5.147) reduces to

$$\begin{aligned} S_f(\omega : \Delta p_z) &= \frac{\sigma_f^2}{2} \int_{-u_0}^{u_0} e^{jk_o \Delta p_z u} du \\ &= \sigma_f^2 \frac{\sin(k_o \Delta p_z u_0)}{k_o \Delta p_z} = \sigma_f^2 u_0 \text{sinc}(k_o \Delta p_z u_0), \end{aligned} \quad (5.150)$$

which is the desired result.

A second example corresponds to a spatial distribution spread around the broadside direction.

Example 5.3.3

We assume

$$\bar{S}_{ou}(\omega : u) = \frac{\sigma_f^2}{\sqrt{2\pi}\sigma_u} e^{-\frac{u^2}{2\sigma_u^2}}, \quad -1 \leq u \leq 1, \quad (5.151)$$

and σ_u is small compared to unity. Then (5.147) reduces to

$$S_f(\omega : \Delta p_z) = \sigma_f^2 e^{-\frac{k_o^2 \Delta p_z^2 \sigma_u^2}{2}} \int_{-1}^1 \frac{1}{\sqrt{2\pi}\sigma_u} e^{-\frac{1}{2\sigma_u^2}(u - jk_o \Delta p_z \sigma_u^2)^2} du. \quad (5.152)$$

For small σ_u , the limits on the integral can be approximated as $-\infty$ to ∞ , so the integral equals unity and

$$S_f(\omega : \Delta p_z) = \sigma_f^2 \exp \left\{ -\frac{k_o^2 \Delta p_z^2 \sigma_u^2}{2} \right\}. \quad (5.153)$$

Other examples are developed in the problems. We now consider 2-D projections.

5.3.4.2 Projection onto two dimensions

In this case, we assume the 2-D surface of interest is the xy -plane. Define

$$\Delta \mathbf{p}_s = \Delta \mathbf{p}|_{p_z=0} = [\Delta p_x \Delta p_y]^T, \quad (5.154)$$

and

$$\mathbf{k}_s = \mathbf{k}|_{k_z=0} = [k_x k_y]^T. \quad (5.155)$$

We first find $S_f(\omega : \Delta \mathbf{p}_s)$. Substituting $\theta_p = \frac{\pi}{2}$ into (5.138), we obtain

$$S_f(\omega_0 : \Delta \mathbf{p}_s) = \int_0^\pi d\theta \int_0^{2\pi} d\phi \frac{\sin \theta}{4\pi} S_o(\omega_0 : \theta, \phi) e^{jk_o r_p \sin \theta \cos(\phi - \phi_p)}. \quad (5.156)$$

We first perform the integration with respect to θ over the regions $[0, \frac{\pi}{2}]$ and $[\frac{\pi}{2}, \pi]$. (This is necessary since two points on the surface of the sphere for

the plane-wave model project to the same point on the 2-D surface.) Now change variables in each region. Define

$$\sin \theta = v, \quad 0 \leq \theta \leq \frac{\pi}{2}, \quad (5.157)$$

and

$$\sin(\pi - \theta) = v, \quad \frac{\pi}{2} < \theta \leq \pi. \quad (5.158)$$

Then (5.156) reduces to

$$\begin{aligned} S_f(\omega_0 : \mathbf{p}_s) = & \frac{1}{4\pi} \int_0^1 \frac{v dv}{\sqrt{1-v^2}} \int_0^{2\pi} d\phi e^{jk_o r_p v \cos(\phi-\phi_p)} \left\{ S_o \left(\omega_0 : \sin^{-1} v, \phi \right) \right. \\ & \left. + S_o \left(\omega_0 : \pi - \sin^{-1} v, \phi \right) \right\}, \end{aligned} \quad (5.159)$$

which is the general result.

If $S_o(\omega_0 : \theta, \phi)$ does not have an azimuthal (ϕ) dependence, then we can perform the integration over ϕ . Rewriting (5.156) for this case,

$$\begin{aligned} S_f(\omega_0 : \mathbf{p}_s) = & \frac{1}{4\pi} \int_0^1 \frac{v dv}{\sqrt{1-v^2}} \left\{ S_o \left(\omega_0 : \sin^{-1}(v) \right) \right. \\ & \left. + S_o \left(\omega_0 : \pi - \sin^{-1} v \right) \right\} \\ & \cdot \int_0^{2\pi} d\phi e^{jk_o r_p v \cos(\phi-\phi_p)}. \end{aligned} \quad (5.160)$$

The inner integral corresponds to a zero-order Bessel function. Thus,

$$\begin{aligned} S_f(\omega_0 : \mathbf{p}_s) = & \frac{1}{2} \int_0^1 \frac{dv J_0(k_o r_p v)}{\sqrt{1-v^2}} \left\{ S_o \left(\omega_0 : \sin^{-1}(v) \right) \right. \\ & \left. + S_o \left(\omega_0 : \pi - \sin^{-1} v \right) \right\}. \end{aligned} \quad (5.161)$$

At this point, we must specify $S_f(\omega_0 : \theta)$ in order to proceed. We consider the sector distribution in Figure 5.8.

Example 5.3.4

We define

$$v_0 = \sin \theta_0. \quad (5.162)$$

Then, (5.161) reduces to

$$S_f(\omega_0 : \Delta \mathbf{p}_s) = \frac{S_o(\omega_0)}{2} \int_0^{v_0} \frac{vdv J_0(k_o r_p v)}{\sqrt{1-v^2}}. \quad (5.163)$$

The integral in (5.163) can be evaluated numerically.

Several other spatial distributions corresponding to various ambient noise or signal models are developed in the problems.

5.3.4.3 Summary

In this section, we have developed both a second-moment representation and a Gaussian process representation for space-time random processes. We now study how arrays and apertures respond to these space-time processes.

5.4 Arrays and Apertures

In this section, we discuss how arrays and apertures respond to space-time random processes. In Chapter 2, we showed that a plane wave was the basis function for a linear time-invariant system. In Section 5.2, we modeled the space-time processes as collections of statistically independent plane waves. We now combine these two models. We begin our discussion with arrays.

5.4.1 Arrays

5.4.1.1 Sampling

We first consider a uniformly spaced linear array. The linear array samples the space-time process at spatial intervals d , where d is the interelement spacing. The space-time field is bandlimited in wavenumber space:

$$|k| = \frac{2\pi}{\lambda} \text{ radians/meter} = \frac{1}{\lambda} \text{ cycles/meter} , \quad (5.164)$$

and

$$|k_z| \leq \frac{2\pi}{\lambda} \text{ radians/meter} = \frac{1}{\lambda} \text{ cycles/meter} . \quad (5.165)$$

Since wavenumber and position are conjugate Fourier transform variables, we know that we must sample at

$$d \leq \frac{1}{2\left(\frac{1}{\lambda}\right)} = \frac{\lambda}{2} , \quad (5.166)$$

in order to be able to reconstruct the space-time process without spatial aliasing. This is the same interelement spacing that we found in Chapter 2 using a grating lobe argument.

In two dimensions,

$$|k_x| \leq \frac{2\pi}{\lambda} , \quad (5.167)$$

and

$$|k_y| \leq \frac{2\pi}{\lambda} , \quad (5.168)$$

so that, if we use a rectangular sampling grid, we require

$$d_x \leq \frac{\lambda}{2}, \quad (5.169)$$

and

$$d_y \leq \frac{\lambda}{2}. \quad (5.170)$$

In [PM62], Peterson and Middleton discussed alternate sampling strategies and showed that using the hexagonal array discussed in Section 4.4 with spacing,

$$d_x = \frac{\lambda}{2}, \quad (5.171)$$

$$d_y = \frac{\sqrt{3}}{4}\lambda, \quad (5.172)$$

is the sampling strategy that completely specifies the space-time field with the smallest number of samples (e.g., [PM62], [Mer79] or [DM84]).

5.4.1.2 Spectral matrices

We now consider the output of an N -element array when the input is a sample function of a random space-time process. If the input to the array is the space-time process $x(t, \mathbf{p})$, then the output of the array, in the absence of sensor noise, is

$$\mathbf{x}(t, \mathbf{p}) = \begin{bmatrix} x(t, \mathbf{p}_0) \\ x(t, \mathbf{p}_1) \\ \vdots \\ x(t, \mathbf{p}_{N-1}) \end{bmatrix}, \quad (5.173)$$

where \mathbf{p}_i denotes the position of the i th element.

The spatial spectral matrix is $\mathbf{S}_x(\omega)$ whose ij element is

$$[\mathbf{S}_x(\omega)]_{ij} = \mathbf{S}_x(\omega : \mathbf{p}_i - \mathbf{p}_j), \quad (5.174)$$

where $\mathbf{S}_x(\omega : \mathbf{p}_i - \mathbf{p}_j)$ is the temporal frequency spectrum-spatial correlation function defined in (5.91).

We use the frequency-domain snapshot model of Section 5.2 to obtain $\mathbf{X}_{\Delta T}(\omega_m, k)$. We use the approximation discussed in Section 5.2:

$$E \left[\mathbf{X}_{\Delta T}(\omega_m, k) \mathbf{X}_{\Delta T}^H(\omega_m, k) \right] \simeq \mathbf{S}_x(\omega_m). \quad (5.175)$$

In the beamforming application, $\mathbf{X}(\omega_m, k)$ is processed with a matrix filter $\mathbf{W}^H(\omega_m)$ as shown in Figure 5.9. Then,

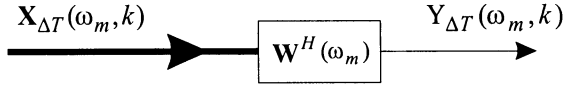


Figure 5.9 Matrix filter.

$$Y_{\Delta T}(\omega_m, k) = \mathbf{W}^H(\omega_m) \mathbf{X}_{\Delta T}(\omega_m, k), \quad (5.176)$$

and the spectrum of $Y_{\Delta T}(\omega_m, k)$ is

$$\begin{aligned} S_y(\omega_m) &= E[Y_{\Delta T}(\omega_m, k) Y_{\Delta T}^*(\omega_m, k)] \\ &= \mathbf{W}^H(\omega_m, k) [E[\mathbf{X}(\omega_m, k) \mathbf{X}^H(\omega_m, k)] \mathbf{W}(\omega_m)], \end{aligned} \quad (5.177)$$

or

$$S_y(\omega_m) = \mathbf{W}^H(\omega_m) \mathbf{S}_x(\omega_m) \mathbf{W}(\omega_m). \quad (5.178)$$

5.4.1.3 Beam patterns in frequency-wavenumber space

An alternative expression for $S_y(\omega_m)$ is useful in order to interpret the result in terms of beam patterns and the frequency-wavenumber spectrum.

We can write

$$Y_{\Delta T}(\omega_m, k) = \sum_{n=0}^{N-1} W_n^*(\omega_m) X(\omega_m, k : \mathbf{p}_n). \quad (5.179)$$

The output spectrum is given by (5.177). Using (5.179) in (5.177) and (5.174) in the result gives

$$S_y(\omega_m) = \sum_{n=1}^N \sum_{l=1}^N W_n^*(\omega_m) S_x(\omega : \mathbf{p}_n - \mathbf{p}_l) W_l(\omega_m). \quad (5.180)$$

Using (5.95) in (5.180) gives

$$\begin{aligned} S_y(\omega_m) &= \int_{-\infty}^{\infty} \int_{-\infty}^{\infty} \int_{-\infty}^{\infty} \frac{d\mathbf{k}}{(2\pi)^3} \sum_{n=1}^N \sum_{l=1}^N W_n^*(\omega_m) W_l(\omega_m) \\ &\quad \cdot P_x(\omega : \mathbf{k}) e^{-j\mathbf{k}(\mathbf{p}_n - \mathbf{p}_l)}. \end{aligned} \quad (5.181)$$

Using the definition of the beam pattern, (5.181) can be written as

$$S_y(\omega_m) = \int_{-\infty}^{\infty} \int_{-\infty}^{\infty} \int_{-\infty}^{\infty} |B(\omega_m, \mathbf{k})|^2 P_x(\omega_m, \mathbf{k}) \frac{d\mathbf{k}}{(2\pi)^3}, \quad (5.182)$$

where $B(\omega_m, \mathbf{k})$ is the beam pattern at frequency ω_m and wavenumber \mathbf{k} and $P_x(\omega_m, \mathbf{k})$ is the frequency-wavenumber spectrum at the array.

This result is useful in terms of analyzing the performance of an array and in designing suitable beam patterns. It is analogous to the scalar spectral result,

$$S_{\text{out}}(\omega_m) = |H(\omega_m)|^2 S_{\text{in}}(\omega_m). \quad (5.183)$$

5.4.1.4 Co-arrays

It is useful to explore the relationship in (5.182) further. The term $|B(\omega, \mathbf{k})|^2$ represents the power pattern of the array. We can define an aperture auto-correlation function corresponding to the power pattern. Thus,⁹

$$R_W(\omega : \mathbf{p}) = \int_{-\infty}^{\infty} \cdot \int_{-\infty}^{\infty} |B(\omega, \mathbf{k})|^2 e^{j\mathbf{k}^T \mathbf{p}} \frac{d\mathbf{k}}{(2\pi)^3}, \quad (5.184)$$

where the integral is over the appropriate dimension and \mathbf{p} takes on discrete values corresponding to the element positions. For one dimension,

$$R_W(\omega : p_x) = \int_{-\infty}^{\infty} |B(\omega, k_x)|^2 e^{jk_x p_x} \frac{dk_x}{2\pi}, \quad (5.185)$$

and for two dimensions,

$$R_W(\omega : p_x, p_y) = \int_{-\infty}^{\infty} \int_{-\infty}^{\infty} |B(\omega, \mathbf{k})|^2 e^{j[k_x p_x + k_y p_y]} \frac{dk_x dk_y}{(2\pi)^2}. \quad (5.186)$$

From the transform relationship between the aperture weighting function and the beam pattern, we see $R_W(\omega : \mathbf{p})$ is just the convolution of $\mathbf{W}(\omega)$ with itself. For an N -element linear array (not necessarily equally spaced)

$$R_W(\omega : |m|) = \sum_{n=0}^{N-1} W(n) W^*(n + m), \quad m = 0, \pm 1, \dots, \pm N, \quad (5.187)$$

where the symmetry of $R_W(\omega : |m|)$ follows from the symmetry of $P_B(\omega : k_x)$ in k_x .

We encountered co-arrays previously in Section 3.9.2 in our discussion of minimum redundancy arrays. This discussion develops the idea from a more fundamental viewpoint of sampling $P_x(\omega : \mathbf{k})$ and showing how the samples of $P_x(\omega : \mathbf{k})$ can be used to reconstruct $P_x(\omega : \mathbf{k})$.

⁹This function was defined in [Bag76]. The application of co-arrays is discussed in [Hau68] and [Kre71].

For simplicity we consider the 1-D case. The function $P_x(\omega : k_z)$ is bandlimited in k_z -space,

$$|k_z| \leq \frac{2\pi}{\lambda}. \quad (5.188)$$

Therefore, from the sampling theorem, if the co-array has elements at

$$md = m \left(\frac{\lambda}{2} \right), \quad -\infty < m < \infty, \quad (5.189)$$

we could reconstruct $P_x(\omega : k_z)$ exactly. In practice, m will be limited by the physical extent of the array. However, we want to have the value at md for all m within the range allowed by the aperture size.

The reason that we use the co-array in the sampling theorem is the relationship to $P_x(\omega : \mathbf{k})$ in (5.182). Thus, as long as the co-array does not have gaps, the sampling theorem will hold. As we saw in Section 3.9.2, the array itself may have significant gaps.

5.4.1.5 Sensor noise

In all physical systems there is noise associated with the observation process. At a minimum, there is noise generated internally by the electronics in the system. We model this as a zero-mean spatially uncorrelated Gaussian random process that we denote by $\mathbf{n}_{su}(t)$. This is the noise introduced in Section 5.2. The contribution to the spatial spectral matrix is

$$\mathbf{S}_{\mathbf{n}_{su}}(\omega_m) = S_n(\omega_m) \mathbf{I}. \quad (5.190)$$

In most cases, we also assume that the temporal spectrum is flat. Then,

$$\mathbf{S}_{\mathbf{n}_{su}}(\omega_m) = \sigma_w^2 \mathbf{I}, \quad (5.191)$$

where σ_w^2 is height of the white noise spectrum.¹⁰ We denote noise vectors satisfying (5.191) as $\mathbf{w}(t)$.

The spectrum at the output of the array processor due to a white noise input is given by substituting (5.191) into (5.178), which results in,

$$S_{y_W}(\omega_m) = \sigma_w^2 |\mathbf{W}(\omega_m)|^2, \quad (5.192)$$

or

$$S_{y_W}(\omega_m) = \sigma_w^2 \sum_{i=1}^N |W_i(\omega_m)|^2. \quad (5.193)$$

¹⁰We use N_0 as the spectral height for the continuous spectral case. When we use the frequency-domain snapshot model we label the snapshot variance σ_w^2 to be consistent with the literature ($\sigma_w^2 = N_0$).

5.4.2 Apertures

All of the results developed for arrays carry over to apertures in a straightforward manner.

The input to the aperture is the space-time process $f(t, p)$. The aperture weighting function is $w(t, p)$. The output of the system is

$$y(t) = \int_{-\infty}^{\infty} d\tau \int_{\mathcal{R}^A} \cdot \int w^*(\tau, \mathbf{p}) f(t - \tau, \mathbf{p}) d\mathbf{p}, \quad (5.194)$$

where \mathcal{R}^A denotes the aperture region. For a linear aperture,

$$y(t) = \int_{-\infty}^{\infty} d\tau \int_{-\frac{L}{2}}^{\frac{L}{2}} w^*(\tau, p_x) f_1(t - \tau, p_x) dp_x, \quad (5.195)$$

where the subscript “1” on $f(\cdot)$ denotes that it is a 1-D representation of the input. If we started with a 2-D representation of the input, then

$$y(t) = \int_{-\infty}^{\infty} d\tau \int_{-\frac{L}{2}}^{\frac{L}{2}} \int_{L_y} w^*(\tau, p_x) \delta(p_y) f_2(t - \tau, p_x, p_y) dp_x dp_y, \quad (5.196)$$

for a linear array on the x -axis.

If we use the frequency domain snapshot model and let $\omega_m = \omega$, then we can also write

$$Y(\omega) = \int_{\mathcal{R}^A} \cdot \int W^*(\omega, \mathbf{p}) F(\omega, \mathbf{p}) d\mathbf{p}. \quad (5.197)$$

The output spectrum is

$$\begin{aligned} S_y(\omega) &= \int_{\mathcal{R}^A} \cdot \int \int_{\mathcal{R}^A} \cdot \int W^*(\omega, \mathbf{p}_\alpha) \Delta T^{-1} E [F(\omega, \mathbf{p}_\alpha) F^*(\omega, \mathbf{p}_\beta)] \\ &\quad W(\omega, \mathbf{p}_\beta) d\mathbf{p}_\alpha d\mathbf{p}_\beta, \end{aligned} \quad (5.198)$$

or

$$S_y(\omega) = \int_{\mathcal{R}^A} \cdot \int \int_{\mathcal{R}^A} \cdot \int W^*(\omega, \mathbf{p}_\alpha) S_f(\omega : \mathbf{p}_\alpha, \mathbf{p}_\beta) W(\omega, \mathbf{p}_\beta) d\mathbf{p}_\alpha d\mathbf{p}_\beta, \quad (5.199)$$

where $S_f(\omega : \mathbf{p}_\alpha, \mathbf{p}_\beta)$ is the temporal frequency spectrum spatial correlation function of the input space-time process defined in (5.91). Using (5.95) in (5.199), and performing the integration over p_α and p_β gives

$$S_y(\omega) = \int_{-\infty}^{\infty} \int_{-\infty}^{\infty} \int_{-\infty}^{\infty} |B(\omega, \mathbf{k})|^2 P_f(\omega, \mathbf{k}) \frac{d\mathbf{k}}{(2\pi)^N}, \quad (5.200)$$

which is identical to (5.182).

To define the sensor noise we specify the dimension of the aperture first. For a linear aperture,

$$K_W(t, u : p_1, p_2) = N_o \delta(t - u) \delta(p_1 - p_2). \quad (5.201)$$

For a planar aperture,

$$K_W(t, u : p_{x_1}, p_{y_1}, p_{x_2}, p_{y_2}) = N_o \delta(t - u) \delta(p_{x_1} - p_{x_2}) \delta(p_{y_1} - p_{y_2}). \quad (5.202)$$

The results in (5.197) and (5.200) are important when the effect of non-isotropic sensors are included in the model. Then the frequency domain snapshot at the output of the n th sensor is

$$X_n(\omega) = \int_{R^A} \cdot \int W_{el}^*(w, \mathbf{p}) F(w, \mathbf{p}) d\mathbf{p}, \quad (5.203)$$

and

$$S_{x_n}(\omega) = \int_{-\infty}^{\infty} \int_{-\infty}^{\infty} \int_{-\infty}^{\infty} |B_{el}(\omega, \mathbf{k})|^2 P_f(\omega, \mathbf{k}) \frac{d\mathbf{k}}{(2\pi)^N}. \quad (5.204)$$

In most of the subsequent discussions (and in most of the array processing literature), the sensor output is assumed to be the value of the space-time field at the sensor location. However, in an actual system design both the temporal and spatial response characteristics should be taken into account.

5.5 Orthogonal Expansions

In Chapter 3 of DEMT I [VT68], [VT01a], we saw the utility of Karhunen-Loëve expansion for scalar Gaussian processes. It provided an orthogonal series expansion whose coefficients are statistically independent Gaussian random variables.¹¹ In Section 3.7 of [VT68], [VT01a], we introduced the corresponding expansion for vector random processes.

By using a frequency-domain snapshot model we have gone directly to a sequence of complex Gaussian random variables whose spatial spectral matrix is $\mathbf{S}_x(\omega_m)$. The model assumes that the snapshots are statistically independent so we can focus on a single snapshot $\mathbf{X}(\omega_m, k)$.¹² Writing $\mathbf{X}(\omega_m, k)$ as a weighted sum of orthonormal vectors gives

$$\mathbf{X}(\omega_m, k) = \sum_{i=1}^N x_i \Phi_i, \quad (5.205)$$

¹¹The Karhunen-Loëve expansion deals with second moments and produces *uncorrelated* coefficients if we do not impose the Gaussian assumption.

¹²For notational simplicity, the “ ΔT ” subscript is omitted.

where the ω_m and k dependence are suppressed on the right side of (5.205). The Φ_i are orthonormal vectors,

$$\Phi_i^H \Phi_j = \delta_{ij}, \quad i, j = 1, \dots, N, \quad (5.206)$$

and the coefficients are

$$x_i = \Phi_i^H \mathbf{X}(\omega_m, k), \quad i = 1, \dots, N. \quad (5.207)$$

The Φ_i are chosen so that

$$E[x_i x_j^*] = \lambda_i \delta_{ij}, \quad i, j = 1, \dots, N. \quad (5.208)$$

Substituting (5.207) into (5.208) gives

$$E[\Phi_i^H \mathbf{X}(\omega_m, k) \mathbf{X}^H(\omega_m, k) \Phi_j] = \lambda_i \delta_{ij}, \quad i, j = 1, \dots, N, \quad (5.209)$$

or

$$\Phi_i^H \mathbf{S}_x(\omega_m) \Phi_j = \lambda_i \delta_{ij}, \quad i, j = 1, \dots, N. \quad (5.210)$$

The solution to (5.210) is

$$\lambda_i \Phi_i = \mathbf{S}_x(\omega_m) \Phi_i, \quad i = 1, \dots, N. \quad (5.211)$$

The result in (5.211) is familiar as the matrix eigendecomposition problem that is reviewed in Section A.4.¹³

For simplicity we can suppress ω_m and i in the notation to obtain

$$\lambda \Phi = \mathbf{S}_x \Phi. \quad (5.212)$$

The λ_i , $i = 1, \dots, N$ are the eigenvalues and the Φ_i , $i = 1, \dots, N$ are eigenvectors. The spatial spectral matrix is a non-negative definite Hermitian matrix whose eigenvalues are real non-negative numbers. We order the eigenvalues in decreasing size,

$$\lambda_{max} \triangleq \lambda_1 \geq \lambda_2 \cdots \lambda_N = \lambda_{min}. \quad (5.213)$$

The coefficients in the expansion, x_i , $i = 1, \dots, N$, are zero-mean circular complex Gaussian random variables with variance λ_i .

In many cases, it is useful to expand \mathbf{S}_x using the eigenvalue and eigenvectors,

$$\mathbf{S}_x = \sum_{i=1}^N \lambda_i \Phi_i \Phi_i^H. \quad (5.214)$$

¹³A brief review of Section A.4 at this point may be useful.

Recall that spatially white noise had a diagonal spectral matrix. From (5.191),

$$\mathbf{S}_w = \sigma_w^2 \mathbf{I}. \quad (5.215)$$

It can be expanded using any set of orthogonal vectors. In particular, if the input spectrum is

$$\mathbf{S}_x = \mathbf{S}_c + \sigma_w^2 \mathbf{I}, \quad (5.216)$$

then $\mathbf{S}_x(\omega)$ can be expanded as

$$\mathbf{S}_x = \sum_{i=1}^N \left[\lambda_i^c + \sigma_w^2 \right] \Phi_i \Phi_i^H, \quad (5.217)$$

where the λ_i^c are the eigenvalues of \mathbf{S}_c and the Φ_i are the eigenvectors of \mathbf{S}_c .

In many cases of interest, the rank of \mathbf{S}_c is less than N so that some of the λ_i^c will equal zero. For example, if the rank is $D < N$, then

$$\lambda_i = \begin{cases} \lambda_i^c + \sigma_w^2, & i = 1, 2, \dots, D, \\ \sigma_w^2, & i = D+1, \dots, N, \end{cases} \quad (5.218)$$

so that there are $N - D$ equal eigenvalues due to the white noise. The inverse of \mathbf{S}_x can be written as

$$\begin{aligned} \mathbf{S}_x^{-1} &= \sum_{i=1}^N \left[\frac{1}{\lambda_i^c + \sigma_w^2} \right] \Phi_i \Phi_i^H \\ &= \frac{1}{\sigma_w^2} \mathbf{I} - \sum_{i=1}^N \frac{\lambda_i^c}{\sigma_w^2 (\lambda_i^c + \sigma_w^2)} \Phi_i \Phi_i^H. \end{aligned} \quad (5.219)$$

We study the behavior of the eigenvalues and eigenvector for various signal configurations. We first consider plane-wave signals.

5.5.1 Plane-wave Signals

In this section, we look at the special case in which $\mathbf{x}(t)$ consists of D directional plane-wave processes plus white sensor noise. The frequency-domain snapshots are

$$\mathbf{X} = \sum_{d=1}^D \mathbf{v}_k(\mathbf{k}_d) \mathbf{F} + \mathbf{W}, \quad (5.220)$$

where we have suppressed both ω_m and k . We define \mathbf{V} as an $N \times D$ -dimensional array manifold matrix,¹⁴

$$\mathbf{V} \triangleq \left[\begin{array}{c|c|c|c} \mathbf{v}(\mathbf{k}_1) & \mathbf{v}(\mathbf{k}_2) & \cdots & \mathbf{v}(\mathbf{k}_D) \end{array} \right]. \quad (5.221)$$

From (5.67),

$$\mathbf{S}_x = \mathbf{V}\mathbf{S}_f\mathbf{V}^H + \sigma_w^2\mathbf{I}. \quad (5.222)$$

We assume that no two signals are coherent. This implies that \mathbf{S}_f is positive definite. We will discuss the coherent signal case later. We examine the eigendecomposition of the first term in (5.222). The columns of \mathbf{V} define a D -dimensional subspace that contains all of the signal energy. The eigenvectors provide an orthogonal basis for that subspace. Therefore, each Φ_i can be obtained from \mathbf{V} by a linear transformation:

$$\Phi_i = c_{1i}\mathbf{v}(\mathbf{k}_1) + c_{2i}\mathbf{v}(\mathbf{k}_2) + \cdots + c_{Di}\mathbf{v}(\mathbf{k}_D), \quad (5.223)$$

or

$$\Phi_i = \mathbf{V}\mathbf{c}_i, \quad i = 1, 2, \dots, D, \quad (5.224)$$

where \mathbf{c}_i is a $D \times 1$ vector. The eigendecomposition equation is

$$\lambda\Phi = \mathbf{V}\mathbf{S}_f\mathbf{V}^H\Phi. \quad (5.225)$$

Using (5.224) in (5.225) gives

$$\lambda\mathbf{V}\mathbf{c}_i = \mathbf{V}\mathbf{S}_f\mathbf{V}^H\mathbf{V}\mathbf{c}_i. \quad (5.226)$$

Equation (5.226) can be written as

$$\mathbf{V} [\lambda\mathbf{I} - \mathbf{S}_f\mathbf{V}^H\mathbf{V}] \mathbf{c}_i = \mathbf{0}. \quad (5.227)$$

In order for (5.227) to be satisfied, we require

$$[\lambda\mathbf{I} - \mathbf{S}_f\mathbf{V}^H\mathbf{V}] \mathbf{c}_i = \mathbf{0}. \quad (5.228)$$

This is a homogeneous equation that has a solution for D values of $\lambda_i, i = 1, 2, \dots, D$. The \mathbf{c}_i are the eigenvectors of $\mathbf{S}_f\mathbf{V}^H\mathbf{V}$. In order for (5.228) to have a non-trivial solution, we require

$$\det [\lambda\mathbf{I} - \mathbf{S}_f\mathbf{V}^H\mathbf{V}] = 0, \quad (5.229)$$

¹⁴We have deleted the subscript “ \mathbf{k} ” for simplicity.

which will have D solutions, which we denote as $\lambda_1^s \geq \lambda_2^s \geq \dots \geq \lambda_D^s$. The superscript “ s ” emphasizes that these eigenvalues are associated with the signal component of \mathbf{X} .

For each λ_i^s we can find the corresponding \mathbf{c}_i , which determines the corresponding $\Phi_i, i = 1, 2, \dots, D$. The eigenvectors corresponding to distinct eigenvalues are orthogonal and we normalize them so that

$$\Phi_i^H \Phi_j = \delta_{ij}. \quad (5.230)$$

The eigenvectors corresponding to equal eigenvalues can be chosen to be orthonormal. The \mathbf{c}_i specified by (5.228) contain an arbitrary scale factor because (5.228) is a homogeneous equation. The normalization in (5.230) determines the magnitude of the scale factor. We can collect the eigenvectors into an $N \times D$ matrix,

$$\mathbf{U}_S \triangleq \left[\begin{array}{c|c|c|c} \Phi_1 & \Phi_2 & \cdots & \Phi_D \end{array} \right]. \quad (5.231)$$

The range space of \mathbf{U}_S is referred to as the signal subspace. We can write

$$\mathbf{U}_S = \mathbf{V}\mathbf{C}, \quad (5.232)$$

where \mathbf{C} is a non-singular $D \times D$ matrix whose columns are $\mathbf{c}_i, i = 1, 2, \dots, D$.

We also observe that the ij th element of $\mathbf{V}^H \mathbf{V}$ is

$$[\mathbf{V}^H \mathbf{V}]_{ij} = \mathbf{v}^H(\mathbf{k}_i) \mathbf{v}(\mathbf{k}_j) \triangleq N B_c(\mathbf{k}_j : \mathbf{k}_i), \quad (5.233)$$

which is just the conventional beam pattern of the array steered to \mathbf{k}_i and evaluated at \mathbf{k}_j . We will use this identification shortly.

Returning to (5.222), we observe that the noise component spans the N -dimensional space. Thus, to represent it, we must add $(N - D)$ more orthonormal vectors. Any set of vectors that are orthogonal with each other and orthogonal to \mathbf{U}_S are satisfactory. We denote this set by the $N \times (N - D)$ matrix,

$$\mathbf{U}_N \triangleq \left[\begin{array}{c|c|c|c} \Phi_{D+1} & \Phi_{D+2} & \cdots & \Phi_N \end{array} \right]. \quad (5.234)$$

The range space of \mathbf{U}_N is referred to as the orthogonal subspace or the noise subspace. The corresponding eigenvalues are σ_w^2 . Notice that when we expand \mathbf{S}_x , the $\sigma_w^2 \mathbf{I}$ term adds σ_w^2 to each signal eigenvalue. Thus, the total expansion is

$$\mathbf{S}_x = \sum_{k=1}^N \lambda_k \Phi_k \Phi_k^H, \quad (5.235)$$

where

$$\lambda_k = \begin{cases} \lambda_k^s + \sigma_w^2, & k = 1, 2, \dots, D, \\ \sigma_w^2, & k = D+1, \dots, N. \end{cases} \quad (5.236)$$

Thus, although the noise subspace contains only noise, the signal subspace contains both signal and noise.

We can also write \mathbf{S}_x as

$$\mathbf{S}_x = \mathbf{U}_S \Lambda_S \mathbf{U}_S^H + \mathbf{U}_N \Lambda_N \mathbf{U}_N^H, \quad (5.237)$$

where

$$\Lambda_S = \text{diag } [\lambda_1, \lambda_2, \dots, \lambda_D], \quad D \times D, \quad (5.238)$$

and

$$\Lambda_N = \text{diag } [\sigma_w^2, \dots, \sigma_w^2] = \sigma_w^2 \mathbf{I}, \quad (N-D) \times (N-D). \quad (5.239)$$

The notion of dividing the observation space into a signal subspace is fundamental to many of the optimum processing schemes that we develop in the text. We observe that this idea of a signal subspace is just the vector version of our signal subspace derivation in Chapter 4 of DEMT I [VT68], [VT01a].

We now discuss the following example to illustrate the concepts.

Example 5.5.1¹⁵

The example of interest is the case of two directional signals $F_1(\omega)$ and $F_2(\omega)$, which are frequency-domain snapshots of sample functions of a zero-mean stationary vector random process with spectral matrix,

$$\mathbf{S}_f = \begin{bmatrix} S_1 & S_{12} \\ S_{21} & S_2 \end{bmatrix}. \quad (5.240)$$

The covariance matrix of \mathbf{X} is

$$\mathbf{S}_x = \mathbf{V} \mathbf{S}_f \mathbf{V}^H. \quad (5.241)$$

The wavenumbers of the two signals are \mathbf{k}_1 and \mathbf{k}_2 . So the array manifold vectors are $\mathbf{v}(\mathbf{k}_1)$ and $\mathbf{v}(\mathbf{k}_2)$. Thus,

$$\begin{aligned} \mathbf{v}_1 &= \mathbf{v}(\mathbf{k}_1) \\ \mathbf{v}_2 &= \mathbf{v}(\mathbf{k}_2). \end{aligned} \quad (5.242)$$

¹⁵The solution for the eigenvalues for two plane-wave sources was published by Kwok and Brandon [KB79a], [KB79b] and Morgan [Mor78] and is utilized by Hudson [Hud81] and Kaveh and Barabell ([KB86a] and [KB86b]).

Inserting (5.240) and \mathbf{V} into (5.229) gives,

$$\det \left[\lambda \mathbf{I} - N \begin{bmatrix} S_1 & S_{12} \\ S_{21} & S_2 \end{bmatrix} \begin{bmatrix} 1 & B_c^{12} \\ B_c^{21} & 1 \end{bmatrix} \right] = 0, \quad (5.243)$$

where we have defined

$$B_c^{mn} = B_c(\mathbf{k}_n : \mathbf{k}_m) = \frac{\mathbf{v}^H(\mathbf{k}_m)\mathbf{v}(\mathbf{k}_n)}{N}, \quad m, n = 1, 2, \quad (5.244)$$

and we observe that

$$B_c^{21} = [B_c^{12}]^*, \quad (5.245)$$

and

$$S_{21} = S_{12}^*. \quad (5.246)$$

The B_c^{mn} terms represent the spatial correlation between the signals, and the S_{mn} terms represent the temporal correlation.

The determinant in (5.243) is a quadratic equation in λ ,

$$\lambda^2 - b\lambda + c = 0, \quad (5.247)$$

where

$$b = N [S_1 + S_2 + 2\operatorname{Re}[S_{12}B_c^{21}]], \quad (5.248)$$

and

$$c = N^2 S_1 S_2 [(1 - |\rho|^2)(1 - |B_c^{12}|^2)], \quad (5.249)$$

where

$$\rho = \frac{S_{12}}{(S_1 S_2)^{\frac{1}{2}}}, \quad (5.250)$$

is the temporal signal correlation. Then,

$$\lambda = \frac{b}{2} \left[1 \pm \sqrt{1 - \frac{4c}{b^2}} \right]. \quad (5.251)$$

Using (5.248) and (5.249) in (5.251) gives

$$\begin{aligned} \lambda_{1(2)} &= \frac{1}{2} N \left[S_1 + S_2 + 2(S_1 S_2)^{\frac{1}{2}} \operatorname{Re}[\rho^* B_c^{12}] \right] \\ &\cdot \left[1 \pm \sqrt{1 - \frac{4S_1 S_2 (1 - |B_c^{12}|^2)(1 - |\rho|^2)}{[S_1 + S_2 + 2(S_1 S_2)^{\frac{1}{2}} \operatorname{Re}[\rho^* B_c^{12}]]^2}} \right], \end{aligned} \quad (5.252)$$

where λ_1 corresponds to the plus sign and λ_2 corresponds to the minus sign.

The two eigenvectors are given by (5.224),

$$\Phi_1 = c_{11}\mathbf{v}(\mathbf{k}_1) + c_{12}\mathbf{v}(\mathbf{k}_2), \quad (5.253)$$

$$\Phi_2 = c_{21}\mathbf{v}(\mathbf{k}_1) + c_{22}\mathbf{v}(\mathbf{k}_2), \quad (5.254)$$

where $\mathbf{c}_i, i = 1, 2$, is obtained from (5.228) using the eigenvalues obtained from (5.247).

Note that all of the results to this point are for an arbitrary array and the array geometry enters through the conventional beam pattern.

For the case of uncorrelated signals

$$\lambda_{1(2)} = \frac{1}{2}N[(S_1 + S_2)] \left[1 \pm \sqrt{1 - \frac{4S_1S_2(1 - |B_c^{12}|^2)}{(S_1 + S_2)^2}} \right]. \quad (5.255)$$

For equal-power uncorrelated signals, (5.255) reduces to

$$\lambda_{1(2)} = NS_1 [1 \pm |B_c^{12}|], \quad (5.256)$$

and

$$\mathbf{c}_1 = \frac{1}{\sqrt{2N[1 + |B_c^{12}|]}} \begin{bmatrix} 1 \\ e^{-j\phi(B_c^{12})} \end{bmatrix}, \quad (5.257)$$

$$\mathbf{c}_2 = \frac{1}{\sqrt{2N[1 - |B_c^{12}|]}} \begin{bmatrix} 1 \\ -e^{-j\phi(B_c^{12})} \end{bmatrix}, \quad (5.258)$$

where $\phi(B_c^{12})$ denotes the phase of B_c^{12} . The corresponding normalized eigenvectors are

$$\Phi_{1(2)} = \frac{\mathbf{v}(\mathbf{k}_1) \pm e^{-j\phi(B_c^{12})}\mathbf{v}(\mathbf{k}_2)}{\sqrt{2N[1 \pm |B_c^{12}|]}}. \quad (5.259)$$

For a standard linear array,

$$B_c^{12} = \frac{1}{N} \frac{\sin\left(\frac{N}{2}\pi\Delta u\right)}{\sin\left(\frac{1}{2}\pi\Delta u\right)}. \quad (5.260)$$

In Figure 5.10, we plot $\frac{\lambda_1}{NS_1}$ and $\frac{\lambda_2}{NS_1}$ in dB versus $\frac{\Delta u}{BW_{NN}}$ on a log scale. The behavior is what we would expect. For small Δu , the largest eigenvalue approaches 2 and the smallest approaches zero. We see that the plot is linear for $\frac{\Delta u}{BW_{NN}} \leq 0.2$ and that λ_2 has a slope of $\frac{20 \text{ dB}}{\text{decade}}$. When B_c^{12} has a null, the two eigenvalues are equal because the two directional signals already defined a 2-D subspace with an orthogonal base. Once Δu goes beyond the first null in the beam pattern ($\Delta u = \frac{2}{N}$), the value of B_c^{12} is low (≤ 13.4 dB) so that the two eigenvalues are approximately equal.

In Figure 5.11, we plot the eigenbeams¹⁶ for two signals placed symmetric around $u = 0$ for various values of $\frac{\Delta u}{BW_{NN}}$.

A second case of interest is the unequal signal case when one signal is much larger (≥ 10 dB) than the other. In Figure 5.12, we show the eigenvalue behavior for the case when $\frac{S_1}{S_2} = 0$ dB, 3 dB, 10 dB, and 20 dB.

From (5.252), we see that temporal correlation has the same effect as spatial correlation. In Figure 5.13, we plot the two eigenvalues versus ρ , for various Δu . Note the importance of the phase of $\rho; \phi_\rho$, in the eigenvalue behavior.

If $|\rho| = 1$, then (5.252) shows that $\lambda_2 = 0$. Thus, the signal subspace is 1-D instead of 2-D. This situation occurs when the two signals are coherent.

¹⁶An eigenbeam is a beam obtained when the Hermitian transpose of an eigenvector is used as the weight vector.

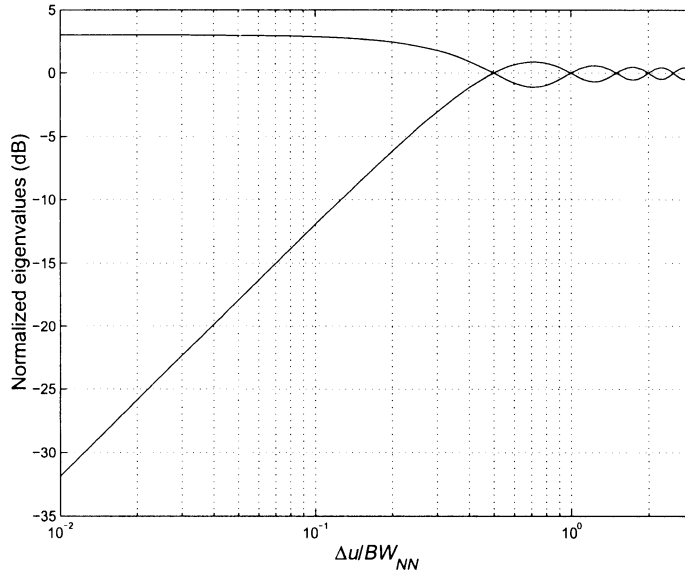


Figure 5.10 Normalized eigenvalues versus $\Delta u/BW_{NN}$.

One of the difficult cases that we encounter in various applications is the case when Δu is small (i.e., the plane waves are arriving from almost the same direction). For small Δu , we define¹⁷

$$\varepsilon^2 = 1 - |B_c^{12}|^2. \quad (5.261)$$

Then for small ε^2 ,

$$\lambda_1 \simeq N(S_1 + S_2), \quad (5.262)$$

and

$$\lambda_2 \simeq N \frac{S_1 S_2 \varepsilon^2}{S_1 + S_2}. \quad (5.263)$$

For small Δu and a standard linear array,

$$B_c^{12} \simeq 1 - \frac{N^2 - 1}{24} (\pi \Delta u)^2 = 1 - \frac{N^2 - 1}{24} (\Delta\psi)^2. \quad (5.264)$$

For closely spaced sources with high correlation,

$$\lambda_1 \simeq N(S_1^{\frac{1}{2}} + S_2^{\frac{1}{2}})^2, \quad (5.265)$$

and

$$\lambda_2 \simeq \frac{2N S_1 S_2 \varepsilon_u^2 \varepsilon_p^2}{(S_1^{\frac{1}{2}} + S_2^{\frac{1}{2}})^2}. \quad (5.266)$$

¹⁷The results are contained in [Hud81].

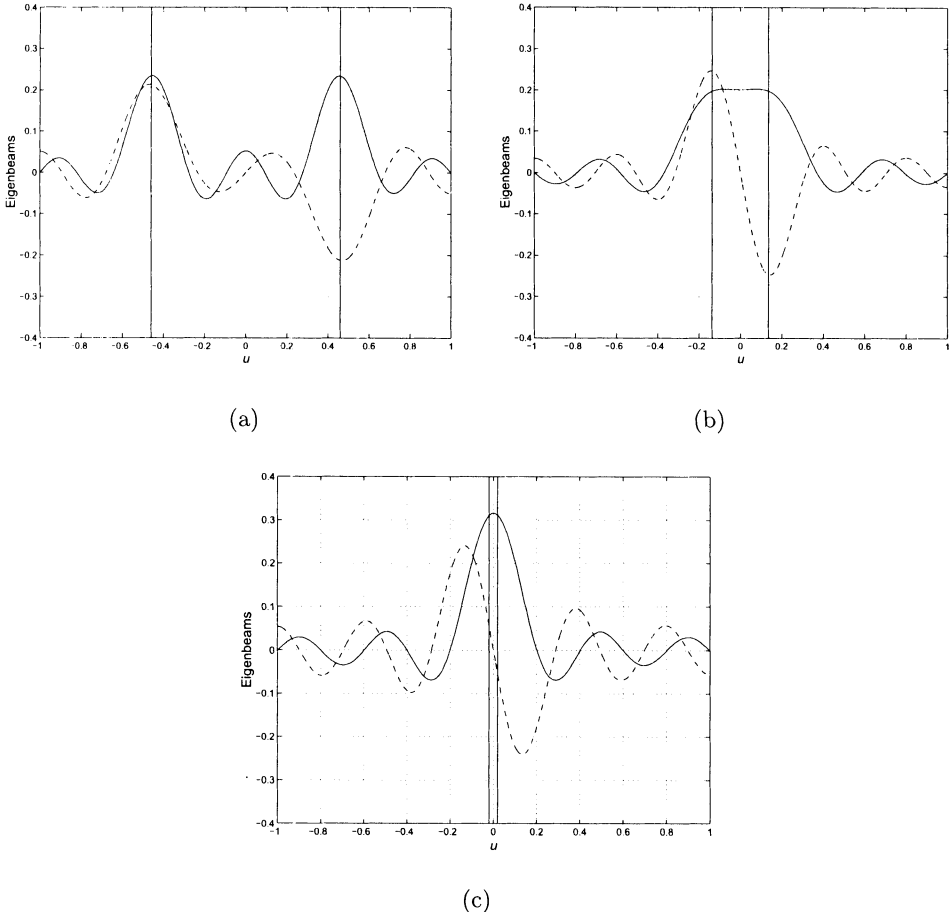


Figure 5.11 Eigenbeams for the two directional signals case: 10-element standard linear array (a) $\Delta u = 2.3BW_{NN}$; (b) $\Delta u = 0.68BW_{NN}$; (c) $\Delta u = 0.1BW_{NN}$.

For more than two directional signals at arbitrary angles, (5.228) must be solved numerically. There are various algorithms that enable this to be accomplished in a straightforward manner (e.g., [KSL94]). For certain geometries and array configurations, we can solve the 3- and 4-directional signal cases analytically by exploiting the centrosymmetric and persymmetric nature of $\mathbf{S}_f \mathbf{V}^H \mathbf{V}$. Various other signal and array geometries are studied in the problems.

For temporally uncorrelated signals, the conventional beam pattern matrix $[\mathbf{V}^H \mathbf{V}]$ is the key factor in the eigenvalue calculations. If the directional

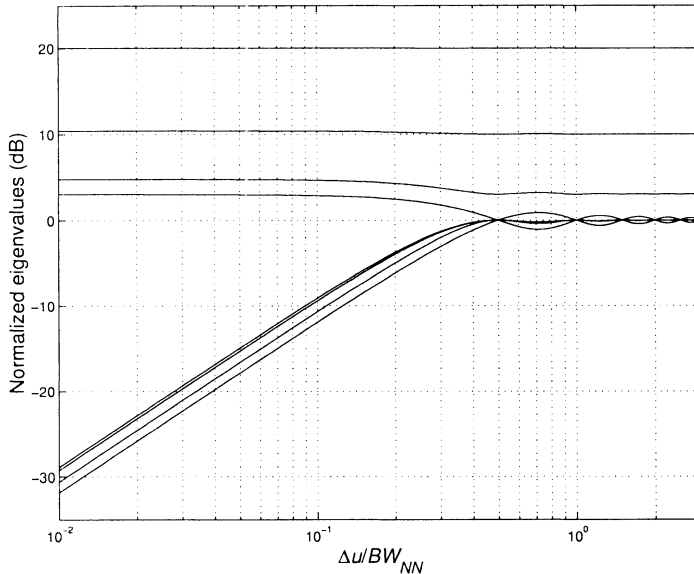


Figure 5.12 Eigenvalue behavior for unequal signals: $S_1/S_2 = 0$ dB, 3 dB, 10 dB, and 20 dB.

signals have the same spectrum and are outside the main lobes of the beams formed by the other directional signals, then the eigenvalues will approach N times the spectral heights of the various signals and the signals will have only modest impact on each other.

5.5.2 Spatially Spread Signals

We now consider an example of spatially spread signals to illustrate the eigendecomposition process.

Example 5.5.2

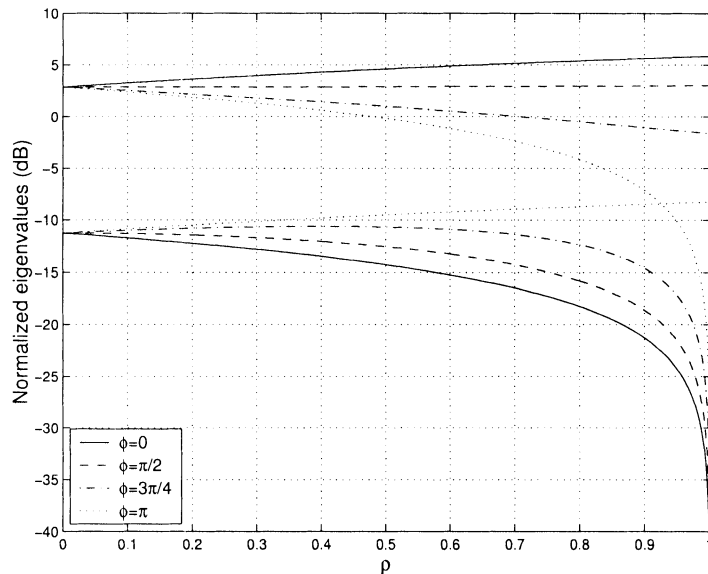
Consider an N -element standard linear array. The array manifold vector for a signal arriving from direction u is,

$$[\mathbf{v}(u)]_n = e^{j(n-\frac{N-1}{2})\pi u}, \quad n = 0, 1, \dots, N-1. \quad (5.267)$$

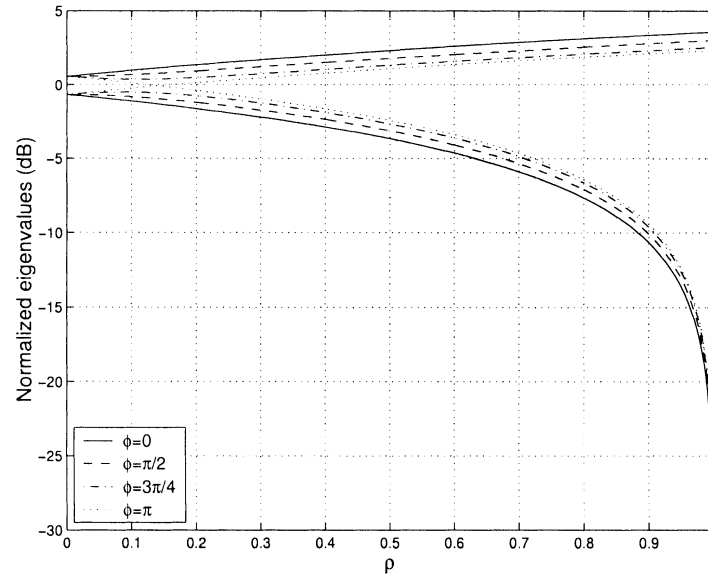
The resulting spectral matrix for a signal with unity power is

$$\begin{aligned} [\mathbf{S}_x]_{nm} &= e^{j(n-\frac{N-1}{2})\pi u} e^{-j(m-\frac{N-1}{2})\pi u} \\ &= e^{j(n-m)\pi u}. \end{aligned} \quad (5.268)$$

Now assume that the signal direction is centered at broadside and is spread uniformly in

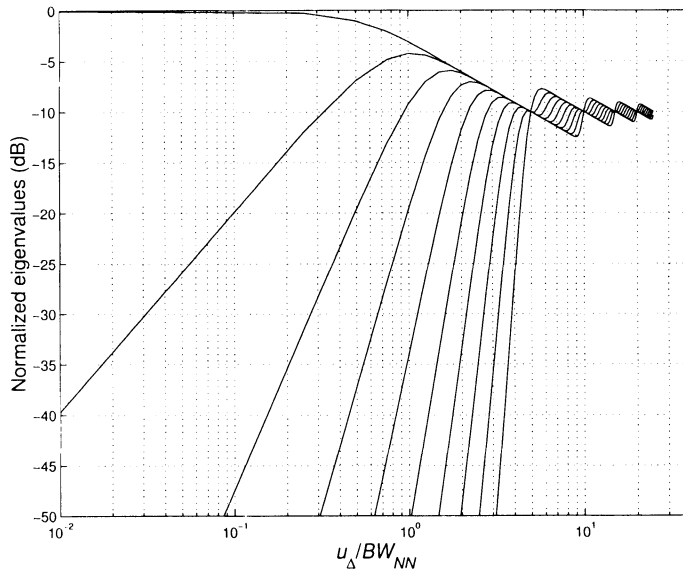


(a)



(b)

Figure 5.13 Eigenvalues for two correlated signals: $SNR_1 = SNR_2 = 0$ dB
 (a) $\Delta u = 0.0433$; (b) $\Delta u = 0.5$.

Figure 5.14 Eigenvalues as a function of u_Δ/BW_{NN} .

u-space,

$$P_1(\omega : u) = \begin{cases} \frac{\sigma_s^2}{u_\Delta}, & |u| \leq \frac{u_\Delta}{2}, \\ 0, & \text{elsewhere.} \end{cases} \quad (5.269)$$

Then,

$$\begin{aligned} [\mathbf{S}_x]_{nm} &= \int_{-u_\Delta/2}^{u_\Delta/2} \frac{\sigma_s^2}{u_\Delta} e^{-j(n-m)\pi u} \\ &= \sigma_s^2 \operatorname{sinc}\left((n-m) \frac{\pi u_\Delta}{2}\right). \end{aligned} \quad (5.270)$$

Using (5.270) in (5.214) and writing out the matrix multiplication gives

$$\lambda \Phi_n = \sigma_s^2 \sum_{m=1}^N \operatorname{sinc}\left((n-m) \frac{\pi u_\Delta}{2}\right) \Phi_m, \quad n = 1, \dots, N. \quad (5.271)$$

We see that this is exactly the same problem as in Section 3.1 (see Figure 3.5), so the eigenvectors will consist of the *discrete prolate spheroidal sequences*.

In Figure 5.14, we plot the normalized eigenvalues for a 10-element array and various values of u_Δ/BW_{NN} . As u_Δ goes to zero, the wavenumber spectrum approaches that of a single directional signal. As u_Δ goes to 2, the wavenumber spectrum corresponds to “one-dimensional” isotropic noise.

The number of significant eigenvalues is

$$N_{SE} = \frac{u_\Delta}{2} N + 1. \quad (5.272)$$

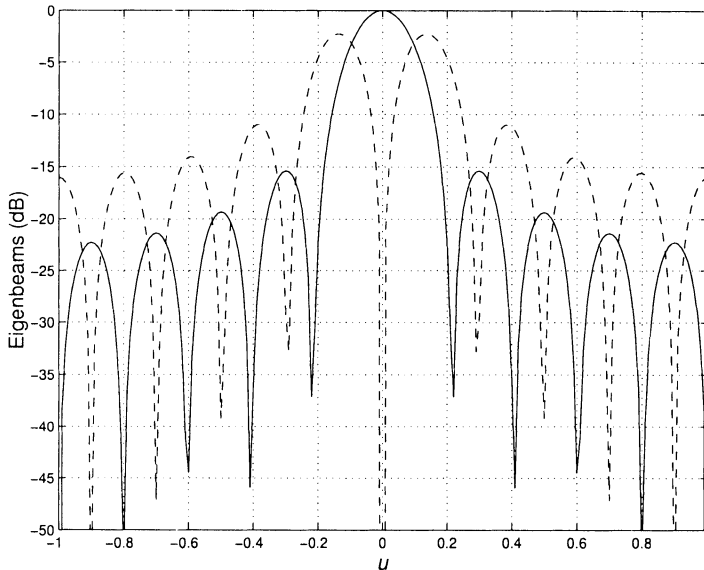


Figure 5.15 Eigenbeams for $u_\Delta = 0.2$.

This is the number we would expect from our sampling discussion in Section 2.4.6 and Section 5.2.4. In Figure 5.15, we show the eigenvectors and eigenbeams corresponding to $u_\Delta = 0.2$. Note that the second eigenvector is asymmetric so the corresponding beam pattern is imaginary and asymmetric. Thus, the eigenbeams correspond to sum and difference beams.

From Figure 5.14, we see that for very small u_Δ there is only one significant eigenvalue. As u_Δ increases, the second eigenvalue increases to a significant level. In later sections, we design an optimum processing algorithms under the assumption that the signal is not spread. We would like to be able to test how large u_Δ can be without violating the assumption. We hypothesize that we can test the behavior by examining the behavior of the second eigenvalue.¹⁸

In order to get a simple expression, we replace the spatially spread signal by two point sources placed symmetrically about $u = 0$. We choose the spacing so that the variances match. The variance in (5.269) is

$$\sigma_u^2 = \sigma_s^2 \frac{u_\Delta^2}{12}. \quad (5.273)$$

Therefore, we use two uncorrelated point source plane-wave signals with power $\sigma_s^2/2$ located at

$$u_s = \pm \frac{u_\Delta}{2\sqrt{3}}. \quad (5.274)$$

¹⁸This approach is developed in the context of finite bandwidth signals by Zatman [Zat98]. We consider that model in Section 5.5.3.

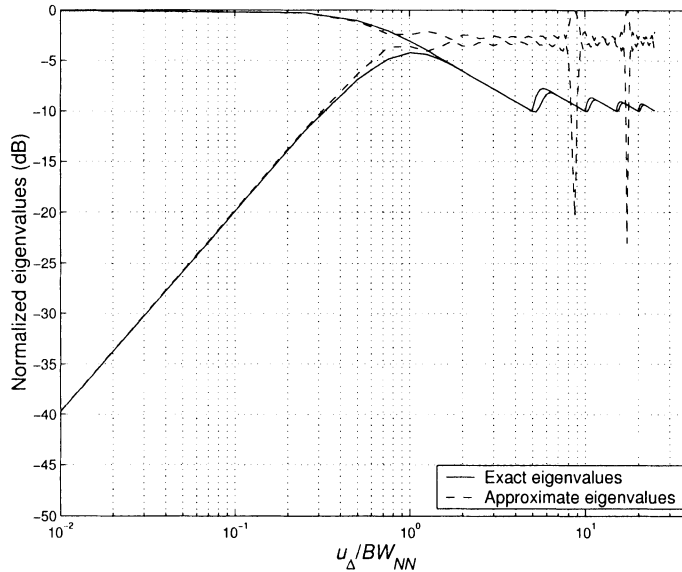


Figure 5.16 Behavior of two largest eigenvalues of a spatially spread signal.

Using (5.274) in (5.256), we obtain

$$\lambda_{1(2)} = \frac{N\sigma_s^2}{2} [1 \pm |B_c^{12}|], \quad (5.275)$$

where, from (2.97),

$$B_c^{12} = \frac{\sin(N\pi u_s)}{N \sin(\pi u_s)} = \frac{\sin(\frac{N\pi u_\Delta}{2\sqrt{3}})}{N \sin(\frac{\pi u_\Delta}{2\sqrt{3}})}. \quad (5.276)$$

In Figure 5.16, we plot the exact value of $\lambda_{1(2)}$ from (5.271) and the approximate value of $\lambda_{1(2)}$ from (5.275). We see that the approximation is accurate for $u \leq 0.5BW_{NN}$.

In most cases of interest we observe the signals of interest in the presence of additive white noise of spectral height σ_w^2 being added to each eigenvalue. We hypothesize that if the second eigenvalue is less than the noise eigenvalue that the performance of algorithms designed for point source signals will not be degraded significantly when the signal is spatially spread. Thus,

$$\frac{N\sigma_s^2}{2} \left(1 - \left| \frac{\sin(\frac{N\pi u_\Delta}{2\sqrt{3}})}{N \sin(\frac{\pi u_\Delta}{2\sqrt{3}})} \right| \right) \leq \sigma_w^2, \quad (5.277)$$

is a tentative criterion. We will revisit it later in the text.

5.5.3 Frequency-spread Signals

In most of our discussions we have assumed that the signals were narrowband. In Section 2.2 (following (2.47)) we gave a heuristic definition of the narrowband assumption. We now revisit the question in the context of the behavior of the eigenvalues.

In this section, we find the eigenvalues and eigenvectors of a point source whose temporal bandwidth is non-zero. In Section 5.5.2, we found that each point source resulted in one eigenvalue in \mathbf{S}_x . We find that, for a non-zero bandwidth signal, there are N non-zero eigenvalues. However, for the bandwidths of interest in the present discussion, only the first and second eigenvalues are significant.

The effect of finite bandwidth on the eigenvalues has been analyzed by Hudson (see pp.144–148 of [Hud81]). Compton [Com88] also discusses bandwidth effects in the context of array performance.

We restrict our attention to a uniform linear array. Most of the results carry over to other array geometries. We consider a single point source arriving from $u_s = \cos \theta_s$ in u -space.

The array manifold vector is

$$[\mathbf{v}(\psi)]_n = e^{j(n-\frac{N-1}{2})\psi}, \quad n = 0, \dots, N-1, \quad (5.278)$$

where

$$\psi = \frac{2\pi d}{\lambda} u_s = \frac{2\pi df}{c} u_s. \quad (5.279)$$

The interelement time delay is

$$\tau_{nm} = \frac{(n-m)d}{c} u_s. \quad (5.280)$$

If we assume the array design frequency is f_c , then an array with $\lambda_c/2$ spacing has¹⁹

$$d = \frac{\lambda_c}{2} = \frac{c}{2f_c}. \quad (5.281)$$

Using (5.281) in (5.280) and (5.279) gives

$$\tau_{nm} = \frac{(n-m)}{2f_c} u_s \quad (5.282)$$

and

$$\psi = \frac{\pi f}{f_c} u_s. \quad (5.283)$$

¹⁹In many cases, the design frequency of the array will be the highest frequency, $f_u = f_c + B_s/2$. A similar result to (5.290) can be derived.

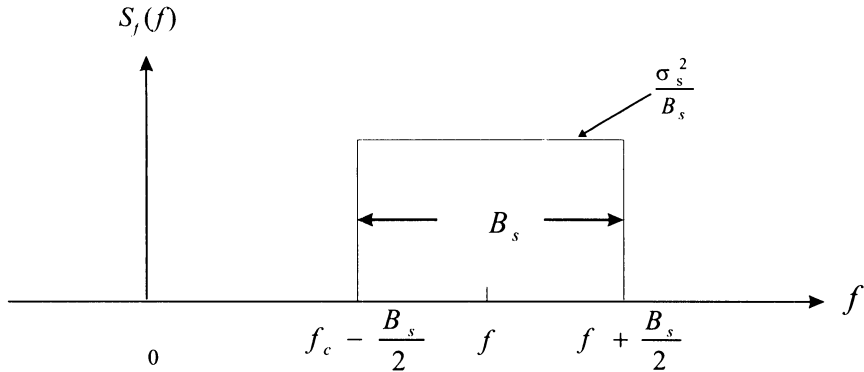


Figure 5.17 Frequency-spread source signal.

For simplicity, we assume the source has the temporal spectrum shown in Figure 5.17. We have assumed narrowband processing, so the spatial spectral matrix for $\omega_\Delta = 0$ is the matrix of interest:

$$[\mathbf{S}_x(f_c)]_{nm} = \int_{f_c-B_s/2}^{f_c+B_s/2} \frac{\sigma_s^2}{B_s} e^{j(n-\frac{N-1}{2})\psi} e^{-j(m-\frac{N-1}{2})\psi} df. \quad (5.284)$$

Using (5.283) and (5.282) in (5.284) gives

$$[\mathbf{S}_x(f_c)]_{nm} = \frac{\sigma_s^2}{B_s} \int_{f_c-B_s/2}^{f_c+B_s/2} e^{j2\pi\tau_{nm}f} df, \quad (5.285)$$

which reduces to

$$[\mathbf{S}_x(f_c)]_{nm} = \sigma_s^2 \text{sinc}(\pi\tau_{nm}B_s), \quad (5.286)$$

or

$$[\mathbf{S}_x(f_c)]_{nm} = \sigma_s^2 \text{sinc}\left(\frac{\pi}{2}(n-m)B_f u_s\right), \quad (5.287)$$

where

$$B_f \triangleq \frac{B_s}{f_c} \quad (5.288)$$

is the ratio of the signal bandwidth to the center frequency.

Comparing (5.287) and (5.270), we see that if we let

$$B_f u_s = u_\Delta, \quad (5.289)$$

the two expressions are identical. Thus the eigenvalue plot in Figure 5.14 applies to the frequency-spread case if we relabel the axis.

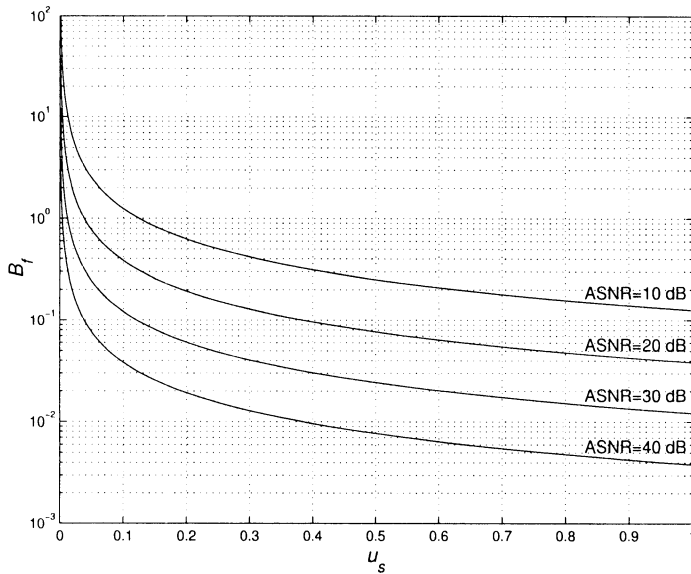


Figure 5.18 Threshold SNR for narrowband assumption: standard linear array.

The subsequent discussion leading to (5.277) also applies. Thus, we can hypothesize a test for the narrowband assumption as²⁰

$$\frac{N\sigma_s^2}{2} \left(1 - \left| \frac{\sin(\frac{N\pi B_f u_s}{2\sqrt{3}})}{N \sin(\frac{\pi B_f u_s}{2\sqrt{3}})} \right| \right) \leq \sigma_w^2. \quad (5.290)$$

We investigate the validity of this criterion later in the text. In Figure 5.18, we plot (5.290) with an equality sign for various array signal-to-noise ratios ($ASNRs$), where

$$ASNR = \frac{N\sigma_s^2}{\sigma_w^2}. \quad (5.291)$$

The duality between spatial spreading and frequency spreading holds for linear arrays. For other array geometries, the effects must be analyzed individually.

In our discussion, we used a uniform temporal frequency spectrum. The results for other spectral shapes follow in a straightforward manner.

²⁰This criterion is due to Zatman [Zat98].

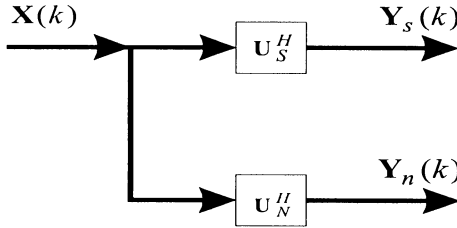


Figure 5.19 Eigenvector beamspace processor.

5.5.4 Closely Spaced Signals

One of the important cases that we encounter in subsequent chapters is the one in which we have D signals that are closely spaced (or clustered) in ψ -space.

Lee [Lee92] has developed approximate expressions for the eigenvalues and eigenvectors that are useful in some analyses. The derivation is lengthy, so we refer the reader to [Lee92] for the derivation and discussion.

5.5.5 Beamspace Processors

In many applications, we will find it useful to interpret the eigenvector decomposition as a beamspace processor. The model is shown in Figure 5.19. The input consists of a Gaussian signal plus additive independent Gaussian sensor noise. In the snapshot model,

$$\mathbf{X}(k) = \mathbf{V}\mathbf{F}(k) + \mathbf{W}(k), \quad k = 1, 2, \dots, K. \quad (5.292)$$

The signal subspace processor is \mathbf{U}_S^H , where

$$\mathbf{U}_S = \left[\begin{array}{c|c|c|c} \Phi_1 & \Phi_2 & \cdots & \Phi_D \end{array} \right], \quad (5.293)$$

is an $N \times D$ matrix of the normalized eigenvectors of $\mathbf{V}\mathbf{S}_f\mathbf{V}^H$.

The noise subspace processor is \mathbf{U}_N^H , where

$$\mathbf{U}_N = \left[\begin{array}{c|c|c|c} \Phi_{D+1} & \Phi_{D+2} & \cdots & \Phi_N \end{array} \right], \quad (5.294)$$

is an $N \times (N - D)$ matrix whose columns are orthogonal to \mathbf{U}_S .

The advantage of this interpretation is that $\mathbf{Y}_s(k)$, the output of the signal subspace processor, is a sufficient statistic and the output $\mathbf{Y}_n(k)$ can be discarded. All of our subsequent processing deals with the $D \times 1$ vector $\mathbf{Y}_s(k)$.

Note that there is still noise in $\mathbf{Y}_s(k)$. However, since \mathbf{U}_S has orthonormal columns, it is white noise:

$$E \left[\mathbf{Y}_s(k) \mathbf{Y}_s^H(k) \right] = \mathbf{U}_S^H \mathbf{V} \mathbf{S}_f \mathbf{V}^H \mathbf{U}_S + \sigma_w^2 \mathbf{U}_S^H \mathbf{I} \mathbf{U}_S. \quad (5.295)$$

Using (5.237) and (5.238),

$$\mathbf{S}_{\mathbf{Y}_s} = \mathbf{\Lambda}_S + \sigma_w^2 \mathbf{I}. \quad (5.296)$$

Thus, our eigenvector beamspace processor has uncorrelated (statistically independent in the Gaussian model) outputs.

5.5.6 Subspaces for Spatially Spread Signals

For directional signal models in the presence of white noise, the concept and construction of a D -dimensional subspace is straightforward. The columns of the \mathbf{V} matrix define a D -dimensional subspace and the corresponding eigenvectors form an orthonormal basis for the subspace.

The subspace concept is also useful for spatially spread signals in which the number of significant eigenvalues is less than N . We can illustrate this idea with a simple example.

Example 5.5.3

Consider the standard linear array in Example 5.5.1 and the wavenumber function in (5.269).

We define $D_s(M)$ as the dimension of the subspace. M is $-10 \log$ (percentage of the signal power outside the subspace). In Figure 5.20, we plot $D_s(M)$ for several M for a standard 11-element array versus u_Δ/BW_{NN} .

We see that, for $u_\Delta < BW_{NN}$, the number of eigenvalues required is not sensitive to the specific value of $D_s(M)$. In many applications, we use $M = 20$ dB (or 0.01 signal power outside the subspace).

5.6 Parametric Wavenumber Models

In Section 5.3, we modeled space-time fields by starting with a distribution in space that was based on some knowledge of the environment. Once the statistical properties of the space-time field were specified we could find the statistical properties of the array input.²¹

In this section we take a different approach. We create a parametric model of the mechanism that generates a random field whose spatial spectrum matches observed data at the array. The process generation model is

²¹This section may be omitted at first reading by readers who are primarily interested in plane-wave models.

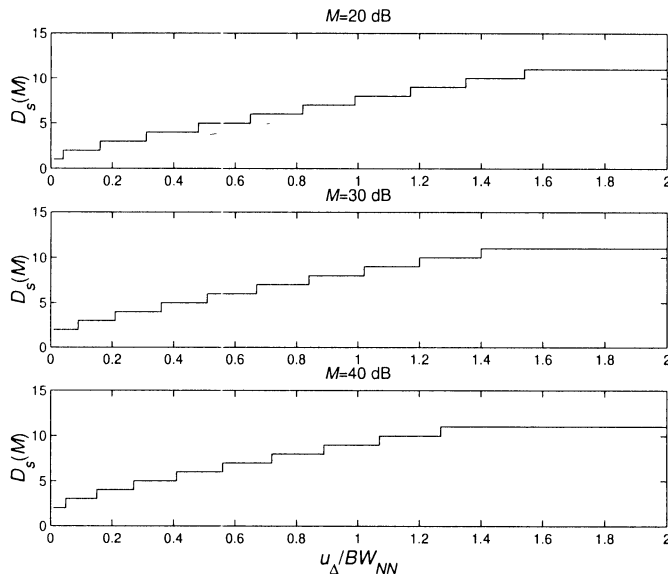


Figure 5.20 Dimension of approximate signal subspace: Number of eigenvalues required for various $D_s(M)$ versus u_Δ/BW_{NN} : $M = 20$ dB, 30 dB, and 40 dB.

not necessarily related to the actual physical mechanism that generates the observed spatial spectra.

The technique was originally used in the estimation of temporal power spectrum.²² We restrict our attention to a standard N element linear array.

We refer to the model that we develop as a rational transfer function model. These models have been widely used in both continuous and discrete time problems for a number of years.

5.6.1 Rational Transfer Function Models

For the purpose of developing the model, we assume the input sequence to the digital system shown in Figure 5.21 is a white noise sequence $u(n)$ and the output sequence is $x(n)$. Note that $u(n)$ is used to develop the model and is not an actual input to the array. In the array context, $x(n)$ is a complex variable that represents the frequency-domain snapshot from the

²²There are number of good discussions of parametric models (for example, [Kay88], [Mar87], [PRLN92], [Hay91]). Our discussion is similar to Chapter 5 of [Kay88] and Chapter 6 of [Mar87]. A discussion of various models for spatially spread sources is contained in Wakefield and Kaveh [WK85].

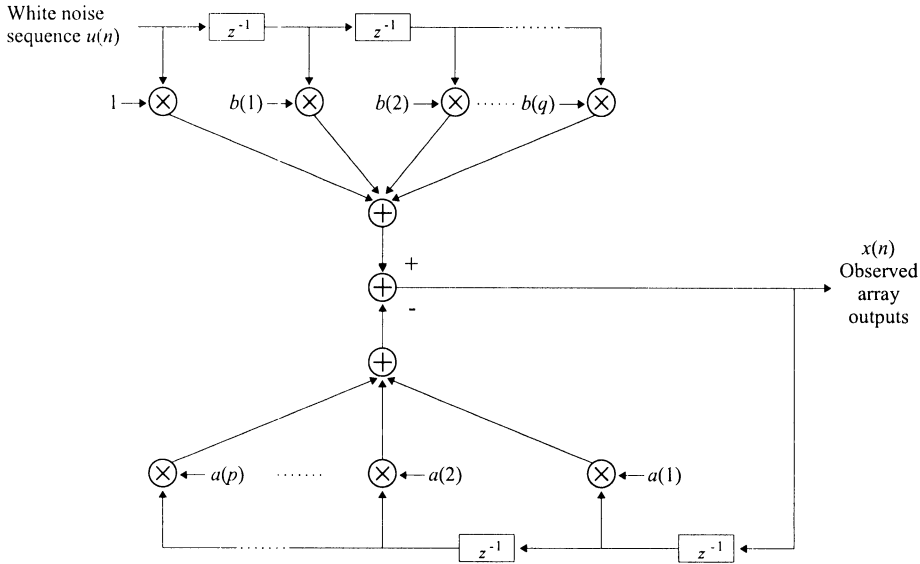


Figure 5.21 Auto-regressive moving average model of random field.

n th element of the array at snapshot time k . Our development does not depend on k , so we suppress k in our notation. We also use $x(n)$ to denote the snapshot instead of $X(n)$ to simplify the subsequent notation.

Our objective is to develop a model for the spatial correlation between sensor outputs. The input and output are related by a linear difference equation

$$x(n) = - \sum_{m=1}^p a(m)x(n-m) + \sum_{m=0}^q b(m)u(n-m), \quad 1 \leq n \leq N. \quad (5.297)$$

The general model is referred to as the ARMA model. It is shown in Figure 5.21. Note that in (5.297), the sequence is across the array at a single snapshot.

The z -transform of the system is

$$H(z) = \frac{B(z)}{A(z)}, \quad (5.298)$$

where

$$A(z) = \sum_{m=0}^p a(m)z^{-m}, \quad (5.299)$$

and

$$B(z) = \sum_{m=0}^q b(m)z^{-m}, \quad (5.300)$$

and we require that all the zeros of $A(z)$ be inside the unit circle. This guarantees that $H(z)$ is a stable, realizable system (e.g., [OS89]).

The output spectrum in the z -domain is

$$P_{xx}(z) = H(z)H^*\left(\frac{1}{z^*}\right)P_{uu}(z) \quad (5.301)$$

$$= \frac{B(z)B^*\left(\frac{1}{z^*}\right)}{A(z)A^*\left(\frac{1}{z^*}\right)}P_{uu}(z). \quad (5.302)$$

Evaluating at $z = e^{j\psi}$ gives the wavenumber spectrum of $x(n)$ in ψ -space.²³ Thus,

$$P_{xx}(z)|_{z=e^{j\psi}} \triangleq \tilde{P}_{xx}(\psi) = \sigma_u^2 \left| \frac{\tilde{B}(\psi)}{\tilde{A}(\psi)} \right|^2, \quad (5.303)$$

where σ_u^2 is the variance of the input process. We can assume $b(0)$ and $a(0)$ equal 1 and incorporate the filter gain in σ_u^2 . This model is referred to as an ARMA(p, q) process.

The corresponding spatial correlation values are obtained by taking the inverse transform of (5.302). We write

$$P_{xx}(z)A(z) = D^*\left(\frac{1}{z^*}\right)B(z)\sigma_u^2, \quad (5.304)$$

where

$$D^*\left(\frac{1}{z^*}\right) = \frac{B^*\left(\frac{1}{z^*}\right)}{A^*\left(\frac{1}{z^*}\right)}. \quad (5.305)$$

The inverse z -transform of (5.304) is

$$\sum_{l=0}^p a(l)r_{xx}(m-l) = \sigma_u^2 \sum_{l=0}^q b(l)d^*(l-m). \quad (5.306)$$

Since $d(m) = 0$ for $m < 0$, (5.306) reduces to

$$r_{xx}(m) = \begin{cases} -\sum_{l=1}^p a(l)r_{xx}(m-l) + \sigma_u^2 \sum_{l=0}^{q-m} d^*(l)b(l+m), & 0 \leq m \leq q, \\ -\sum_{l=1}^p a(l)r_{xx}(m-l), & m \geq q+1. \end{cases} \quad (5.307)$$

²³Recall that $\psi = k_z d = \pi \cos \theta$ so that there is an exact correspondence between ψ in the space domain and ω in time series analysis.

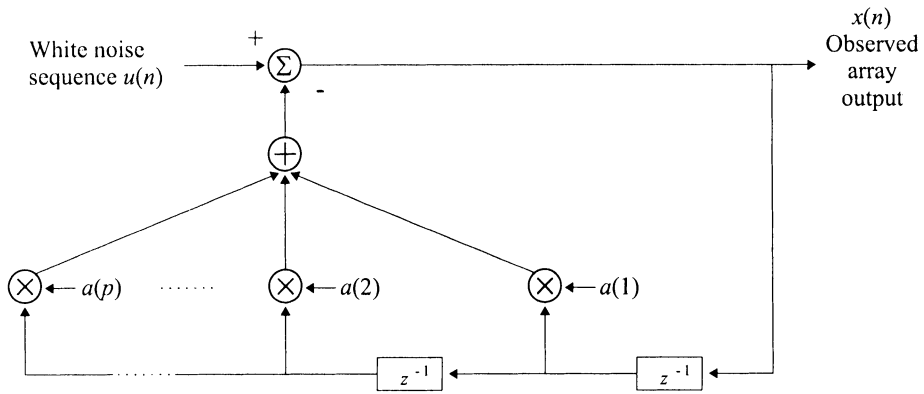


Figure 5.22 Auto-regressive model of random field.

Note that $r_{xx}(m)$ denotes the spatial correlation between the snapshot from sensor element 0 and sensor element m . We focus most of our attention on processes where all of the $b(m)$ except $b(0)$ are equal to zero. In this case,

$$x(n) = - \sum_{m=1}^p a(m)x(n-m) + u(n). \quad (5.308)$$

This model is referred to as an auto-regressive process of order p , AR(p). It is auto-regressive because it is a linear regression model acting on itself. If we define

$$\hat{x}(n) = - \sum_{m=1}^p a(m)x(n-m), \quad (5.309)$$

then

$$x(n) = \hat{x}(n) + u(n), \quad (5.310)$$

so that $u(n)$ corresponds to the error between the weighted sum of past values and the value $x(n)$.

The power spectral density is

$$\tilde{P}_{xx}(\psi) = \frac{\sigma_u^2}{|A(e^{j\psi})|^2}. \quad (5.311)$$

The AR process model is shown in Figure 5.22.

The spatial correlation values follow directly from the process generation model. From (5.311), we have

$$\tilde{P}_{xx}(\psi)A(e^{j\psi}) = \frac{\sigma_u^2}{A^*(e^{j\psi})}. \quad (5.312)$$

Taking the inverse transform of (5.312) gives

$$r_{xx}(m) = \begin{cases} -\sum_{l=1}^p a(l)r_{xx}(-l) + \sigma_u^2, & m = 0, \\ -\sum_{l=1}^p a(l)r_{xx}(m-l), & m \geq 1, \\ r_{xx}^*(-m), & m \leq -1. \end{cases} \quad (5.313)$$

In order to write (5.313) in matrix form, we define a $p \times 1$ vector \mathbf{y} as

$$\mathbf{y} = [x(0) \ x(1) \ \cdots \ x(p)]^T. \quad (5.314)$$

The result for $m \geq 1$ can be written in matrix form as

$$\tilde{\mathbf{R}}_y \mathbf{a} = -\mathbf{r}_y, \quad (5.315)$$

where $\tilde{\mathbf{R}}_y$ is a $p \times p$ matrix,

$$\tilde{\mathbf{R}}_y \triangleq \begin{bmatrix} r_{xx}[0] & r_{xx}[-1] & \cdots & r_{xx}[-(p-1)] \\ r_{xx}[1] & r_{xx}[0] & \cdots & r_{xx}[-(p-2)] \\ \vdots & \vdots & \ddots & \vdots \\ r_{xx}[p-1] & r_{xx}[p-2] & \cdots & r_{xx}[0] \end{bmatrix}, \quad (5.316)$$

which is Hermitian because $r_{xx}(-1) = r_{xx}^*(1)$. $\tilde{\mathbf{R}}_y$ is also Toeplitz.

The matrix \mathbf{a} is a $p \times 1$ matrix,

$$\mathbf{a} = [a(1) \ | \ a(2) \ | \ \cdots \ | \ a(p)]^T, \quad (5.317)$$

and \mathbf{r}_y is a $p \times 1$ matrix,

$$\mathbf{r}_y = [r_{xx}(1) \ | \ r_{xx}(2) \ | \ \cdots \ | \ r_{xx}(p)]^T. \quad (5.318)$$

The equations in (5.313) are referred to as the Yule-Walker equations.²⁴ The result can also be written in augmented form by incorporating the $m = 0$ part of (5.313):

$$\tilde{\mathbf{R}}_y^A \mathbf{a}^A = \sigma_u^2 \mathbf{e}_1, \quad (5.319)$$

²⁴Normally (5.315)–(5.318) are written with \mathbf{x} as the vector. However, in our notation, \mathbf{x} denotes an $N \times 1$ vector of the entire array output.

where

$$\tilde{\mathbf{R}}_y^A = \begin{bmatrix} r_{xx}[0] & r_{xx}[-1] & \cdots & r_{xx}[-p] \\ r_{xx}[1] & r_{xx}[0] & \cdots & r_{xx}[-(p-1)] \\ \vdots & \vdots & \ddots & \vdots \\ r_{xx}[p] & r_{xx}[p-1] & \cdots & r_{xx}[0] \end{bmatrix}, \quad (5.320)$$

$$\mathbf{a}^A = \left[1 \mid a(1) \mid \cdots \mid a(p) \right]^T, \quad (5.321)$$

and

$$\sigma_u^2 \mathbf{e}_1 = \left[\sigma_u^2 \mid 0 \mid \cdots \mid 0 \right]^T. \quad (5.322)$$

We consider several examples to illustrate the type of wavenumber spectra that can be generated using the AR process model.

Example 5.6.1

We consider a complex AR (1) process. It follows from (5.313) that

$$r_{xx}(m) = \begin{cases} -a(1)r_{xx}(m-1), & m \geq 1, \\ r_{xx}^*(-m), & m \leq -1, \end{cases} \quad (5.323)$$

or

$$r_{xx}(m) = \begin{cases} r_{xx}(0)(-a(1))^m, & m \geq 1, \\ r_{xx}^*(-m), & m \leq -1, \end{cases} \quad (5.324)$$

and

$$r_{xx}(0) = \frac{\sigma_u^2}{1 - |a(1)|^2}. \quad (5.325)$$

Note that the array spatial spectral matrix \mathbf{S}_x is a Hermitian, Toeplitz matrix whose ij element is a function of $(i-j)$ where $(i-j) = k$ in (5.323) and (5.324). For example, if $N = 4$,

$$\mathbf{S}_x = \begin{bmatrix} r_{xx}(0) & r_{xx}^*(1) & r_{xx}^*(2) & r_{xx}^*(3) \\ r_{xx}(1) & r_{xx}(0) & r_{xx}^*(1) & r_{xx}^*(2) \\ r_{xx}(2) & r_{xx}(1) & r_{xx}(0) & r_{xx}^*(1) \\ r_{xx}(3) & r_{xx}(2) & r_{xx}(1) & r_{xx}(0) \end{bmatrix}. \quad (5.326)$$

The input signal power equals $r_{xx}(0)$. The wavenumber spectrum in ψ -space is

$$\tilde{P}_{xx}(\psi) = \frac{\sigma_u^2}{|1 - z_1 e^{-j\psi}|^2}. \quad (5.327)$$

To examine the behavior, we write

$$z_1 = |z_1| e^{j\pi\phi_1}. \quad (5.328)$$

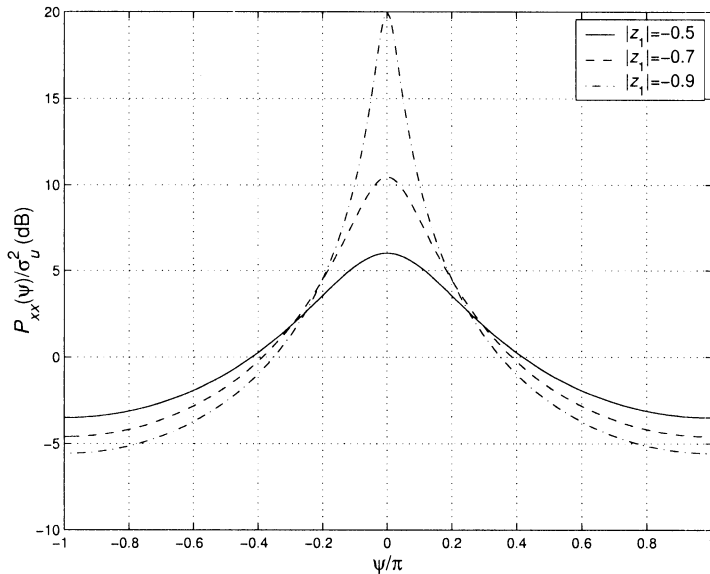


Figure 5.23 Normalized wavenumber spectra for complex AR(1) process: $|z_1| = 0.5, 0.7$, and 0.9 ; $\phi_1 = 0$.

Note that $a(1) = -z_1$. In Figure 5.23, we show the wavenumber spectrum for $|z_1| = 0.5, 0.7$, and 0.9 and $\phi_1 = 0$. We see that it corresponds to a spatially spread signal centered at $\psi = 0$. As $|z_1|$ approaches unity, it approaches the single plane-wave model. In Figure 5.24, we show the spectrum for $|z_1| = 0.7$ and $\phi_1 = 0, 0.6$, and 1.0 . We see that the effect of ϕ_1 is to shift the center of wavenumber spectrum to

$$\psi_c = \pi\phi_1. \quad (5.329)$$

In order to generate multiple peaks in the wavenumber spectrum, we need to use a higher order model.

Example 5.6.2

In this example, we consider a complex AR(2) process. Since we are trying to match an observed wavenumber spectrum, we start with the wavenumber spectrum,

$$\begin{aligned} \tilde{P}_{xx}(\psi) &= \frac{\sigma_u^2}{|(1 - z_1 e^{-j\psi})(1 - z_2 e^{-j\psi})|^2} \\ &= \frac{\sigma_u^2}{|1 - (z_1 + z_2)e^{-j\psi} + z_1 z_2 e^{-j2\psi}|^2} \\ &= \frac{\sigma_u^2}{|1 + a(1)e^{-j\psi} + a(2)e^{-j2\psi}|^2}. \end{aligned} \quad (5.330)$$

In Figure 5.25, we show the wavenumber spectra for $z_1 = 0.9$ and $z_2 = 0.7e^{-j(0.8\pi)}$. In Figure 5.26, we show the wavenumber spectra for $z_1 = 0.9e^{j(0.5\pi)}$, $z_2 = 0.9e^{j(0.7\pi)}$. We

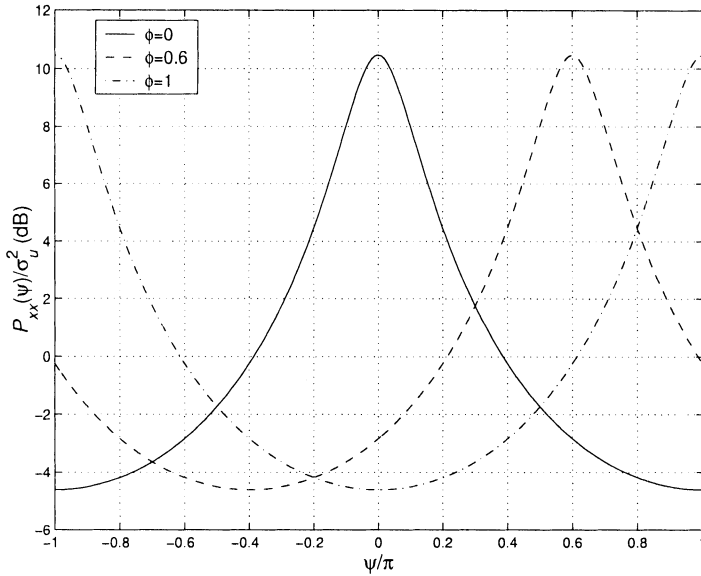


Figure 5.24 Normalized wavenumber spectra for complex AR(1) process: $|z_1| = 0.7$; $\phi_1 = 0, 0.6$, and 1.0 .

see that we can achieve reasonable flexibility in the wavenumber spectra by changing the location of the poles.

The correlation matrix can be found by taking the inverse z -transform of $P_2(\psi)$ or by substituting $a(1)$ and $a(2)$ into (5.313) and solving.

Example 5.6.3

In this example, we consider a complex AR(3) process:

$$\tilde{P}_3(\psi) = \frac{\sigma_u^2}{|(1 - z_1 e^{-j\psi})(1 - z_2 e^{-j\psi})(1 - z_3 e^{-j\psi})|^2}. \quad (5.331)$$

In Figure 5.27, we show the wavenumber spectrum for $z_1 = 0.7e^{-j(0.6\pi)}$, $z_2 = 0.7$, $z_3 = 0.7e^{j(0.6\pi)}$. In Figure 5.28, we show the wavenumber spectrum for $z_1 = 0.9e^{-j(0.7\pi)}$, $z_2 = 0.9e^{-j(0.5\pi)}$, and $z_3 = 0.7e^{j(0.4\pi)}$.

The third process of interest corresponds to the case where all of the $a(n)$ coefficients are zero except for $a[0] = 1$. Then,

$$x(n) = \sum_{m=0}^q b(m)u(n-m), \quad (5.332)$$

and the process is referred to as a moving average (MA) process.

$$\tilde{P}_{MA}(\psi) = \sigma_u^2 |\tilde{B}(\psi)|^2. \quad (5.333)$$

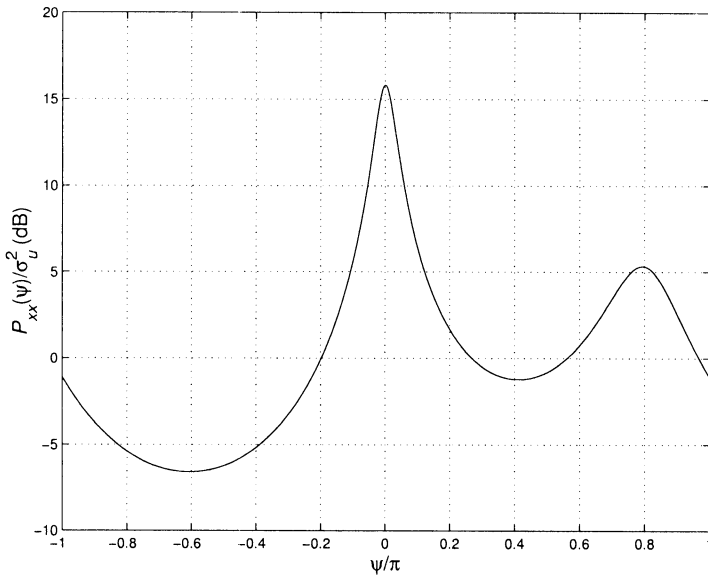


Figure 5.25 Normalized wavenumber spectrum for complex AR(2) process:
 $z_1 = 0.9, z_2 = 0.7 \exp(j(0.8\pi))$.

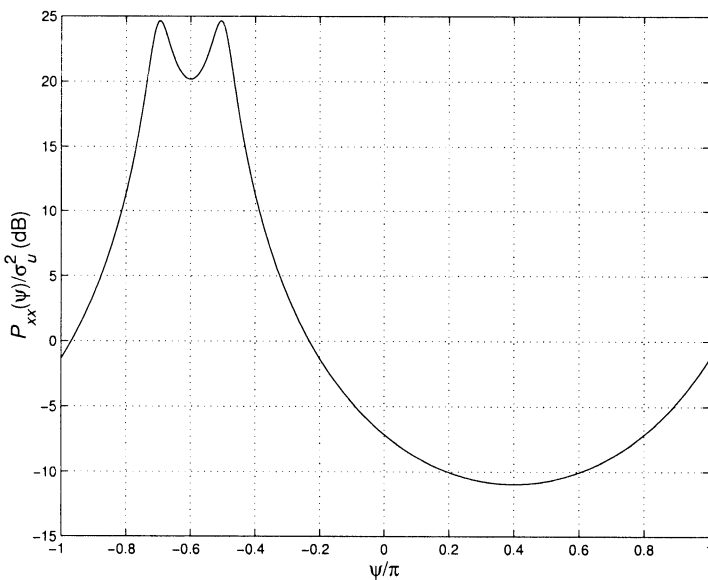


Figure 5.26 Wavenumber spectrum for complex AR(2) process: $z_1 = 0.9 \exp(-j0.5\pi), z_2 = 0.9 \exp(-j0.7\pi)$.

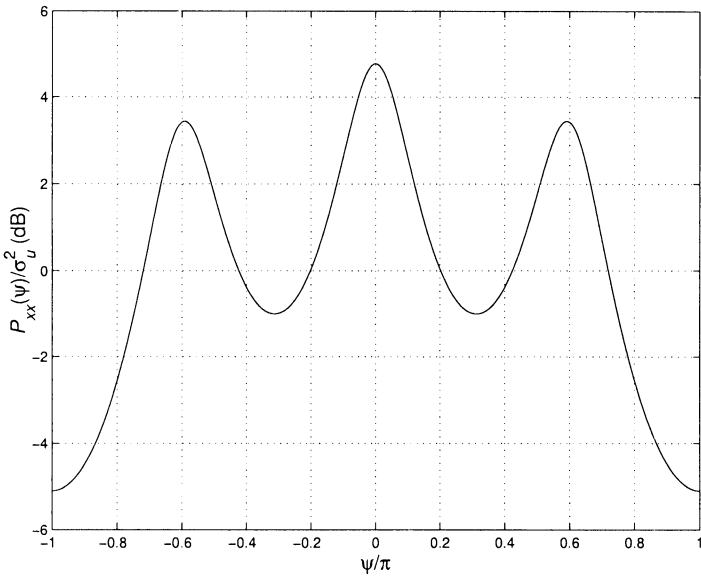


Figure 5.27 Wavenumber spectrum for complex AR(3) process: $z_1 = 0.7 \exp(-j0.6\pi)$, $z_2 = 0.7$, $z_3 = 0.7 \exp(j0.6\pi)$.

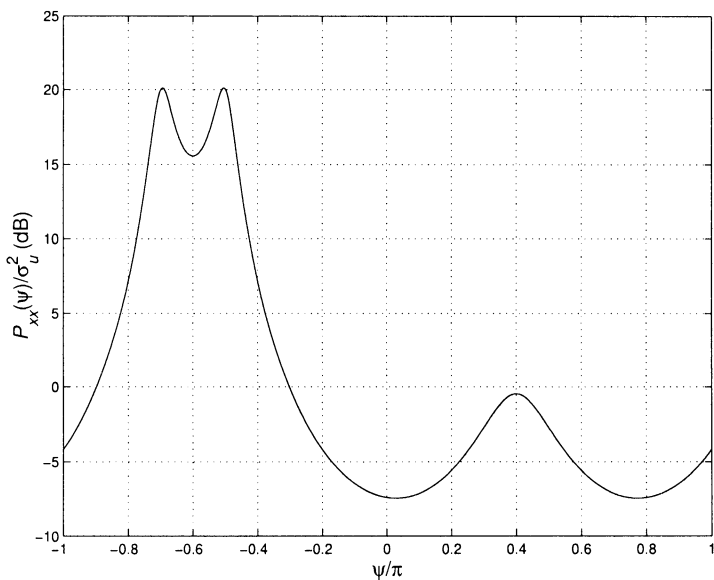


Figure 5.28 Wavenumber spectrum for complex AR(3) process: $z_1 = 0.9 \exp(-j0.7\pi)$, $z_2 = 0.9 \exp(-j0.5\pi)$, $z_3 = 0.7 \exp(j0.4\pi)$.

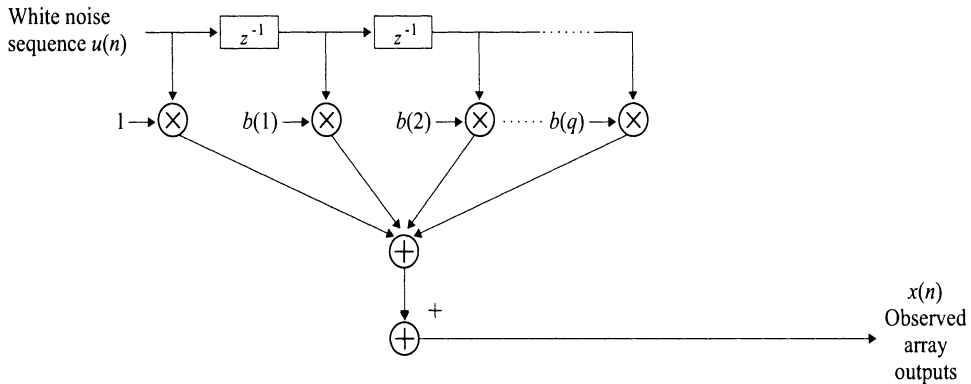


Figure 5.29 Moving average model of random field.

The model is shown in Figure 5.29. The corresponding correlation values can be obtained by letting $a(l) = \delta(l)$ and $d(l) = b(l)$ in (5.307). Then

$$r_{xx}(m) = \begin{cases} \sigma_u^2 \sum_{l=0}^{q-m} b^*(l)b(m+l), & m = 0, 1, \dots, q, \\ 0, & m \geq q+1. \end{cases} \quad (5.334)$$

For a complex MA(1) process,

$$r_{xx}(m) = \begin{cases} \sigma_u^2 [1 + |b(1)|^2], & m = 0, \\ \sigma_u^2 [b(1)], & m = 1, \\ 0, & m \geq 2. \end{cases} \quad (5.335)$$

For a complex MA(2) process,

$$r_{xx}(m) = \begin{cases} \sigma_u^2 [1 + |b(1)|^2 + |b(2)|^2], & m = 0, \\ \sigma_u^2 [b(1) + b^*(1)b(2)], & m = 1, \\ \sigma_u^2 [b(2)], & m = 2, \\ 0, & m \geq 3. \end{cases} \quad (5.336)$$

Thus, the spatial spectral matrix for an N -element array is a banded Hermitian, Toeplitz matrix,

$$\mathbf{S}_x = \begin{bmatrix} r_{xx}(0) & r_{xx}^*(1) & r_{xx}^*(2) & 0 & \cdots & 0 \\ r_{xx}(1) & r_{xx}(0) & r_{xx}^*(1) & r_{xx}^*(2) & \cdots & \cdots \\ r_{xx}(2) & r_{xx}(1) & r_{xx}(0) & r_{xx}^*(1) & \cdots & \cdots \\ \vdots & \vdots & \vdots & \vdots & \ddots & \vdots \\ 0 & \cdots & \cdots & \cdots & r_{xx}(1) & r_{xx}(0) \end{bmatrix}, \quad (5.337)$$

where only the main diagonal and $2q$ adjacent diagonals are non-zero. This banded property is useful in many applications.

In many cases, we model the incoming process as an AR(p) process and need to find \mathbf{S}_x^{-1} in order to implement a desired process. In order to find \mathbf{S}_x^{-1} , we use a representation given by Siddiqui [Sid58] and LeCadre [LeC89] (who attributes the result for real processes to Gohberg [KVM78], [BAS86], see also [BS83]). We can write \mathbf{S}_x^{-1} as

$$\mathbf{S}_x^{-1} = \frac{1}{\sigma_u^2} \left[\mathbf{A}_1 \mathbf{A}_1^H - \mathbf{A}_3 \mathbf{A}_3^H \right], \quad (5.338)$$

where \mathbf{A}_1 and \mathbf{A}_3 are two triangular $N \times N$ Toeplitz matrices defined as,

$$\mathbf{A}_1 = \begin{bmatrix} 1 & & & & \\ a_1 & 1 & & & \mathbf{0} \\ a_2 & a_1 & 1 & & \\ \vdots & a_2 & \ddots & 1 & \\ a_p & \dots & \ddots & \ddots & 1 \\ \ddots & \ddots & \ddots & \ddots & \ddots \\ \mathbf{0} & a_p & \dots & \dots & a_1 & 1 \end{bmatrix}, \quad (5.339)$$

$$\mathbf{A}_3 = \begin{bmatrix} & & \mathbf{0} & & \\ a_p^* & & & & \\ \vdots & a_p^* & & & \mathbf{0} \\ a_3^* & \vdots & \ddots & & \\ a_2^* & a_3^* & \dots & \ddots & \\ a_1^* & a_2^* & a_3^* & \dots & a_p^* \end{bmatrix}. \quad (5.340)$$

We present a simple example to illustrate the result in (5.338).

Example 5.6.4

Consider a complex AR(1) process and an N -element array. Then,

$$\mathbf{A}_1 = \begin{bmatrix} 1 & & & & \\ a_1 & 1 & & & \mathbf{0} \\ 0 & a_1 & \ddots & & \\ \vdots & \dots & \ddots & \ddots & \\ 0 & \dots & \dots & a_1 & 1 \end{bmatrix}, \quad (5.341)$$

and

$$\mathbf{A}_3 = \begin{bmatrix} 0 & \cdots & \cdots & 0 \\ \vdots & \cdots & \cdots & \vdots \\ 0 & \cdots & \cdots & 0 \\ a_1^* & 0 & \cdots & 0 \end{bmatrix}. \quad (5.342)$$

Substituting (5.341) and (5.342) into (5.338), we can obtain \mathbf{S}_x^{-1} .

We see that we can write \mathbf{S}_x^{-1} using triangular matrices that only contain the parameters in the AR(p) model. We find this representation useful in many applications.

5.6.2 Model Relationships

In order to relate the various models, we use results due to Wold [Wol54] and Kolmogorov [Kol41].²⁵ The specific result of interest is a theorem in [Kol41] that says that any ARMA or MA process can be represented by an infinite order AR process. We develop the procedure to find this representation and the corresponding finite order approximation.

We first consider an ARMA (1,1) process. Then,

$$H(z) = \frac{1 + b(1)z^{-1}}{1 + a(1)z^{-1}}. \quad (5.343)$$

The corresponding infinite order AR(∞) process is

$$H(z) = \frac{1}{C(z)} = \frac{1}{1 + c(1)z^{-1} + c(2)z^{-2} + \dots}, \quad (5.344)$$

where

$$C(z) = H^{-1}(z) = \frac{1 + a(1)z^{-1}}{1 + b(1)z^{-1}}. \quad (5.345)$$

One can show that the inverse z -transform of $C(z)$ is

$$c(m) = \begin{cases} 1 & m = 0, \\ [a(1) - b(1)](-b(1))^{m-1} & m \geq 1. \end{cases} \quad (5.346)$$

The $c(m)$ are the coefficients that are used in the AR model (they correspond to the $a(m)$ in (5.299)). In order to approximate this with a finite AR model AR(K), we choose K such that

$$c(K+1) \simeq 0, \quad (5.347)$$

²⁵This discussion follows [Kay88].

or equivalently

$$b(1)^K \simeq 0. \quad (5.348)$$

Thus, as the zero in the ARMA process gets closer to the unit circle, we require a higher order process to get a good approximation.

For a general ARMA (p, q) process the AR (∞) process parameters can be obtained as the inverse z -transform of $H^{-1}(z)$ or by the recursive difference equation

$$c(l) = - \sum_{m=1}^q b(m)c(l-m) + \sum_{m=0}^p a(m)\delta(l-m), \quad l \geq 0, \quad (5.349)$$

with initial conditions; $c(-q), c(-q+1), \dots, c(1)$ set equal to zero.

In our application, we are interested in a particular type of ARMA process, so we will defer an example until we have developed the model.

5.6.3 Observation Noise

It is important to note that our discussion up to this point refers to the signal process of interest (note that the “signal” process might contain various interfering signals that we have sometimes called noise). What we actually observe at the array output is

$$x(n) = f(n) + w(n), \quad (5.350)$$

where $w(n)$ is a zero-mean white observation noise with variance σ_w^2 . This observation noise is statistically independent of the white input process $u(n)$. Then

$$\tilde{P}_{xx}(\psi) = \frac{\sigma_u^2 \left[1 + \frac{\sigma_w^2}{\sigma_u^2} |\tilde{A}(\psi)|^2 \right]}{|\tilde{A}(\psi)|^2}. \quad (5.351)$$

Thus, $x(n)$ corresponds to an ARMA (p, p) process where the transfer function of the MA branch satisfies,

$$\left| B(z)B^* \left(\frac{1}{z^*} \right) \right|^2 = \left[1 + \frac{\sigma_w^2}{\sigma_u^2} A(z)A^* \left(\frac{1}{z^*} \right) \right]. \quad (5.352)$$

Note that we can view this model as one in which a single white noise process generates the composite output spectrum. The presence of this observation noise will cause a problem, both in the development of the algorithms and in the application to actual array processing problems.

In many applications we will approximate the ARMA(p, p) model with a higher order AR model. We consider two examples to illustrate this technique.

Example 5.6.5

Consider a complex AR(1) process in the presence of white noise with spectral height σ_w^2 . Using (5.327) in (5.351), we have

$$\tilde{P}_{xx}(\psi) = \frac{\sigma_u^2 + \sigma_w^2 [1 + a(1)e^{-j\psi}] [1 + a^*(1)e^{j\psi}]}{|1 + a(1)e^{-j\psi}|^2}. \quad (5.353)$$

To find $b(1)$, we equate the MA portion of the wavenumber spectrum to the numerator in (5.353):

$$\sigma_b^2 [1 + b(1)e^{-j\psi}] [1 + b^*(1)e^{j\psi}] = \sigma_u^2 + \sigma_w^2 [1 + a(1)e^{-j\psi} + a^*(1)e^{j\psi} + |a(1)|^2], \quad (5.354)$$

which implies,

$$\sigma_b^2 [1 + |b(1)|^2] = \sigma_u^2 + \sigma_w^2 [1 + |a(1)|^2], \quad (5.355)$$

and

$$\sigma_b^2 b(1) = \sigma_w^2 a(1). \quad (5.356)$$

From (5.356)

$$b(1) = \frac{\sigma_w^2}{\sigma_b^2} a(1). \quad (5.357)$$

Substituting (5.357) into (5.355) gives us a quadratic equation in σ_b^2 , which can be solved. This gives the value of $b(1)$. We substitute $b(1)$ into (5.346) to find $c(k)$.

We have shown the results in Figures 5.30, 5.31, and 5.32 for three values of SNR ($\sigma_u^2/\sigma_w^2 = 10$ dB, 0 dB, and -10 dB), two values of $|z_1|$, and various values of K , the order of AR (K) process. In all cases, $|c(k)| \leq 0.001$ for the highest order process.

As the SNR increases, the model order K that is required to get a good fit decreases. As $|z_1|$ increases, the required model order increases.

Example 5.6.6

In this example, we consider the complex AR(2) process discussed in Example 5.6.2,

$$\tilde{P}_{xx}(\psi) = \frac{\sigma_u^2 + \sigma_w^2 |1 + a(1)e^{-j\psi} + a(2)e^{-j2\psi}|^2}{|1 + a(1)e^{-j\psi} + a(2)e^{-j2\psi}|^2}. \quad (5.358)$$

Proceeding as in Example 5.6.5, we obtain three equations,

$$\sigma_b^2 [1 + |b(1)|^2 + |b(2)|^2] = \sigma_u^2 + \sigma_w^2 [1 + |a(1)|^2 + |a(2)|^2], \quad (5.359)$$

$$\sigma_b^2 [b(1) + b(2)b^*(1)] = \sigma_w^2 [a(1) + a(2)a^*(1)], \quad (5.360)$$

and

$$\sigma_b^2 [b(2)] = \sigma_w^2 a(2). \quad (5.361)$$

We solve these three equations and use the results in (5.349) to find the $c(m)$.

We have shown the results in Figures 5.33, 5.34, 5.35 for several of the models in Example 5.6.2, for three values ($\sigma_u^2/\sigma_w^2 = 10$ dB, 0 dB, and -10 dB) and various values of K , the order of AR(K) process.

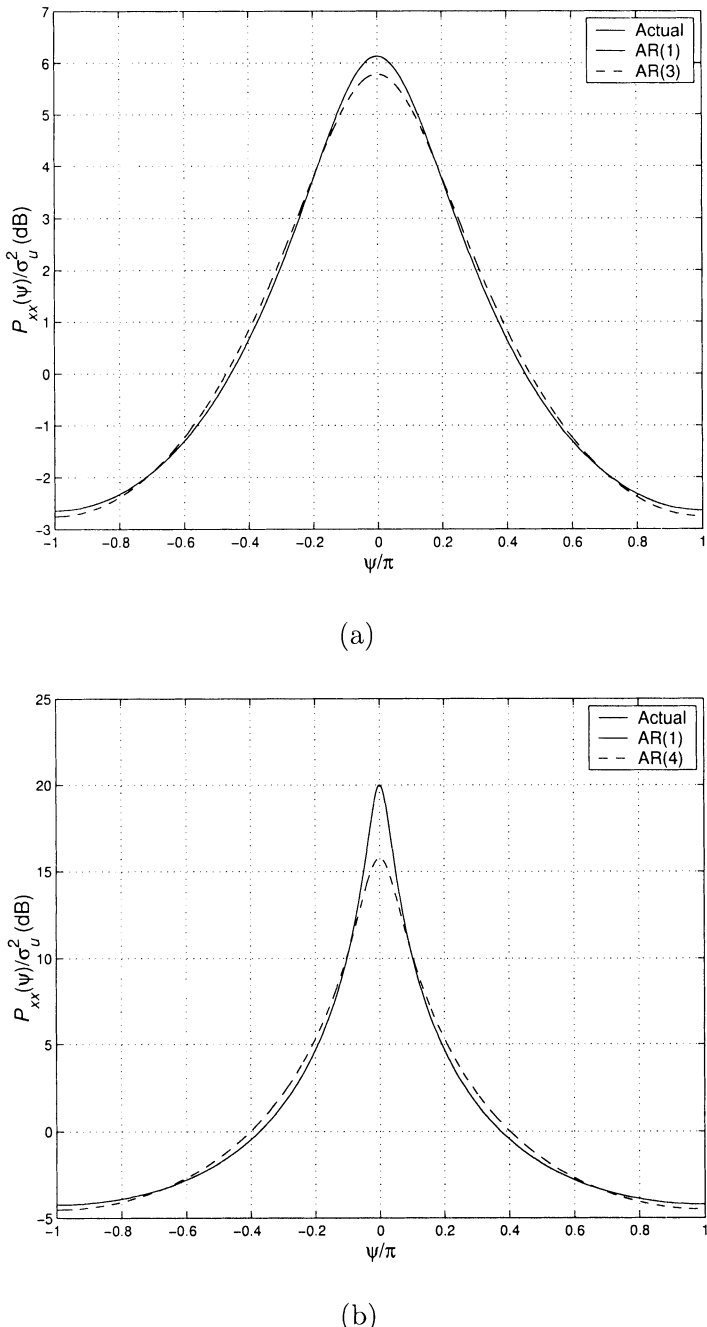


Figure 5.30 Wavenumber spectrum of a complex AR(1) process with additive white noise: $\sigma_u^2/\sigma_w^2 = 10$ dB; (a) $|z_1| = 0.5$; (b) $|z_1| = 0.9$.

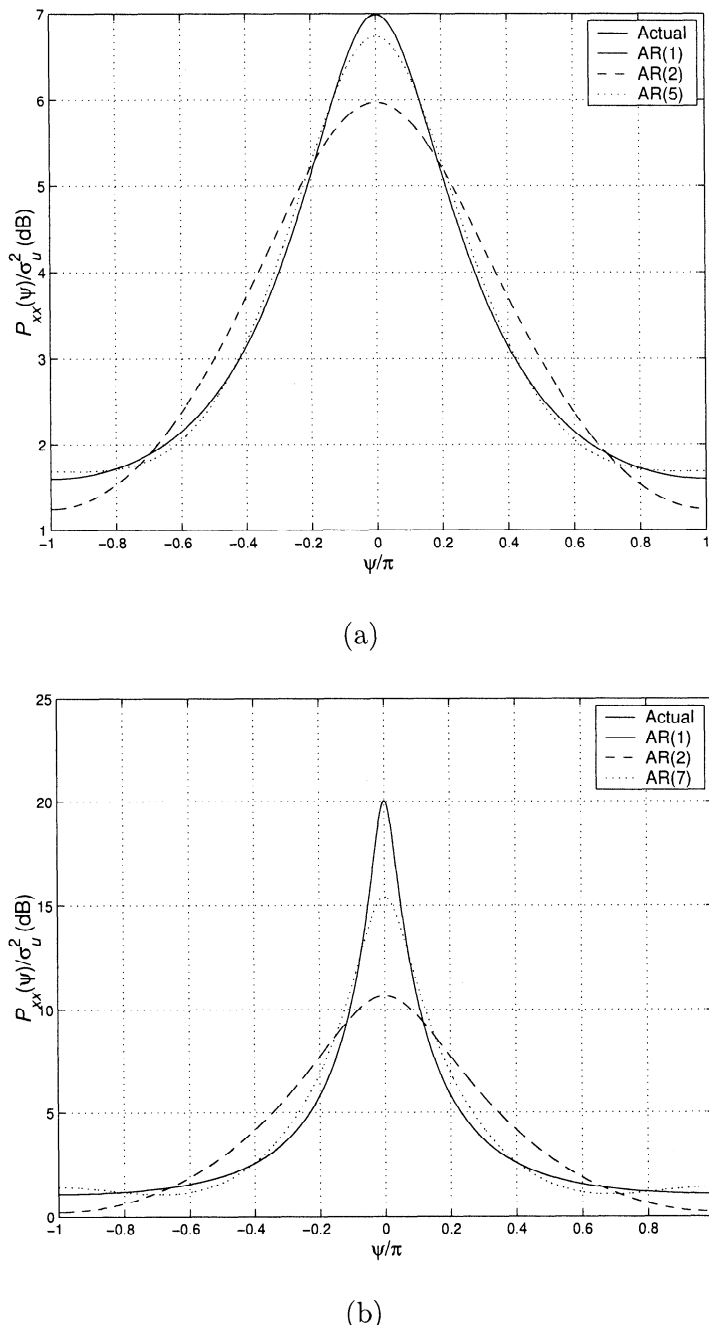


Figure 5.31 Wavenumber spectrum of a complex AR(1) process with additive white noise: $\sigma_u^2/\sigma_w^2 = 0$ dB; (a) $|z_1| = 0.5$; (b) $|z_1| = 0.9$.

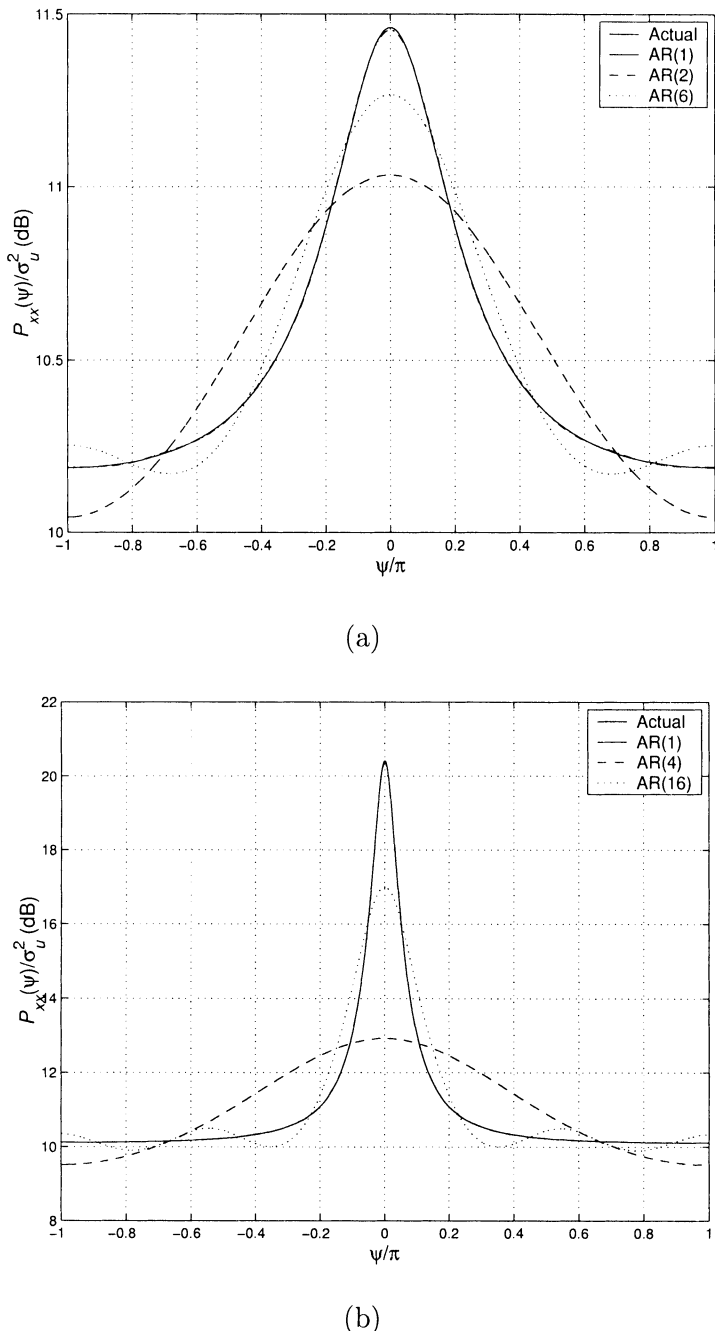


Figure 5.32 Wavenumber spectrum of a complex AR(1) process with additive white noise: $\sigma_u^2/\sigma_w^2 = -10$ dB; (a) $|z_1| = 0.5$; (b) $|z_1| = 0.9$.

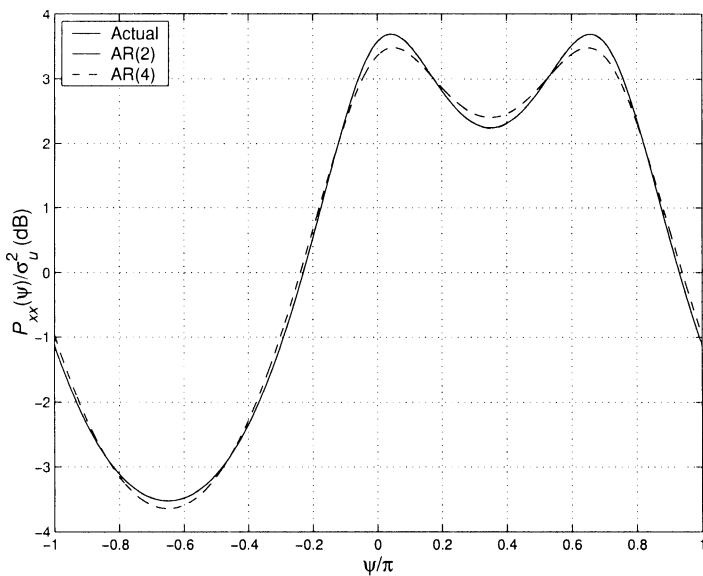


Figure 5.33 Wavenumber spectrum of a complex AR(2) process with additive white noise: $\sigma_u^2/\sigma_w^2 = 10 \text{ dB}$, $z_1 = 0.5$, $z_2 = 0.5e^{j(0.7\pi)}$.

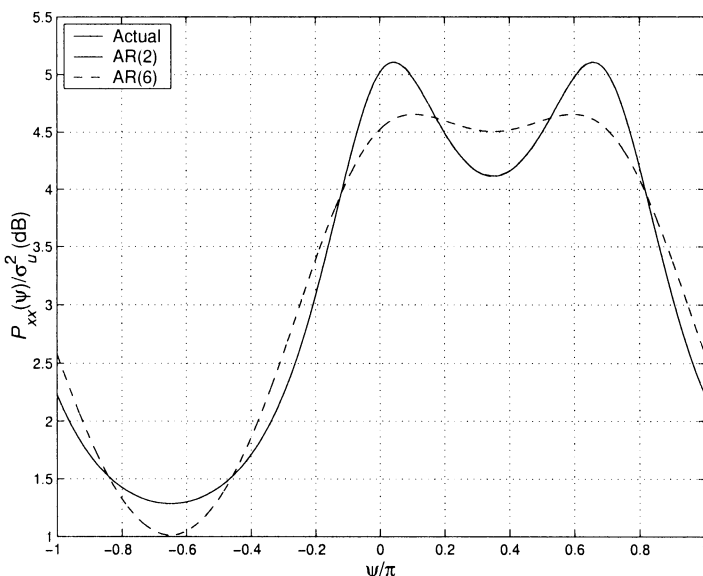


Figure 5.34 Wavenumber spectrum of a complex AR(2) process with additive white noise: $\sigma_u^2/\sigma_w^2 = 0 \text{ dB}$, $z_1 = 0.5$, $z_2 = 0.5e^{j(0.7\pi)}$.

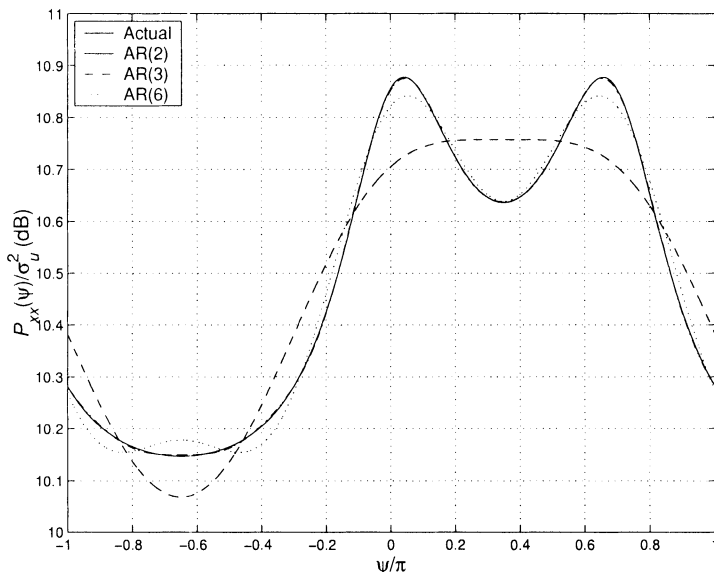


Figure 5.35 Wavenumber spectrum of a complex AR(2) process with additive white noise: $\sigma_u^2/\sigma_w^2 = -10$ dB, $z_1 = 0.5$, $z_2 = 0.5e^{j(0.7\pi)}$.

5.6.4 Summary

Although the ARMA model may seem somewhat artificial, one can show that many spatially spread physical noises (or spread-signal processes) can be modelled by an ARMA model (or an AR model approximation to the ARMA model). (See discussions in [LeC89], [Bur84], [AA66], as well as other references on physical noise models.)

We use AR models to represent various signal and noise processes in subsequent chapters of the text. In the analogous time-domain problem, AR models are widely used for estimation of the power density spectrum of the process. These techniques map directly to the problem of estimating the frequency-wavenumber spectrum of a narrowband process impinging on a standard linear array. We discuss this problem briefly in Chapter 10 but do not pursue it in detail.

5.7 Summary

In this chapter we have developed characterizations for random space-time processes that will be used in our study of optimum array processing.

In Section 5.2, we developed the frequency-domain snapshot model that we use throughout most of the text. We also developed the time-domain snapshot model and saw that, for narrowband processes, the two models give the same results.

In Section 5.3, we introduced a more general model of space-time processes and defined Gaussian space-time processes. This general model could accommodate spatially distributed signal and noise sources that are encountered in many applications.

In Section 5.4, we saw how arrays and apertures respond to these space-time processes. We developed an expression for \mathbf{S}_x , the spatial spectral matrix. This matrix plays the key role in most of our subsequent discussions.

In Section 5.5, we developed an eigendecomposition of the spatial spectral matrix \mathbf{S}_x . The resulting eigenvectors and eigenvalues are the important elements in many of the optimum array processing schemes that we develop in subsequent chapters.

In Section 5.6, we restricted our attention to uniform linear arrays and developed a rational transfer function process model that can be used to model spatially spread signal and noise processes. These AR and ARMA models are widely used to model various physical random processes.

This chapter provides the first part of the background that is needed to develop optimum array processors. In this discussion, we have used ensemble averages and assumed that the various quantities such as \mathbf{S}_f , \mathbf{S}_x , and σ_w^2 were known. In practice, we must estimate these quantities from a finite amount of data. We discuss these issues in Section 7.2.

In Chapter 6, we develop optimum waveform estimation algorithms using the models developed in this chapter.

5.8 Problems

P5.2 Snapshot Models

Problem 5.2.1

Define

$$\mathbf{X}(\omega_m) = \int_0^{\Delta T} \mathbf{x}(t) e^{-j\omega t} dt. \quad (5.362)$$

- (a) Show that

$$E [\mathbf{X}(\omega_m) \mathbf{X}^H(\omega_m)] = \int_0^{\Delta T} (\Delta T - |v|) \mathbf{R}_x(v) \cos \omega_m v dv. \quad (5.363)$$

(b) Show that

$$\lim_{\Delta T \rightarrow \infty} \left\{ \frac{1}{\Delta T} E \left[\mathbf{X}(\omega_m) \mathbf{X}^H(\omega_m) \right] \right\} = \int_{-\infty}^{\infty} \mathbf{R}_x(v) \cos \omega_m v \, dv = \mathbf{S}_x(\omega_m). \quad (5.364)$$

(c) Discuss how large ΔT must be in order for

$$\frac{1}{\Delta T} E \left[\mathbf{X}(\omega_m) \mathbf{X}^H(\omega_m) \right] \simeq \mathbf{S}_x(\omega_m). \quad (5.365)$$

Problem 5.2.2

Consider a standard 10-element linear array. Assume that the signal is a plane wave whose direction cosine is u_s and whose spectrum is shown in Figure 5.2(a). The expression for $\mathbf{S}_{x_{\Delta T}}(m, m)$ is given in Section 5.2.1.3.

- (a) Plot the matrix, $\mathbf{S}_{x_{\Delta T}}(m, m)$, for $B_s \cdot \Delta T = 2^l, l = 0, \dots, 7, |m| = 2^l$, for $u = 0$. Discuss your results.
- (b) Repeat for $u = 0.5$
- (c) Repeat for $u = 0.9$

Problem 5.2.3

Repeat Problem 5.2.2 for $\mathbf{S}_{x_{\Delta T}}(m_1, m_2)$. Consider the cases

$$\begin{aligned} m_1 &= 0, & m_2 &= 1 \\ m_1 &= 0, & m_2 &= 2. \end{aligned} \quad (5.366)$$

Problem 5.2.4

Consider the expression in (5.27). Evaluate it for the plane-wave model in Problem 5.2.2, $l = k + 1$, and $m_1 = m_2$.

P5.3 Space-time Random Processes

Problem 5.3.1 [Bag76]

In an ocean environment, surface or bottom noise can be characterized by

$$S_o(\omega_0 : \theta, \phi) = S_o(\omega_0) [1 + \alpha \cos \theta], \quad (5.367)$$

and has azimuthal (ϕ) symmetry. An intensity plot is shown in Figure 5.36.

- (a) Plot the real and imaginary part of $S_x(\omega_0 : \Delta p)$ versus Δp for various α and $\cos \theta_p$.
- (b) Check your result against the analytic formula

$$S_x(\omega_0 : \Delta p) = S_o(\omega_0) \left\{ \text{sinc}(k_o \Delta p) + j \alpha \frac{1}{k_o \Delta p} [\text{sinc}(k_o \Delta p) - \cos(k_o \Delta p)] \cos \theta_p \right\}. \quad (5.368)$$

Problem 5.3.2 [Bag76]

In an ocean environment, we can model layer noise as

$$S_o(\omega_0 : \theta, \phi) = S_o(\omega_0) \left[1 - \frac{1}{4} \alpha - \frac{3}{4} \alpha \cos(2\theta) \right], \quad (5.369)$$

with azimuthal symmetry. An intensity plot is shown in Figure 5.37.

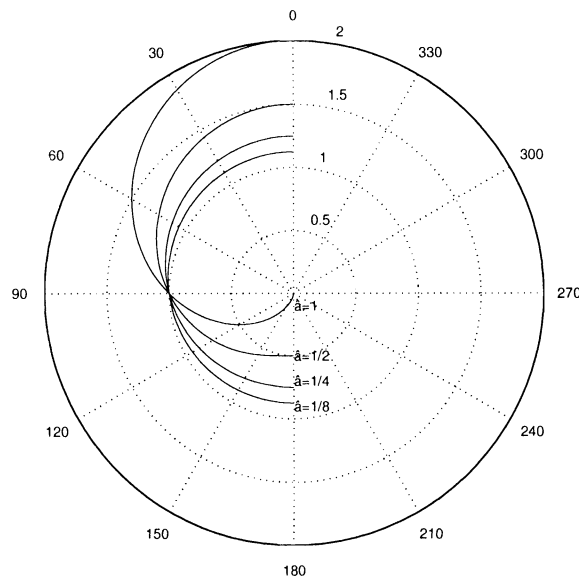


Figure 5.36 Power distribution: surface noise. [From [Bag76]]

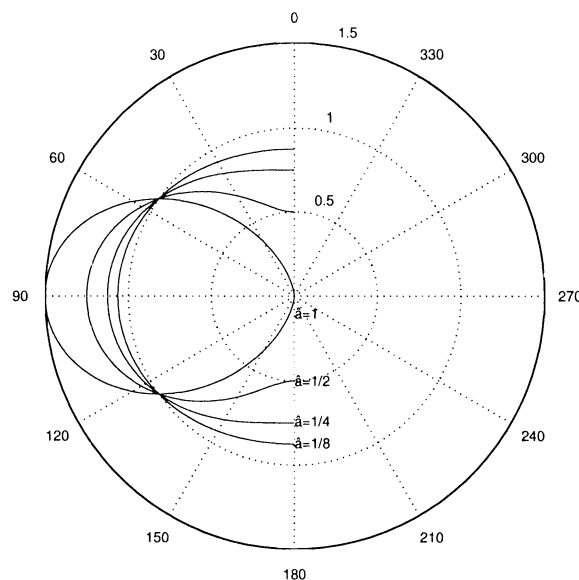


Figure 5.37 Power distribution: layer noise. [From [Bag76]]

- (a) Plot $S_f(\omega_0 : \Delta\mathbf{p})$ versus $\Delta\mathbf{p}$ for various $\cos\theta_p$ and α .
(b) Check your result against the analytic formula

$$S_x(\omega_o : \Delta\mathbf{p}) = S_o(\omega_o) \left\{ \text{sinc}(k_o\Delta\mathbf{p}) + \alpha \left[\left(\frac{3}{(k_o\Delta\mathbf{p})^2} - 1 \right) \text{sinc}(k_o\Delta\mathbf{p}) - \frac{3\cos(k_o\Delta\mathbf{p})}{(k_o\Delta\mathbf{p})^2} \right] \left[\frac{3\cos(2\theta_z) + 1}{4} \right] \right\}. \quad (5.370)$$

Problem 5.3.3 [Bag76]

Consider the 2-D representation of noise that has a high concentration of low wavenumber components. Assume,

$$P_f(\omega : \mathbf{k}) = S_o(\omega) \frac{1}{\pi^2 k_o^2} \left\{ \left(\frac{k_r}{k_o} \right) \left[1 - \left(\frac{k_r}{k_o} \right)^2 \right]^{\frac{1}{2}} \right\}^{-1}. \quad (5.371)$$

- (a) Plot $\frac{S_f(\omega : \Delta\mathbf{p})}{S_o(\omega)}$ versus $\Delta\mathbf{p}$.
(b) Compare your result to the analytic formula,

$$S_f(\omega : \Delta\mathbf{p}) = S_o(\omega) J_o^2 \left(\frac{k_r \Delta\mathbf{p}}{2} \right). \quad (5.372)$$

P5.4 Arrays and Apertures

Problem 5.4.1

Using (5.182) as a starting point, show that

$$S_y(\omega) = \int_{-\infty}^{\infty} \cdot \int_{-\infty}^{\infty} S_x(\omega : \Delta\mathbf{p}) R_W(\omega : \Delta\mathbf{p}) d\Delta\mathbf{p}, \quad (5.373)$$

where $R_W(\omega : \Delta\mathbf{p})$ is defined in (5.184).

Problem 5.4.2

Find the co-array for a standard 4×4 square array.

Problem 5.4.3 [JD93]

Consider a 9-element crossed array with an element at the origin and four equally spaced (d) elements along both the positive x -axis and the positive y -axis.

- (a) Find the co-array.
(b) Plot the beam pattern for uniform weighting.
(c) Compute the directivity and compare to a square 3×3 array with interelement spacing d .

Problem 5.4.4

Repeat Problem 5.4.3 for a symmetric 9-element crossed array along the x - and y -axes with interelement spacing d .

Problem 5.4.5 [JD93]

Consider an equilateral triangle array with four equally spaced (d) elements on each side (nine sensors total).

- (a) Find the co-array.
- (b) Find the beam pattern if the array lies in the xy -plane and the sensors are short dipoles oriented in the z -direction.

P5.5 Orthogonal Expansions

In Problems 5.5.1–5.5.23, the objective is to find the eigenvalues and eigenvectors. The spatial signal (or noise) environment and the array (or aperture) geometry is specified in each problem.

Problem 5.5.1

The input is two equal-power uncorrelated plane waves. The array is a standard 10×10 square array.

- (a) Find the normalized eigenvalues.
- (b) Plot the eigenvectors for several ψ_1 and ψ_2 .

Problem 5.5.2

Repeat Problem 5.5.1 for four equal-power uncorrelated signals that are uniformly spaced in ψ -space.

Problem 5.5.3

The input is three equal-power uncorrelated plane waves that are equally spaced in ψ -space. The array is a standard 10-element linear array.

- (a) Plot the eigenvalues for several $\Delta\psi$.
- (b) Plot the eigenvectors for several $\Delta\psi$.

Problem 5.5.4.

The input is two equal-power uncorrelated plane waves. The array is a standard 19-element hexagonal array (e.g., Section 4.4).

- (a) Find the normalized eigenvalues.
- (b) Plot the eigenvectors for several $\Delta\psi$.

Problem 5.5.5

Repeat Problem 5.5.4 for four equal-power uncorrelated signals that are uniformly spaced in ψ -space.

- (a) Find the normalized eigenvalues.
- (b) Plot the eigenvectors for several $\Delta\psi$.

Problem 5.5.6

Assume that the signal has the spatial correlation function, given by (5.148).

Consider a 20-element linear array along the x -axis with $d = \lambda/2$.

Find the eigenvalues and eigenvectors.

Problem 5.5.7

Assume the signal has the spatial correlation function given by (5.148).

Consider a standard 10-element linear array along the x -axis.

Find the eigenvalues and eigenvectors for various θ_0 .

Problem 5.5.8

Repeat Problem 5.5.7 for the sector noise model with the center of the sector moved to $\theta_1 = 30^\circ, \phi_1 = 0^\circ$.

Problem 5.5.9

Repeat Problem 5.5.7 for a standard 10×10 square array located in the xy -plane.

Problem 5.5.10

Repeat Problem 5.5.8 for a standard 10×10 square array located in the xy -plane.

Problem 5.5.11

The input is two equal-power uncorrelated plane waves. The aperture is a ring aperture with $R = 3\lambda$.

- (a) Find the normalized eigenvalues.
- (b) Plot the eigenvectors for several $\Delta\psi$.

Problem 5.5.12

The input is two equal-power uncorrelated plane waves. The array is 12-element circular array with $R = 3\lambda$.

- (a) Find the normalized eigenvalues.
- (b) Plot the eigenvectors for several $\Delta\psi$.

Problem 5.5.13

Repeat Problem 5.5.11 for a circular aperture with $R = \sqrt{3}\lambda$. Compare the results to the results in Problem 5.5.4.

Problem 5.5.14

Repeat Problem 5.5.13 for a square aperture whose area is the same as the circular aperture in Problem 5.5.13.

Problem 5.5.15

Consider a standard 11-element linear array. The input consists of the spatially spread spectrum described in Example 5.5.1 (with $\psi_\Delta = \pi \cos 15^\circ$) and two equal-power (P) uncorrelated plane waves at $\psi_1 = \pi \cos 15^\circ$ and $\psi_2 = \pi \cos 20^\circ$. Define $\beta = \frac{S_x(\omega) \cdot 2\psi_\Delta}{P}$.

- (a) Find the normalized eigenvalues.
- (b) Check the behavior of the eigenvalues for $\beta = 0$ and $\beta = \infty$.
- (c) Plot the eigenvectors for $\beta = 1$.

Problem 5.5.16

Consider a standard 10-element linear array and four uncorrelated equal-power plane-wave signals at $\psi = \pm\Delta\psi$ and $\psi = \pm2\Delta\psi$. Read [Lee92].

- (a) Use Lee's procedure to find the eigenvalues and eigenvectors.
- (b) Plot the resulting eigenvalues versus $\Delta\psi/BW_{NN}$ using Lee's procedure and compare the results to an exact numerical calculation for several $\Delta\psi$.
- (c) Plot the resulting eigenvectors and plot $|\mathbf{e}_i|$ versus $\Delta\psi/BW_{NN}$.

Problem 5.5.17

- (a) Repeat Problem 5.5.16(a) for a standard 21-element linear array and six uncorrelated equal-power plane-wave signals at $\psi = \pm\Delta\psi, \pm2\Delta\psi, \pm3\Delta\psi$.
- (b) Plot the resulting eigenvalues versus $\frac{\Delta\psi}{BW_{NN}}$.
- (c) Plot the resulting eigenvectors.

Problem 5.5.18 (continuation: Problem 5.5.16)

Consider a standard 10-element linear array and the frequency-wavenumber function in (5.269).

- (a) Use Lee's [Lee92] procedure to find the eigenvalues and eigenvectors.
- (b) Compare the results to the results in Example 5.5.1

Problem 5.5.19

Consider a standard 11-element linear array. The input signal is a complex AR(1) process whose frequency-wavenumber spectrum is given by (5.327). Find the eigenvalues and eigenvectors for different values of $a(1)$. Plot the eigenvalues versus $|a(1)|$ and $\angle a(1)$. Plot selected eigenbeams.

Problem 5.5.20

Repeat Problem 5.5.19 for the complex AR(2) process whose frequency-wavenumber spectrum is given by (5.330).

Problem 5.5.21

Repeat Problem 5.5.19 for the complex ARMA (1,1) process whose frequency-wavenumber spectrum is given by (5.353). Does the structure of $\tilde{P}_x(\psi)$ allow any simplification?

Problem 5.5.22

In Section 5.3.4.1, the function $\bar{S}_o(\omega, u)$ is the 1-D frequency-wavenumber response function evaluated for $k_z = -\frac{2\pi}{\lambda}u$. Let

$$\bar{S}_o(\omega, u) = P_x(\omega, k_z)|_{k_z=-\frac{2\pi}{\lambda}u} = \begin{cases} S_x(\omega) \frac{1}{2u_o}, & |u - u_s| \leq u_o, \\ 0, & \text{otherwise.} \end{cases} \quad (5.374)$$

The signal is spatially spread around the direction-of-arrival u_s with a uniform distribution with spreading factor u_o .

(a) Show that

$$S_x(\omega, \Delta p_z) = S_x(\omega) e^{-j \frac{2\pi}{\lambda} u_s \Delta p_z} \text{sinc}\left(\frac{2\pi}{\lambda} u_o \Delta p_z\right). \quad (5.375)$$

(b) Assume an N -element standard linear array along the z -axis. Find the expression for $S_x(\omega)$.

(c) Plot the eigenvalues and eigenbeams for several directions-of-arrival u_s , and spreading factors u_o .

Problem 5.5.23 (continuation)

Repeat Problem 5.5.22 with

$$\bar{S}_o(\omega, u) = P_x(\omega, k_z)|_{k_z=-\frac{2\pi}{\lambda}u} = S_x(\omega) \frac{1}{\sqrt{2\pi\sigma_o^2}} \exp\left\{-\frac{(u-u_s)^2}{2\sigma_o^2}\right\}, \quad (5.376)$$

and

$$S_x(\omega, \Delta p_z) = S_x(\omega) e^{-j \frac{2\pi}{\lambda} u_s \Delta p_z} \exp\left\{-\frac{1}{2}\left(\frac{2\pi}{\lambda}\sigma_o \Delta p_z\right)^2\right\}. \quad (5.377)$$

The signal is spatially spread around the direction-of-arrival u_s with a Gaussian distribution with spreading factor σ_o . Assume $\sigma_o \ll 1$.

Problem 5.5.24

Derive the results in (5.255) and (5.259).

Problem 5.5.25

Consider a standard 10-element linear array, and two uncorrelated plane waves. Assume $S_1 = 1$. Plot the eigenvalues (normalized by N) and eigenvectors for various separations for (i) $S_2 = S_1$, (ii) $S_2 = 10S_1$, (iii) $S_2 = 100S_1$, (iv) $S_2 = 1000S_1$. Find the eigenvalues and eigenvectors numerically by constructing $\mathbf{S}_x = \mathbf{V}\mathbf{S}_f\mathbf{V}^H$ and verify that eigenvalues are the same as the analytical expression in (5.255).

Problem 5.5.26

Consider a standard 10-element linear array. There are three uncorrelated plane waves impinging on the array:

Signal: $u_s = 0, \sigma_s^2 = 1$

Interferer: $u_1 = 0.3, \sigma_1^2 = 10, 1000$

Interferer: $u_2 = -0.5, \sigma_2^2 = 10, 1000$

(a) Find the eigenvalues and eigenvectors for the four combinations of interferer powers. Plot the eigenbeams.

(b) Assume that the signal actually arrives from $u_a; -0.1 \leq u_a \leq 0.1$. Compute the correlation between $\mathbf{v}(u_a)$ and each of the three eigenvectors in part (a). Plot the results versus u_a for the four cases.

(c) Define

$$\mathbf{v}_p(u_a) = \mathbf{v}^H(u_a) \mathbf{U}_{S+I}, \quad (5.378)$$

where \mathbf{U}_{S+I} is the $N \times 3$ matrix defining the “signal-plus-interference” subspace. Then

$$C(u_a) = \frac{1}{N} \|\mathbf{v}_p(u_a)\|^2, \quad (5.379)$$

measures the amount of the signal power contained in the subspace. Plot $C(u_a)$ versus u_a .

Problem 5.5.27

Consider the same nominal model as in Problem 5.5.26(a). Assume that the sensor positions are perturbed using the model in Section 2.6.3.

(a) Express \mathbf{S}_x as a function of $\Delta\mathbf{p}$.

(b) Define

$$\mathbf{v}_p(\Delta\mathbf{p}) = \mathbf{v}^H(u_s)\mathbf{U}_{S+I}(\Delta\mathbf{p}), \quad (5.380)$$

where $\mathbf{U}_{S+I}(\Delta\mathbf{p})$ is the “signal-plus-interference” subspace calculated using the actual array location. The array manifold vector $\mathbf{v}(u_s)$ is calculated using the nominal location with $u_s = 0$. Define

$$C(\Delta\mathbf{p}) = \frac{1}{N} \|\mathbf{v}_p(\Delta\mathbf{p})\|^2. \quad (5.381)$$

Plot $E[C(\Delta\mathbf{p})]$ versus σ_λ^2 for the case of equal power interferers ($\sigma_I^2 = 10$ dB and 30 dB). Discuss your result.

Problem 5.5.28

Consider an N -element standard linear array. The signal is spatially spread and frequency spread. The signal direction is centered at u_s ,

$$P_1(f, u) = \begin{cases} \frac{\sigma_s^2}{B_s \Delta u}, & |u - u_s| \leq \frac{\Delta u}{2}, |f - f_c| \leq \frac{B_s}{2}, \\ 0, & \text{elsewhere.} \end{cases} \quad (5.382)$$

(a) Find \mathbf{S}_x .

(b) Find the eigenvalues and eigenvectors for a standard 10-element linear array as a function of $u_\Delta/B\omega_{NN}$ and $B_f u_s$.

(c) Develop a test similar to those in (5.277) and (5.290).

P5.6 Parametric Wavenumber Models

Problem 5.6.1

Consider the surface noise model in Problem 5.3.1. Assume we are observing with a standard linear array along the z -axis. Develop a rational transfer model that approximates the frequency-wavenumber function.

Problem 5.6.2

Find the correlation matrix \mathbf{S}_x for the input process whose wavenumber spectrum is given by (5.330). Use the parameter values in Figure 5.25.

Problem 5.6.3

Assume that

$$\mathbf{X}(k) = \mathbf{F}(k) + \mathbf{N}(k), \quad (5.383)$$

where $\mathbf{F}(k)$ is a plane wave from broadside and the $\mathbf{N}(k)$ have the wavenumber spectrum shown in Figure 5.24, with $a(1) = 0.7e^{-j(0.6\pi)}$. We process the input with a standard 10-element linear array. Find the array weighting to maximize the array gain.

Problem 5.6.4

- (a) Find \mathbf{S}_x for the complex AR(2) process in (5.330).
- (b) Indicate how you would implement the spatial whitening filters.

Problem 5.6.5

Consider an $N \times N$ symmetric tridiagonal Toeplitz matrix whose first row is $[a, b, 0, \dots, 0]$. The eigenvalues and eigenvectors are given by

$$\lambda^{(k)} = a + 2b \cos\left(\frac{k\pi}{N} + 1\right), \quad k = 1, \dots, N, \quad (5.384)$$

and

$$\Phi_j^{(k)} = \left(\frac{2}{N} + 1\right)^{1/2} \sin\left(\frac{kj\pi}{N} + 1\right), \quad j, k = 1, \dots, N. \quad (5.385)$$

(e.g., [RB78] or [GK69]).

- (a) Use this result to find an analytic expression for the eigenvalues and eigenvectors of a real AR(1) process.
- (b) Plot the eigenbeams for $N = 10$ and several values of $a(1)$.
- (c) Check the behavior as $a(1) \rightarrow 1$.

Problem 5.6.6

Repeat Problem 5.6.5 for a complex AR(1) process.

Problem 5.6.7

- (a) Find the whitening filter for a complex AR(2) process.
- (b) Write \mathbf{S}_x^{-1} in the form of (5.338).

Problem 5.6.8

Repeat Problem 5.6.7 for a complex AR(3) process.

Problem 5.6.9

Consider the case in which

$$\mathbf{X}(k) = \mathbf{F}(k) + \mathbf{W}(k), \quad (5.386)$$

and $\mathbf{F}(k)$ is a complex AR(1) process.

- (a) Approximate $\mathbf{x}(k)$ by a higher order AR process. Use this result to find an approximate spatial whitening filter. Define a whiteness measure as

$$\varepsilon_w = \|E[\mathbf{Y}\mathbf{Y}^H] - k\mathbf{I}\|_F, \quad (5.387)$$

where $\mathbf{Y}(n)$ is the output of the whitening filter. Show how to compute the whiteness measure.

- (b) Consider a standard 10-element linear array. Apply the result in part (a) to the model with $\sigma_u^2/\sigma_n^2 = -10$ dB, 0 dB, 10 dB, and $|a(1)| = 0.5, 0.7, 0.9$ and 0.99 for several values of ε_w .

Problem 5.6.10

Repeat Problem 5.6.9 for a complex AR(2) process.

Bibliography

- [AA66] E. M. Arase and T. Arase. Correlations of ambient sea noise. *J. Acoust. Soc. Am.*, vol.40, pp. 205–210, February 1966.
- [Bag76] A. B. Baggeroer. Space-time processes and optimal array processing. Technical Report 506, Navy Undersea Center, San Diego, California, December 1976.
- [BAS86] A. Ben Artiz and T. Shalom. On inversion of Toeplitz and close to Toeplitz matrices. *Linear Algebra Appl.*, vol.75, pp. 173–192, March 1986.
- [Bla57] N. M. Blachman. On Fourier series for Gaussian noise. *Inf. Control* vol.1, pp. 56–63, 1957.
- [BS83] A. Botcher and B. Silbermann. *Invertibility and Asymptotics of Toeplitz Matrices*. Akademie Verlag, Berlin, 1983.
- [Bur84] W. S. Burdic. *Underwater Acoustic System Analysis*. Prentice-Hall, Englewood Cliffs, New Jersey, 1984.
- [Com88] R. T. Compton, Jr. *Adaptive Antennas (Concepts and Performance)*. Prentice-Hall, Englewood Cliffs, New Jersey, 1988.
- [DM84] D. E. Dudgeon and R. M. Mersereau. *Multidimensional Digital Signal Processing*. Prentice-Hall, Inc., Englewood Cliffs, New Jersey, 1984.
- [Doo53] J. Doob. *Stochastic Processes*. Wiley, New York, 1953.
- [DR58] W. B. Davenport and W. L Root. *An Introduction to the Theory of Random Signals and Noise*. McGraw-Hill, New York, 1958.
- [DR87] W. B. Davenport and W. L Root. *An Introduction to the Theory of Random Signals and Noise*. IEEE Press, New York, 1987.
- [Fuh98] D. Fuhrmann. Complex random variables and stochastic processes, In V. Madisetti and D. Williams, editors., *Digital Signal Processing Handbook*, CRC Press, Boca Raton, Florida, 1998.
- [GK69] R. T. Gregory and D. L. Karney. *A Collection of Matrices for Testing Computational Algorithms*. Wiley-Interscience, New York, 1969.
- [Hau68] R. A. Haubrich. Array design. *Bull. Seismol. Soc. Am.*, vol.58, pp. 977–991, June 1968.
- [Hay91] S. Haykin. *Adaptive Filter Theory*. Prentice-Hall, Englewood Cliffs, New Jersey, second edition, 1991.
- [Hel91] C. W. Helstrom. *Probability and Stochastic Processes for Engineers*. Prentice-Hall, Englewood Cliffs, New Jersey, second edition, 1991.
- [HN76] W. S. Hodgkiss and L. W. Nolte. Covariance between Fourier coefficients representing the time waveforms observed from an array of sensors. *J. Acoust. Soc. Am.*, vol.59, pp. 582–590, March 1976.
- [Hud81] J.E. Hudson. *Adaptive Array Principles*. Peter Peregrinus, New York and London, 1981.
- [JD93] D. H. Johnson and D. E. Dudgeon. *Array Signal Processing*. Prentice-Hall, Englewood Cliffs, New Jersey, 1993.
- [Kay88] S. M. Kay. *Modern Spectral Estimation: Theory and Application*. Prentice-Hall, Englewood Cliffs, New Jersey, 1988.

- [KB79a] P. C. K. Kwok and P. S. Brandon. Eigenvalues of the noise covariance matrix of a linear array in the presence of 2 directional interferences. *Electron. Lett.*, vol.15, pp. 50–51, January 1979.
- [KB79b] P. C. K. Kwok and P. S. Brandon. The optimal radiation pattern of an array in the presence of 2 directional interferences. *Electron. Lett.*, vol.15, pp. 251–252, March 1979.
- [KB86a] M. Kaveh and A. J. Barabell. The statistical performance of the MUSIC and the Minimum-Norm algorithms in resolving plane waves in noise. *IEEE Trans. Acoust., Speech, Signal Process.*, vol. ASSP-34, pp. 331–341, April 1986.
- [KB86b] M. Kaveh and A. J. Barabell. Corrections to ‘The statistical performance of the MUSIC and the Minimum-Norm algorithms in resolving plane waves in noise.’ *IEEE Trans. Acoust., Speech, Signal Process.*, vol. ASSP-34, p. 633, June 1986.
- [Kol41] A. N. Kolmogorov. Interpolation and extrapolation von stationären zufälligen folgen. *Bull. Acad. Sci. USSR Ser. Math.*, vol.5, pp. 3–14, January 1941.
- [Kre71] J. L. Kreuzer. A synthetic aperture coherent imaging technique. *Acoust. Hologr.*, vol.3, pp. 287–315, March 1971.
- [KSL94] T. P. Krauss, L. Shure, and J. N. Little. *Signal Processing Toolbox*. The Math Works, Natick, Massachusetts, 1994.
- [KVM78] T. Kailath, A. Vieira, and M. Morf. Inverse of Toeplitz operators, innovations and orthogonal polynomials. *SIAM Rev.*, vol.20, pp. 106–119, January 1978.
- [LeC89] J.-P. LeCadre. Parametric methods for spatial signal processing in the presence of unknown colored noise fields. *IEEE Trans. Acoust., Speech, Signal Process.*, vol. ASSP-37, pp. 965–983, July 1994.
- [Lee92] H. B. Lee. Eigenvalues and Eigenvectors of covariance matrices for signals closely spaced in frequency. *IEEE Trans. Signal Process.*, vol. SP-40, pp. 2518–2535, October 1992.
- [Mar87] S. L. Marple, Jr. *Digital Spectral Analysis*. Prentice-Hall, Englewood Cliffs, New Jersey, 1987.
- [Mer79] R. M. Mersereau. The processing of hexagonally sampled two-dimensional signals. *Proc. IEEE*, vol.67, pp. 930–949, August 1979.
- [Mil74] K. Miller. *Complex Stochastic Processes*. Addison-Wesley, Reading, Massachusetts, 1974.
- [Mor78] D. R. Morgan. Partially adaptive array techniques. *IEEE Trans. Antennas Propag.*, vol. AP-26, pp. 823–833, November 1978.
- [NM93] F. Neeser and J. Massey. The complex random processes with applications to information theory. *IEEE Trans. Inf. Theory*, vol. IT-39, pp. 1293–1302, July 1993.
- [OS89] A. V. Oppenheim and R. W. Schafer. *Discrete-Time Signal Processing*. Prentice-Hall, Englewood Cliffs, New Jersey, 1989.
- [Ows85] N. L. Owsley. Overview of adaptive array processing. In *Adaptive Methods in Underwater Acoustics*, pp. 355–374, H.G. Urban, editor, Reidel, Dordrecht, The Netherlands, 1985.

- [PM62] D. P. Peterson and D. Middleton. Sampling and reconstruction of wave-number limited functions in n -dimensional Euclidean spaces. *Inf. Control*, vol.5, pp. 279–323, April 1962.
- [PRLN92] J. G. Proakis, C. M. Rader, F. Ling, and C. L. Nikias. *Advanced Digital Signal Processing*. Macmillan, New York, 1992.
- [RB78] P. A. Roebuck and S. Barnett. A survey of Toeplitz and related matrices. *Int. J. Syst. Sci.*, vol.9, pp. 921–934, 1978.
- [Sid58] M. M. Siddiqui. On the inversion of the sample covariance matrix in a stationary autoregressive process. *Ann. Math. Statist.*, vol.58, pp. 585–588, June 1958.
- [Str41] J. Stratton. *Electromagnetic Theory*. McGraw-Hill, New York, 1941.
- [VT68] H. L. Van Trees. *Detection, Estimation, and Modulation Theory, Part I*. Wiley, New York, 1968.
- [VT71] H. L. Van Trees. *Detection, Estimation, and Modulation Theory, Part III*. Wiley, New York, 1971.
- [VT01a] H. L. Van Trees. *Detection, Estimation, and Modulation Theory, Part I*. Wiley Interscience, New York, 2001.
- [VT01b] H. L. Van Trees. *Detection, Estimation, and Modulation Theory, Part III*. Wiley Interscience, New York, 2001.
- [WK85] G. Wakefield and M. Kaveh. Frequency-wavenumber spectral estimation of the pressure field beneath a turbulent boundary layer. *Proc. Winter Annual Meeting of the American Society of Mechanical Engineers*, NCA, vol.1, Miami Beach, Florida November 1985.
- [Wol54] H. Wold. *A Study in the Analysis of Stationary Time Series*. Almqvist & Wiksell, Stockholm, 1954.
- [Yag57] A. Yaglom. Some classes of random fields in dimensional space, related to stationary random process. *Theory Prob. Appl.*, p. 273, November 1957.
- [Yag60] A. Yaglom. *An Introduction to the Theory of Stationary Random Functions*. Prentice-Hall, Englewood, Cliffs, New Jersey, 1960.
- [Zat98] M. Zatman. How narrow is narrowband? *Conference Record of the Thirty-First Asilomar Conference on Signals, Systems and Computers*, 1997, vol.2, pp. 1341–1345, October 1998.

Copyright of Optimum Array Processing is the property of John Wiley & Sons, Inc. 2002 and its content may not be copied or emailed to multiple sites or posted to a listserv without the copyright holder's express written permission. However, users may print, download, or email articles for individual use.